



Universidade de Aveiro

Ano 2021

**NUNO MIGUEL
SEQUEIRA DE
ALMEIDA**

**SOLDADURA LASER DE COMPÓSITOS DE MATRIZ
TERMOPLÁSTICA**

**LASER WELDING OF THERMOPLASTIC MATRIX
COMPOSITES**



Universidade de Aveiro

Ano 2021

**NUNO MIGUEL
SEQUEIRA DE
ALMEIDA**

**SOLDADURA LASER DE COMPÓSITOS DE MATRIZ
TERMOPLÁSTICA**

**LASER WELDING OF THERMOPLASTIC MATRIX
COMPOSITES**

Dissertação apresentada à Universidade de Aveiro para cumprimento dos requisitos necessários à obtenção do grau de Mestre em Engenharia Mecânica, realizada sob a orientação científica do Doutor António Manuel de Bastos Pereira, Professor Associado c/ Agregação do Departamento de Engenharia Mecânica da Universidade de Aveiro e do Doutor Alfredo Manuel Balacó de Morais, Professor Associado do Departamento de Engenharia Mecânica da Universidade de Aveiro.

Dissertation presented to the University of Aveiro to fulfill the requirements necessary to obtain a Master's degree in Mechanical Engineering, carried out under the scientific guidance of Dr. António Manuel de Bastos Pereira, Associate Professor with Aggregation at the Department of Mechanical Engineering at the University of Aveiro and of Dr. Alfredo Manuel Balacó de Morais, Associate Professor at the Department of Mechanical Engineering at the University of Aveiro.

Este trabalho teve o apoio financeiro dos projetos UIDB/00481/2020 e UIDP/00481/2020 - FCT - Fundação para Ciência e Tecnologia; e CENTRO-01-0145-FEDER-022083 - Programa Operacional Regional do Centro (Centro2020), no âmbito do Acordo de Parceria Portugal 2020, através do Fundo Europeu de Desenvolvimento Regional.

o júri

presidente

Prof. Doutor Joaquim Alexandre Mendes de Pinho da Cruz

Professor Auxiliar da Universidade de Aveiro

Prof. Doutor Francisco José Gomes da Silva

Professor Coordenador do Instituto Superior de Engenharia do Porto

Prof. Doutor António Manuel de Bastos Pereira

Professor Associado *c/* Agregação da Universidade de Aveiro

**agradecimentos/
acknowledgements**

Ao meu orientador, Doutor António Manuel de Bastos Pereira pela orientação e apoio dado ao longo deste trabalho.

Ao meu coorientador, Doutor Alfredo Manuel Balacó de Morais pelo *feedback* e esclarecimentos.

Ao Engenheiro Ricardo Beja pelo apoio técnico para realização de ensaios.

Aos meus pais pelo apoio e suporte que sempre recebi deles.

Aos meus amigos e colegas que me ajudaram não só neste trabalho como também ao longo do curso.

palavras-chave

Soldadura por transmissão a laser, compósitos, polímeros, termoplásticos, otimização de parâmetros, poliamida, Nd:YAG, soldadura pulsada.

resumo

Nos últimos anos, a necessidade de construções leves aumentou a procura por polímeros e compósitos, seguindo o princípio de *design* conhecido como “substituição de materiais”. Conseqüentemente, surgiram novos métodos de soldadura como a Soldadura a Laser por Transmissão (*LTW*) para superar as limitações dos convencionais.

O objetivo deste estudo foi encontrar os melhores parâmetros para a soldadura LASER pulsado Nd:YAG de polímeros termoplásticos com compósitos de matriz termoplástica.

O efeito dos parâmetros de soldadura a laser, como potência de pico, duração do impulso, sobreposição, diâmetro do feixe e velocidade, na resistência da soldadura foi investigado. Os resultados obtidos foram usados para inferir a janela do processo, que, por sua vez, serviu como um guia para encontrar os parâmetros ideais.

Durante o procedimento experimental, observou-se que é difícil obter resultados consistentes na soldadura a laser de polímeros dissimilares, mesmo quando são compatíveis. A soldadura a laser de um polímero com um compósito com o mesmo material na matriz é, comparativamente, mais fácil de soldar.

Dos resultados obtidos conclui-se que a resistência de soldadura (N/mm) aumenta com a potência de pico, duração do impulso, sobreposição e diâmetro do laser até um limiar, diminuindo para além deste ponto. Quanto à velocidade, a resistência de soldadura atinge valores mais altos em velocidades baixas, como sugere a literatura.

Não obstante, a eficiência de soldadura mais elevada (95% de eficiência do cordão de soldadura e 35% de eficiência da junta de soldadura) é obtida em potências de pico baixas em combinação com percentagens elevadas de sobreposição.

keywords

Laser transmission welding, composites, polymers, thermoplastics, parameter optimization, polyamide, Nd:YAG, pulsed welding.

abstract

In recent years, the need for lightweight constructions has increased the demand for polymers and composites, following the design principle known as *material substitution*. Consequently, new welding methods such as LTW (Laser Transmission Welding) have emerged to overcome the limitations of conventional ones.

The aim of this study was to find the best parameters for pulsed Nd:YAG LASER welding of thermoplastic polymers to thermoplastic matrix composites. The effect of laser welding parameters such as peak power, pulse width, overlap, beam diameter and speed on weld strength was investigated. The results obtained were used to infer the process window, which in turn served as a guide to find the optimal parameters.

During the experimental procedure, it was observed that it is difficult to achieve consistent results when laser welding dissimilar polymers, even when they are compatible. Laser welding of a polymer to a composite with the same material in the matrix is comparatively easier to weld.

From the results obtained, it can be concluded that weld strength (N/mm) increases with Peak Power, Pulse Width, Overlap and beam diameter up to a threshold, decreasing beyond this point. Regarding scan speed, the weld strength achieves higher values at low welding speeds, as the literature suggests.

Nevertheless, the highest weld efficiency (95% weld bead efficiency and 35% weld joint efficiency) is obtained at low Peak Powers in combination with high overlap percentages.

CONTENTS

List of Figures	v
List of Tables	viii
Acronyms	ix
1 Introduction	1
1.1 Background.....	1
1.1.1 The Past	1
1.1.2 The Present.....	1
1.2 Objectives.....	2
1.3 Contents	2
2 Literature Review	3
2.1 Introduction.....	3
2.2 Process Fundamentals.....	3
2.2.1 Laser Welding Methods	3
2.2.2 Process Variants	4
2.2.3 Joint Configurations.....	5
2.2.4 Laser Systems	5
2.3 Innovative Approaches.....	6
2.3.1 LTW Using Filler Material.....	6
2.3.2 Plasma Activation Technique.....	7
2.3.3 Inter-layer Material	7
2.4 Compositions and pre-welding conditions	8
2.4.1 Colorants	8
2.4.2 Reinforcements	9
2.4.3 Crystallinity and Surface Finish	10
2.4.4 Part Thickness.....	11
2.4.5 Air Gap.....	12
2.5 Nd:YAG laser.....	13
2.5.1 Pulsed Mode.....	13
2.5.2 Weld Types	13
2.5.3 Seam Welding.....	13
2.5.4 Pulse Shaping.....	14
2.5.5 Optimizing Peak Power and Pulse Width.....	14



2.5.6	Pulsed Laser Parameters	15
2.6	LTW Parameters	17
2.6.1	Line Energy	17
2.6.2	Laser Power	18
2.6.3	Welding Speed.....	19
2.6.4	Laser Beam Diameter	19
2.6.5	Clamp Pressure.....	20
2.6.6	Laser Wavelength	20
2.7	Weld Quality.....	22
2.7.1	Weld Strength.....	22
2.7.2	Failure Modes.....	22
2.7.3	Weld Pool Dimensions.....	23
2.8	Material Aspects.....	25
2.8.1	Polymers.....	25
2.8.2	Composites	29
2.8.3	Laser Weldability of Polymers	30
2.8.4	Laser Weldability of Composites	32
2.9	Conclusion.....	34
2.9.1	Summary	34
2.9.2	Literature Gaps.....	34
3	Experimental Procedure.....	35
3.1	Introduction.....	35
3.2	Material Selection	35
3.2.1	TECAMID 66 Natural	36
3.2.2	ERTALON® 6 SA.....	37
3.2.3	ERTALON® 66 GF30.....	38
3.3	Material Characterization.....	39
3.4	Test Pieces for Welding	40
3.4.1	Preparation.....	40
3.4.2	Dimensions	42
3.5	Workstation.....	43
3.5.1	Main Components	44
3.6	Clamping Device	45
3.6.1	Components	45



3.6.2	Configuration.....	46
3.6.3	Pressure Calculation	46
3.7	Optimization Process.....	48
3.7.1	Introduction.....	48
3.7.2	Material Comparison	48
3.7.3	Process Window Definition	48
3.7.4	Optimal Parameters	53
3.8	Lap Shear Tests.....	54
3.9	Diameter Measurement	58
4	Results and Discussion	62
4.1	Material Characterization.....	62
4.2	Material Comparison.....	66
4.3	Process Window Definition	68
4.3.1	Evaluation of Peak Power	68
4.3.2	Evaluation of Pulse Width.....	69
4.3.3	Evaluation of Overlap	70
4.3.4	Evaluation of Laser Beam Diameter.....	71
4.3.5	Evaluation of Scan Speed.....	72
4.4	Optimal Parameters	73
4.5	Global Results.....	74
4.6	Comparison to the Base Material	75
5	Conclusions	76
6	Future Work	77
	References	78
	Appendix A.....	83
A.1	TECAMID 66 Natural Datasheet.....	83
A.2	ERTALON 6 SA Datasheet	84
A.3	ERTALON PA66 GF30 Datasheet	85
	Appendix B.....	86
B.1	Diameter Measurements for PA6N/PA66 GF30	86
	Appendix C.....	89
C.1	Stress-Strain Curves (group H).....	89
C.2	Weld Strength-Strain Curves (group A)	90
C.3	Weld Strength-Strain Curves (group B)	92



C.4	Weld Strength-Strain Curves (group C).....	94
C.5	Weld Strength-Strain Curves (group D)	96
C.6	Weld Strength-Strain Curves (group F)	98
C.7	Weld Strength-Strain Curves (group X).....	100
C.8	Stress-Strain Curves (Best Sample)	103

LIST OF FIGURES

Figure 2.1 - Typical joint configuration for (left) laser butt welding, and (right) through-transmission laser welding (TTLW), [12].	3
Figure 2.2 - Schematics of the basic process types used in TTLW, more specifically (a) Contour welding, (b) Quasi-simultaneous welding, (c) Simultaneous welding and (d) Mask welding [14].	4
Figure 2.3 - Various possible joint configurations for the LTW process, in particular, (a) lap joint, (b) stepped joint, (c) scarf joint, (d) single v-groove joint, (e) butt-joint, (f) corner joint, (g) stepped corner joint, (h) I-beam joint. [15].	5
Figure 2.4 - Schematic illustration of the laser transmission welding process using filler material [13].	6
Figure 2.5 - Principle of the intermediate layer technique [16].	7
Figure 2.6 - Effect of CB content on the absorption coefficient of PA6GF, PA6, and PC [21].	8
Figure 2.7 - Effect of GF reinforcement contents on laser transmittance of PA6 and PA66 at 1.064 μm [22].	9
Figure 2.8- Scattering of light in (a) amorphous polymer, and (b) semi-crystalline polymer [11].	10
Figure 2.9 - Apparent absorption coefficient and total reflection of several unreinforced polymers [24].	10
Figure 2.10 - Effect of part thickness on laser transmittance of unfilled PA6 at 1.064 μm [22].	11
Figure 2.11 - Tensile strength per length with different gaps in contour welding and quasi-simultaneous welding [29].	12
Figure 2.12 - Schematic representation of overlap versus effective penetration depth for various overlap percentage [33].	14
Figure 2.13 - Most common pulse shapes used in pulsed laser welding, such as (a) square, (b) spike, (c) downward ramp [34].	14
Figure 2.14 - Effect on weld dimensions of increasing pulse width and peak power on weld dimensions [33].	15
Figure 2.15- Important parameters of pulsed laser welding [33].	16
Figure 2.16 - Characteristic curve of an LTWed polymer (left) and microtome cuts of welded PP samples (right) [35].	17
Figure 2.17 - Effect of line energy on the lap-shear strength for different power levels [36].	18
Figure 2.18 – Influence of power on weld strength at different welding speeds [37].	18
Figure 2.19 - Lap-shear strength (MPa) with varying scanning speed for amorphous (left) and semi-crystalline (right) polymers [38].	19
Figure 2.20 - Tensile shear strength of lap joints and required energy per unit length as a function of welding speed [5].	19
Figure 2.21 - Weld strength as a function of weld pressure for different power/speed combinations [42].	20
Figure 2.22 - Absorption spectra of different polymer samples with the thickness $d=1.6\text{ mm}$ [12].	21
Figure 2.23 - Comparison between PC and PMMA spectroscopy [43].	21
Figure 2.24 - Influence of wavelength on absorption properties for natural PA [44].	22
Figure 2.25 - Main types of failure modes in LTW, more specifically, (a) interfacial, (b) substrate type-I, (c) substrate type-II, (d) mixed type-I, (e) mixed type-II. [38].	23

Figure 2.26 - a) cross-sectional view of the weld pool, where WW= weld width, DT = depth of penetration (LT), DA = depth of penetration (LA) [28]; b) Top view of the weld pool [45].	23
Figure 2.27 - Principles of the T-type butt joint and the formation of the melt pool within the heat affected zone for LTW [46].	24
Figure 2.28 - Sample with visible bond width and HAZ [38].	24
Figure 2.29 - Variation of the weld strength with weld width [47].	25
Figure 2.30 - Classification of plastics [10].	26
Figure 2.31 - Specific volume versus temperature, upon cooling from the liquid melt, for totally amorphous (curve A), semicrystalline (curve B), and crystalline (curve C) polymers.	27
Figure 2.32 - Temperature behavior of amorphous thermoplastics [10].	28
Figure 2.33 - Temperature behavior of semicrystalline thermoplastics [10].	28
Figure 2.34 - The stress–strain behavior for brittle (curve A), plastic (curve B), and highly elastic (elastomeric) (curve C) polymers [49].	29
Figure 2.35 – Schematic representations of (a) continuous and aligned, (b) discontinuous and aligned, and (c) discontinuous and randomly oriented fiber–reinforced composites [49].	30
Figure 2.36 - Cross-sections of LTWed polymers: similar polymers, material joint - (a), (b); dissimilar polymers, form joint – (c), (d) [12].	31
Figure 2.37 - Laser weldability chart for possible polymer combinations [10].	32
Figure 2.38 - Weld strength as a function of line energy for different laser powers [42].	33
Figure 3.1 - Photograph of the materials used in rod format.	35
Figure 3.2 - Examples of applications of Polyamide 66 Natural [55].	36
Figure 3.3 - Examples of applications of ERTALON® 6 SA [58].	37
Figure 3.4 - Examples of applications of ERTALON® 66 GF30 [61].	38
Figure 3.5 - Specimens used in material characterization tests, adapted from [62].	39
Figure 3.6 - Machined specimens of (a) PA66 GF30, (b) PA66N and (c) PA6N.	39
Figure 3.7 - Photograph of the TECAMID 66 rod (a), of an ERTALON 66 GF30 rod section (b) and of an ERTALON 6 SA rod section (c).	40
Figure 3.8 - (a) Lathing operation to turn the rods into discs and (b) ERTALON 66 GF30 discs.	41
Figure 3.9 – Milling operation of the discs.	41
Figure 3.10 - Photographs of the specimen of (a) PA66 GF30, (b) PA66N and (c) PA6N in their final dimensions.	42
Figure 3.11 – Specimen configuration and final dimensions.	42
Figure 3.12 - SISMA SWA-300 [63].	43
Figure 3.13 - SISMA-SWA 300 working page [64].	44
Figure 3.14 - SISMA SWA 300 console [64].	44
Figure 3.15 – Main components of the clamping device, including (A) two springs, (B) an aluminum base, (C) a shim, (D) two metal plates.	45
Figure 3.16 - Clamping device in its final configuration (a) and positioning of the specimens (b).	46
Figure 3.17 – Force vs. displacement curve obtained through the spring tensile test.	47
Figure 3.18 - Photograph of the welded specimens of Group A.	49
Figure 3.19 - Photograph of the specimens of Group A after the tensile test had been performed.	49
Figure 3.20 - Cylindrical rod before (a) and after (b) being subjected to a uniaxial tensile force 'F' [66].	54
Figure 3.21 - (a) Unstressed body; (b) Body subjected to tensile stress; (c) Body subjected to pure shear forces 'S' acting over surface areas 'A' [66].	56



Figure 3.22 – (a) Universal testing machine Shimadzu AGS-X (10 kN); (b) close-up of the test fixtures.	57
Figure 3.23 - a) Schematic representation of a lap shear test in which flexure of the parts occurs due to bending moments; b) Schematic representation of a lap shear test where shims were added to reduce flexure.	58
Figure 3.24 - Photograph of the welding spot corresponding to the sample N1-2 (a) and of the measuring process (b).	58
Figure 4.1 - Bar chart comparing the Weld Bead Shear Strength and Efficiency of PA6 and PA66N (Group H).....	66
Figure 4.2 - Bar chart comparing the Weld Joint Strength and Efficiency of PA6 and PA66N (Group H).....	67
Figure 4.3 - Effect of Peak Power on Weld Strength (Group A).	68
Figure 4.4 - Effect of Pulse Width on Weld Strength (Group B).....	69
Figure 4.5 - Effect of Overlap on Weld Strength (Group C).	70
Figure 4.6 - Effect of the Laser Beam Diameter on Weld Strength (Group D).	71
Figure 4.7 - Effect of the Scan Speed on Weld Strength (Group F).	72
Figure 4.8 - Bar Graph comparing the weld strength obtained for the samples of the optimal parameters (Group X).	73
Figure 4.9 - Bar chart comparing all the samples welded during the experimental procedure.	74
Figure 4.10 - Average Weld Bead Strength and Efficiency obtained in the sample C3	75
Figure 4.11 - Average Weld Joint Strength and Efficiency obtained in the sample C3	75



LIST OF TABLES

Table 3.1 - Relevant properties of TECAMID 66 Natural [53], [22].	36
Table 3.2 - Relevant properties of ERTALON® 6 SA [22], [56].	37
Table 3.3 - Relevant properties of ERTALON® 66 GF30 [59].	38
Table 3.4 - Technical specifications of SISMA-SWA 300 [63].	43
Table 3.5 – Pressure calculation data.	47
Table 3.6 - Comparison between PA66N and PA6N when welded with PA66 GF30.	48
Table 3.7 - Evaluation of Peak Power.	50
Table 3.8 - Evaluation of Pulse Width.	50
Table 3.9 - Evaluation of Overlap.	51
Table 3.10 - Evaluation of Laser Beam Diameter.	51
Table 3.11 - Evaluation of Scan Speed.	52
Table 3.12 - Combination of the optimal parameter ranges.	53
Table 3.13 - Measurements of the spot diameter generated in the laser absorbing part for the PA66N/PA66 GF30 pair.	59
Table 4.1 - Summary of the tensile test results for PA66N.	63
Table 4.2 - Summary of the tensile test results for PA6N.	64
Table 4.3 - Summary of the tensile test results for PA66 GF30.	65
Table 4.4 - Parameter set corresponding to the sample C3.	74



ACRONYMS

Al	Aluminum
BR	Polybutadiene rubber
CB	Carbon Black
CF	Carbon-Fiber Reinforced
DA	Penetration in the absorbing polymer part
DT	Penetration in the transparent polymer part
GF	Glass-Fiber Reinforced
HAZ	Heat Affected Zone
IR-light	Infrared light
LA	Laser Absorbent
LSS	Lap Shear Strength
LT	Laser Transparent
LTW	Laser Transmission Welding
Nd:YAG	Neodymium-doped yttrium aluminum garnet
NIR	Near Infrared
PA6	Polyamide 6
PA66	Polyamide 66
PBT	Polybutylene terephthalate
PC	Polycarbonate
PE	Polyethylene
PEEK	Polyether ether ketone
PE-LD	Low-density polyethylene
PET	Polyethylene terephthalate
PMMA	Polymethyl methacrylate
POM	Polyoxymethylene
PP	Polypropylene
PPS	Polyphenylene sulfide
PS	Polystyrene
PUR	Polyurethane
PVC	Polyvinyl chloride
RSM	Response Surface Methodology
SBR	Styrene-butadiene rubber
TTLW	Through-transmission laser welding
TWIST	Transmission Laser Welding using Incremental Scanning Technique
WW	Weld width



1 INTRODUCTION

1.1 BACKGROUND

1.1.1 The Past

In the early half of the 20th century, during World War II, shortages in metals such as steel urged scientists to research alternative synthetic materials [1]. Polymers such as Nylon and PTFE became widely used to make items such as ropes, tents, parachutes and as coating [1].

At the end of World War II, polymers that were restricted for military use became available for peacetime use. This resulted in a so-called polymer revolution [1].

1.1.2 The Present

Presently, lightweight constructions are indispensable in the automotive and aviation industries due to the demanding legislation requirements on safety, fuel efficiency, and emission of carbon dioxide [2]. One way to meet these requirements without losing performance, is through material substitution [2]. This design principle describes the process of putting the right material with the right properties at the right place [2].

Due to their simultaneous availability of excellent properties such as low weight and high stiffness, fiber-reinforced polymers are widely used in these industries [3]. However, in order to manufacture structural elements, often, many components have to be joined together into complex assemblies [4]. As such, welding between dissimilar materials such as polymer to composites is commonplace, even if it is still limited in some cases due to poor compatibility between materials [5], [6].

Conventional welding methods such as adhesive bonding, mechanical joining, friction stir welding, microwave welding, and hot plate welding are currently used in a variety of applications, however, they possess clear disadvantages such as poor joining quality and low efficiency [6]. Consequently, laser transmission welding has emerged as one of most suitable welding techniques among polymers, and their combinations with composites and even metals [1], [6].



1.2 OBJECTIVES

The aim of this study is to find the best parameters for pulsed Nd:YAG LASER welding of thermoplastic polymers to thermoplastic matrix composites.

1.3 CONTENTS

This document is organized into six chapters. Chapter 1 aims to introduce the main topics of this dissertation. It starts by providing some background information regarding polymers, composites and laser welding, which is followed by the objectives of the document.

Chapter 2 consists of a literature review on laser welding, where the process fundamentals, current state of the art, and material aspects are presented.

Chapter 3 describes the methodology followed in order to achieve the set goals. This included material selection and characterization, test piece preparation, clamping device chosen, workstation used, welding parameters analyzed, and lap shear tests that were performed.

Chapter 4 is dedicated to the analysis of the results and subsequent discussion. This is followed by the conclusion, in Chapter 5 and finally, in Chapter 6, some recommendations for future work are made.

2 LITERATURE REVIEW

2.1 INTRODUCTION

Laser welding is a relatively new polymer welding technique that shows several advantages over other conventional methods such as: adhesive bonding, hot plate bonding, ultrasonic welding and vibration welding [7]. Upon comparison, laser welding shows its superiority due to being highly accurate, allowing high joining speeds, affecting materials mostly locally and allowing dissimilar materials to be joined [8].

Even though, the first attempt at joining polymers using a laser beam dates back to the 70s, it was only in the 90s that this method started being thoroughly explored [9]. Currently, this welding technique has a wide range of applications in fields such as electronics, medical technology, automotive, aerospace and ship building industries [8].

2.2 PROCESS FUNDAMENTALS

2.2.1 Laser Welding Methods

There are two major types of polymer laser welding (Figure 2.1): butt-joint (direct) welding and through-transmission laser welding (TTLW) [10]. The latter is the most common and consists of welding a laser-transparent specimen (on top) to a laser-absorbent one (at the bottom), in a lap joint configuration [10]. Due to transparency, the laser beam reaches the interface between the parts, and is then absorbed by the opaque specimen [10]. When the temperature is high enough, a melt pool forms at the interface, joining both parts due to heat conduction [10].

Butt-joint (direct) welding, on the other hand, consists of joining two polymer parts which are placed side by side [7]. The laser beam (tangent to the joint interface) then fuses together the parts at the interface to form the joint [7], [11].

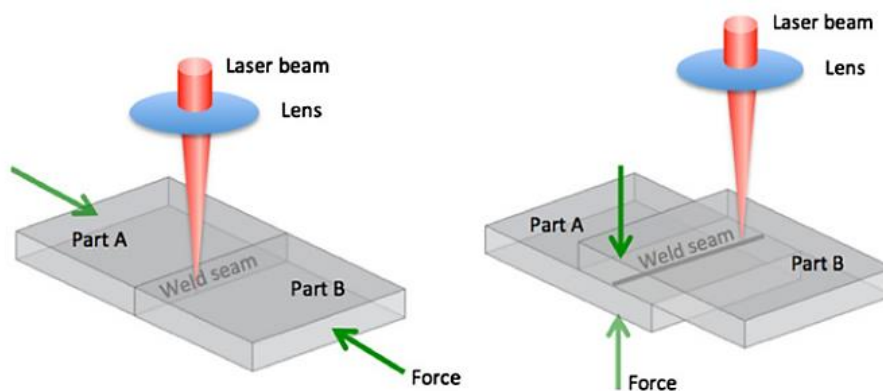


Figure 2.1 - Typical joint configuration for (left) laser butt welding, and (right) through-transmission laser welding (TTLW), [12].

2.2.2 Process Variants

There are four common process types in TTLW [10]. These are: contour, quasi-simultaneous, simultaneous, and mask welding [10]. These can be described as follows:

- **Contour welding** (Figure 2.2-a): a single focused laser beam is moved along the joint path on the work piece [10]. This variant is the most common [13] and will be applied during the experimental procedure in this work.
- **Quasi-simultaneous welding** (Figure 2.2-b): based on a single focused laser beam which is moves several times along the joint geometry at high speed [10].
- **Simultaneous welding** (Figure 2.2-c): the entire joint path is irradiated by laser radiation at the same time and will generate the laser-welded joint without moving the part or the laser beam during processing [10].
- **Mask welding** (Figure 2.2-d): the desired joint contour will be generated by a metallic mask which is positioned above the workpiece [10]. To weld the work piece the mask is illuminated by line-shaped laser radiation that will be moved along the mask [10].

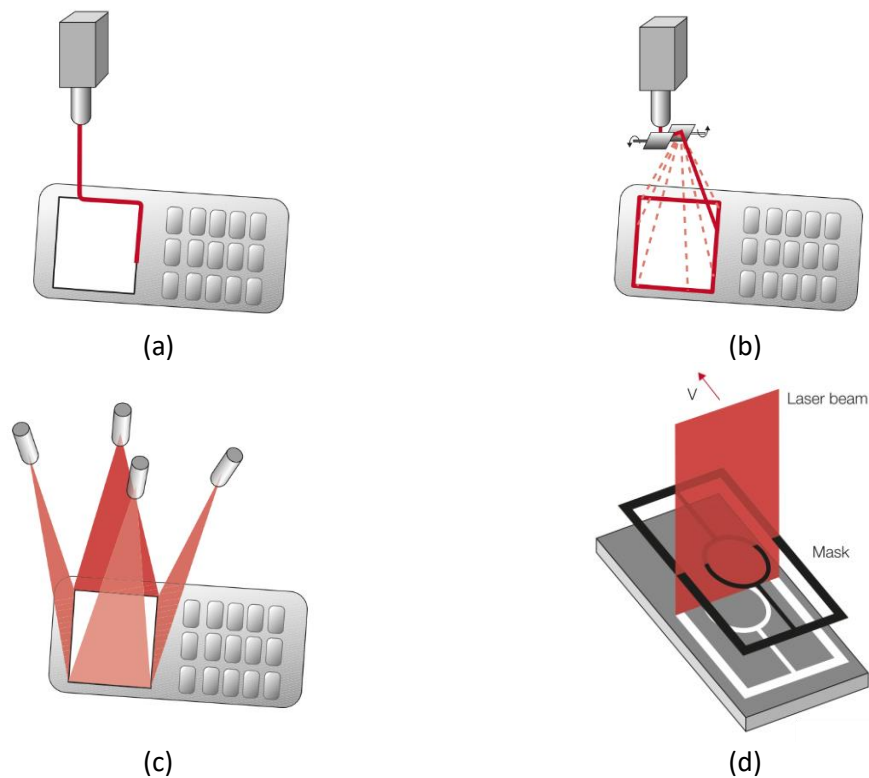


Figure 2.2 - Schematics of the basic process types used in TTLW, more specifically (a) Contour welding, (b) Quasi-simultaneous welding, (c) Simultaneous welding and (d) Mask welding [14].

2.2.3 Joint Configurations

Figure 2.3 showcases the different joint configurations possible using LTW (Laser Transmission Welding). The most common one is the lap joint configuration followed by the T-joint configuration [11]. A butt joint, on the other hand, is very difficult to accomplish as it requires high penetration depth [11].

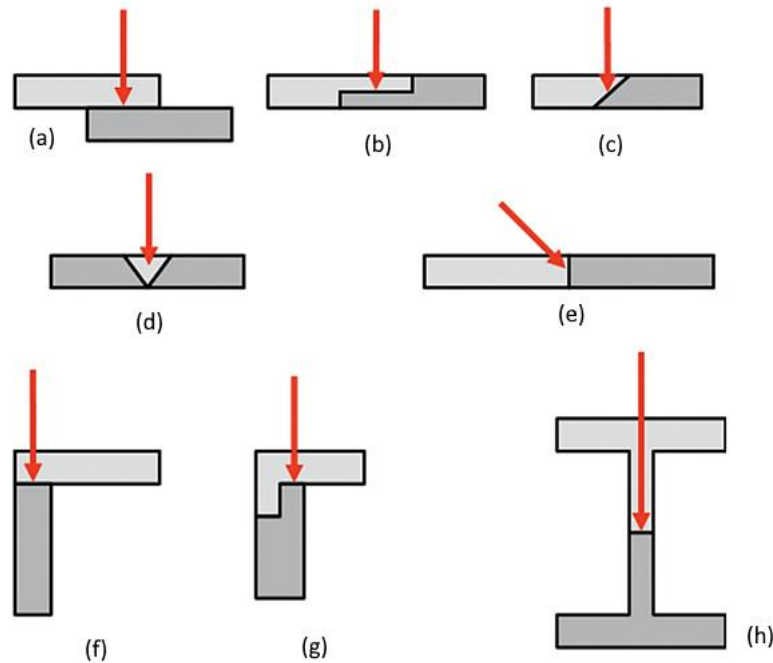


Figure 2.3 - Various possible joint configurations for the LTW process, in particular, (a) lap joint, (b) stepped joint, (c) scarf joint, (d) single v-groove joint, (e) butt-joint, (f) corner joint, (g) stepped corner joint, (h) I-beam joint. [15].

2.2.4 Laser Systems

The main types of laser used for transmission laser welding are diode, Nd:YAG and fiber in the wavelength range 800-1100 nm [15]. However, currently, laser sources with wavelengths up to 2000 nm are available [10]. These laser systems are characterized as follows:

- **Nd:YAG lasers:** solid-state lasers with wavelength of 1064 nm which are known for their low process reliability, short laser working life, relatively high maintenance costs and low plug efficiency (3%), but high beam quality¹ [10], [15].
- **Diode lasers:** operating at wavelengths between 800-2000 nm, these are one of the most important laser sources for industrial applications, as they possess excellent plug efficiency (40%) and reliability [10]. The main disadvantage of this type of laser system is their comparatively much lower beam quality [10].
- **Fiber lasers:** are the latest development of laser sources for material processing applications and are characterized for their excellent beam quality, reliability and plug

¹ Beam quality is the ability to focus the beam to a small spot size with a high energy density [15].

efficiency (30%) [10]. In LTW of polymers they typically emit radiation in the range of 1000-2100 nm [15].

- **CO₂ lasers:** these gas lasers working at 10.6 μm are not common laser sources for laser plastic welding, but are widely used in industry for cutting plastics and for some special applications like welding of thin thermoplastic films [10], [15]. They have a plug efficiency of only 10%, but possess a high beam quality [15].

2.3 INNOVATIVE APPROACHES

Besides the main LTW variants mentioned above, there are, presently, many other innovative techniques such as hybrid welding, clear welding, absorber-free welding, TWIST (Transmission Laser Welding using Incremental Scanning Technique), GLOBO welding system, etc. [7] which are beyond the scope of this review. Therefore, only LTW techniques relevant to welding of composites and dissimilar materials, such as LTW using: filler material, plasma activation technique and inter-layer material, are mentioned.

2.3.1 LTW Using Filler Material

This innovative approach provides a way to combine two opaque joining partners as the upper joining partner does not have to be transparent to the laser radiation [13]. In this case, the filler material acts as the transmissive part, being provided as an endless synthetic monofilament of the same material as the matrix of the joining partners [13], as shown in Figure 2.4.

Berger et al. [13] attempted to weld PA CF42 (Carbon-Fiber Reinforced Polyamide wt.% 42) organic sheets using natural PA6 (Polyamide 6) as filler material. Using this technique, it was possible to reach a weld factor of 0.89 relative to unreinforced PA 6 [13].

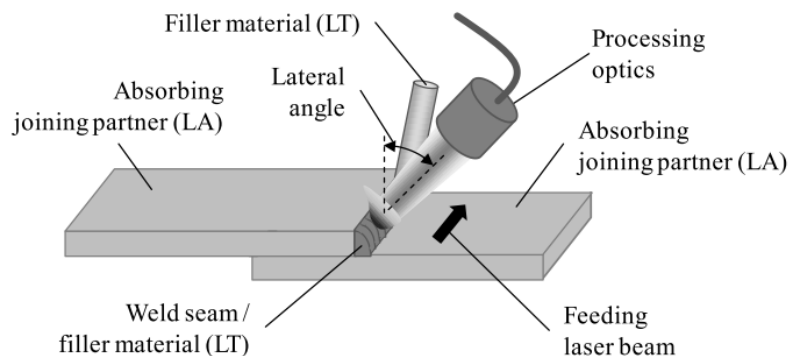


Figure 2.4 - Schematic illustration of the laser transmission welding process using filler material [13].

2.3.2 Plasma Activation Technique

The pre-treatment of surfaces to be joined using plasma is an innovative approach which, in combination with LTW, opens up new possibilities for welding incompatible polymers [16].

Liu et al. [6] preheated PE (Polyethylene) and POM (Polyoxymethylene) using plasma in order to enhance their weld strength, as these polymers are highly incompatible. Using this method, these materials were successfully welded by LTW, due to the formation of mechanical micro-interlocking achieved through surface roughness as well as the generation of homogeneous bubbles [6].

2.3.3 Inter-layer Material

In this process variant, an absorbing layer is introduced at the interface between the joining parts, Figure 2.5 [16]. Both test pieces are joined by heat conduction as the inter-layer melts due to the absorption of radiation [16]. Using this method with a proper choice of the film properties, it is possible to achieve weld strengths of 80% relative to conventional laser welding [16].

Wang et al. [17] used a PC (Polycarbonate) film as intermediate material to enhance weld strength in LTW of PMMA (Polymethyl methacrylate) and PBT (Polybutylene terephthalate). The authors observed that weld strength of specimens with PC film is up to four times stronger than the weld strength without PC film [17].

Hopmann et al. [16] demonstrated that LTW of PP (Polypropylene) and PA6 is possible using multilayer and monolayer films with an adhesive agent. Moreover, results show that thicker films lead to a significant reduction of the achievable weld strengths [16].

Liu et al. [18] applied the magnetron sputtering technology to weld PVC (Polyvinyl chloride) with PA66 (Polyamide 66), using a 20 μm -thick aluminum film. Using this technology, it was possible to successfully weld two incompatible polymers, reaching a maximum joining strength of 4 MPa [18].

Liu et al. [19] also cold sprayed a 20 μm -thick aluminum film on PA66-GF (Glass-Fiber Reinforced Polyamide 66) in order to laser weld it to PC. Using this technique, a maximum tensile strength of 4 MPa was, again, reached [19]. It was concluded that the chemical bonding between Al (Aluminum) and PC is the main reason for the successful weld [19].

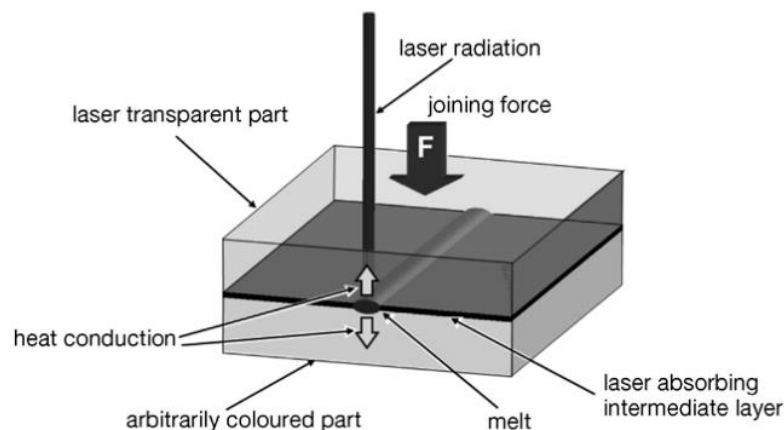


Figure 2.5 - Principle of the intermediate layer technique [16].

2.4 COMPOSITIONS AND PRE-WELDING CONDITIONS

The laser transmission and absorption within a polymer depend mainly on the type and proportion of additives, present in the polymer matrix [11]. The presence of other constituents, like reinforcements, also affects laser transmissivity due to scattering effects [11]. In the following section, common additives used to change polymer properties will be discussed.

2.4.1 Colorants

Natural thermoplastic polymers have low absorption within the NIR (Near Infrared) spectral range from 800 to 1200 nm [10]. In order to successfully weld polymers using the LTW technique, additives, such as colorants, have to be mixed with the resin to increase the absorption of NIR radiation [10].

Colorants can be divided into pigments and dyes [20]. Pigments, unlike dyes, dissolve into polymers and are generally preferred for the coloration of thermoplastics due to superior fastness properties, heat stability and migration resistance [20]. These can be further classified into organic and inorganic [20]. Organic pigments have greater transmission, when compared to inorganic ones such as titanium dioxide and carbon black which are highly light scattering [20]. These are the most widely used inorganic color pigments for manufacturing white and black opaque polymer parts, respectively [11].

Chen et al. [21] described the total laser energy attenuation in scattering polymers with and without carbon black (CB). They observed a linear relationship between the absorption coefficient and the carbon black concentration for PA6, PA6GF, and PC, Figure 2.6 [21].

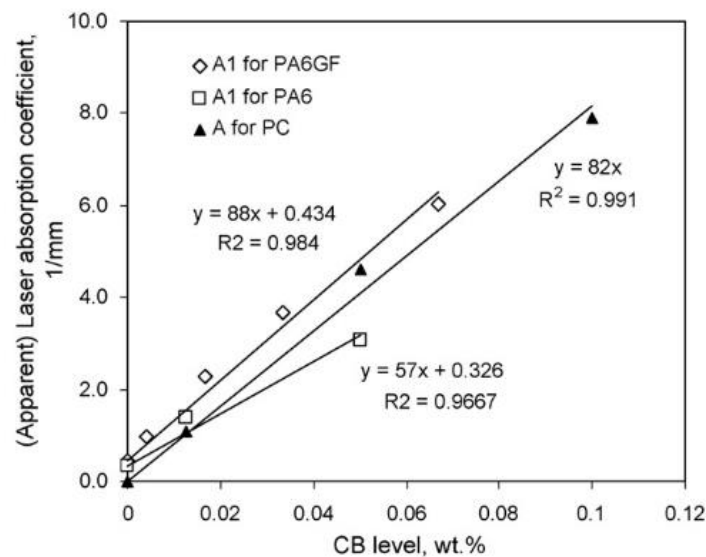


Figure 2.6 - Effect of CB content on the absorption coefficient of PA6GF, PA6, and PC [21].

2.4.2 Reinforcements

Glass fibers (GF) and carbon fibers (CF) are the most common used reinforcements in polymers [11]. Reinforcements are used to enhance the mechanical properties of polymers, however, they also affect their optical properties [11].

Fiber reinforced polymers have been successfully welded as laser the laser transparent partner using LTW [13]. However, carbon fibers are not suitable to reinforce LT partner due to their absorption properties [13].

Adding glass fiber reinforcements to a polymer increases scattering which, in turn, decreases its transmittance [3].

Kagan et al. [22] evaluated the effect of specific nylon composition factors, such as fiber glass, etc. on the NIR transmission characteristics. For short GF reinforced PA6, results show that transmittance decreases with increasing GF content, Figure 2.7 [22]. In this case, the authors found that scattering is responsible, as mentioned previously.

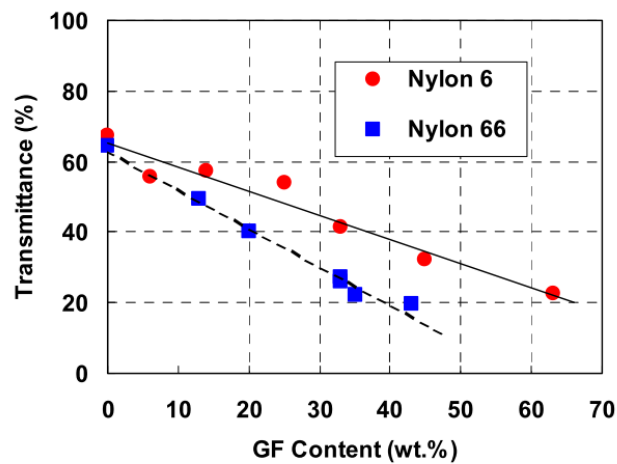


Figure 2.7 - Effect of GF reinforcement contents on laser transmittance of PA6 and PA66 at 1.064 μm [22].

2.4.3 Crystallinity and Surface Finish

Semi-crystalline polymers tend to scatter light to a larger extent than amorphous polymers due to the co-existence of the amorphous and crystalline phases, Figure 2.8 [23]. Scattering produces a longer laser path length, leading to higher absorption [11].

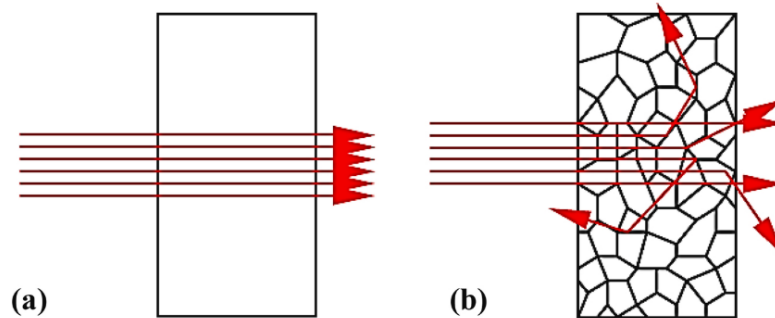


Figure 2.8- Scattering of light in (a) amorphous polymer, and (b) semi-crystalline polymer [11].

Semi-crystalline polymers such as PA6, PA66, PP and PE, show higher values of absorption when compared to amorphous polymers like PC, due to the presence of crystalline structure, Figure 2.9 [24]. Furthermore, PA66 has lower transmittance when compared to PA6, due to higher level of crystallinity in PA66 [11].

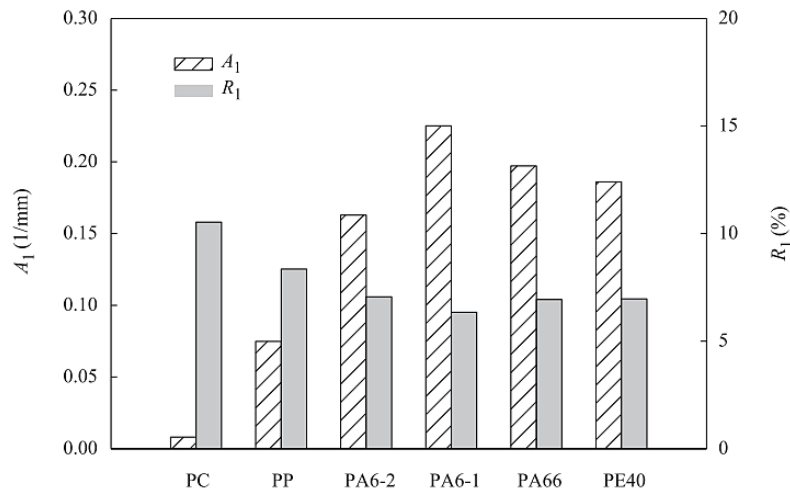


Figure 2.9 - Apparent absorption coefficient and total reflection of several unreinforced polymers [24].

The light reflection and scattering are found to be extremely dependent on the sample surface finish [11]. Wang et al. [25] investigated the optical properties of PC among other polymers and concluded that scattering increases with increasing surface roughness.

2.4.4 Part Thickness

Part thickness is not a major concern for laser transmission in amorphous polymers [11]. Rhew et al. [26] measured the effects of thickness for PC. They concluded that the effect of thickness on transmittance or reflectance for PC is negligible [26].

On the other hand, for semi-crystalline polymers, laser transmission is dependent on part thickness, due to the presence of various phases, which produce more scattering as the level of interactions between the laser beam and the phase boundaries increase [11]. The transmissivity of natural PA6 decreases from 81 % to 70 % when increasing the part thickness from 1 mm to 3 mm [5]. Moreover, Kagan et al. [22] observed that the transmittance decreases with increasing thickness for unfilled PA6, Figure 2.10.

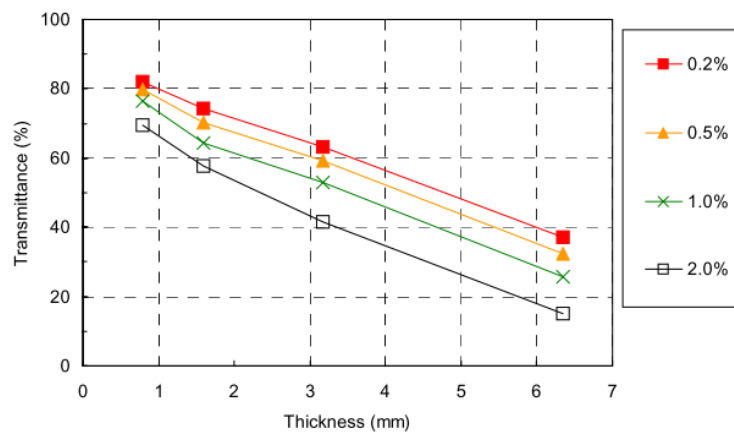


Figure 2.10 - Effect of part thickness on laser transmittance of unfilled PA6 at 1.064 μm [22].

2.4.5 Air Gap

The LTW process benefits from the non-existence of gaps between the parts [27]. If the gap is too large, no heat transfer will occur [27]. Consequently, weld strength decreases with an increase in the part gap [28].

Jansson et al. [29], investigated the effect of air gap in the weld strength. The results showed that tensile strength decreases considerably when increasing part gap from 0 mm to 0.12 mm, Figure 2.11 [29].

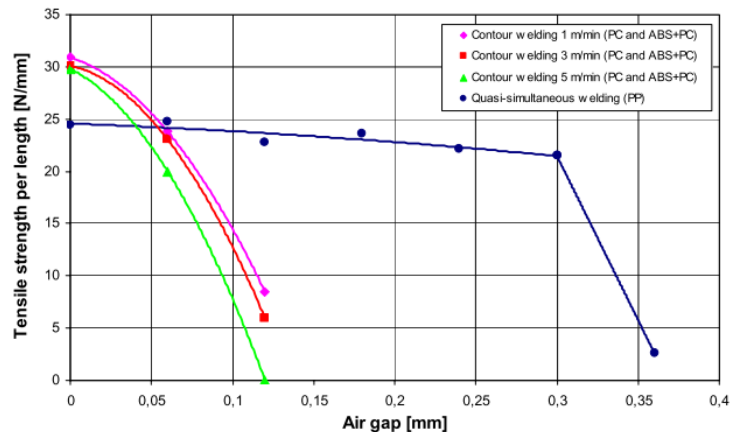


Figure 2.11 - Tensile strength per length with different gaps in contour welding and quasi-simultaneous welding [29].

Van de Ven et al. [30] assessed the influence of part gap for PVC samples welded in a T-joint geometry. The weld strength was found to reduce from 16.1 MPa to 10 MPa when increasing the part gap from 12.7 μm to 25.4 μm [30].

The presence of gaps in LTW using the contour method is a bigger concern, relative to other methods, because the process relies on thermal contact conduction between the absorptive part and the transmissive part [30].

Russek et al. [31] compared the gap bridging capability for contour and simultaneous welding. The gap bridge for simultaneous welding was consistently higher (150 μm) than for contour welding, which varied depending on the polymer (PA: 50 μm ; PC: 100 μm ; PP: 50 μm) [31].



2.5 ND:YAG LASER

The Nd:YAG laser is a versatile, robust and compact laser source used in materials processing [32]. The possibility to transmit the laser beam through optical fibers, is one of the features that contributed to its success [32].

There are two types of Nd:YAG laser welders: continuous wave and pulsed [33]. The former uses average power and remains on continuously until stopped, while the pulsed mode creates welds through individual pulses, where the peak power produced is greater than its average power [21,22]. This allows the pulsed laser to use less energy to create the weld, with a smaller heat affected zone [33].

2.5.1 Pulsed Mode

The pulsed mode is commonly used for drilling, cutting and marking, due to the high peak powers they generate, but can also be used for welding [32]. This mode allows the laser to transmit a burst of energy for a brief length of time (milliseconds), which can reach peak pulse powers 30 times greater than the maximum average power levels [32].

2.5.2 Weld Types

A weld can be created either as an individual spot or a seam weld [34]. With pulsed lasers a seam weld is created by a series of overlapping spot welds, whereas, or a continuous weld the laser remains on for the duration of the seam [34]. As a consequence, pulsed laser has unrivalled spot welding performance and minimal heat input seam welding [33].

2.5.3 Seam Welding

Seam welding involves placing a series of spot welds on a part with a specific physical separation [34]. The weld spot overlap percentage is defined by the percentage of the previous spot that is covered by the subsequent one [34]. For hermetic or seam seal welding, this is typically 80-90%, while for strength-only welds, about 60-70 percent is more common [34]. The spot overlap percentage is a function of speed, pulse repetition rate and focused spot diameter, and is given by Equation 2.1 [34].

$$OL(\%) = \left(1 - \frac{v}{\varphi * f}\right) * 100$$

Equation 2.1

The effective seam penetration is a function of the weld spot overlap. Increasing overlap percentage provides a penetration closer to the maximum penetration of the spot, Figure 2.12 [34].

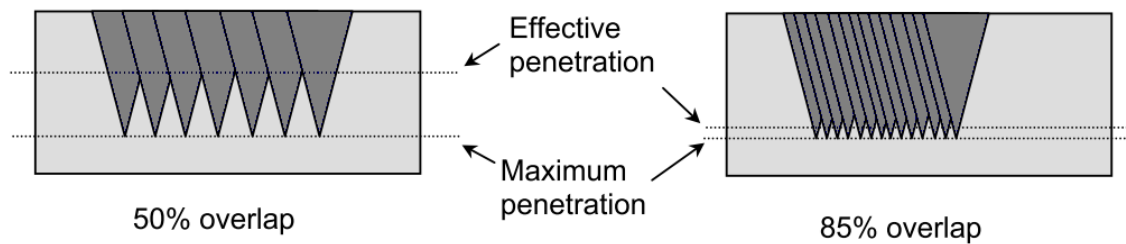


Figure 2.12 - Schematic representation of overlap versus effective penetration depth for various overlap percentage [33].

2.5.4 Pulse Shaping

Most pulsed welding applications use a simple square pulse shape, Figure 2.13-a [34]. However, there are situations in which the use of programmed pulse shaping can enhance welding [34]. One of these is a spike pulse (Figure 2.13-b), which is used to overcome highly reflective materials such as copper and aluminum [33]. Another common pulse is the annealing one (Figure 2.13-c), used to minimize the thermal cycling experienced by the part during welding for materials susceptible to cracking [33], as well as, to reduce weld porosity, or to improve the weld's visual appearance [34].

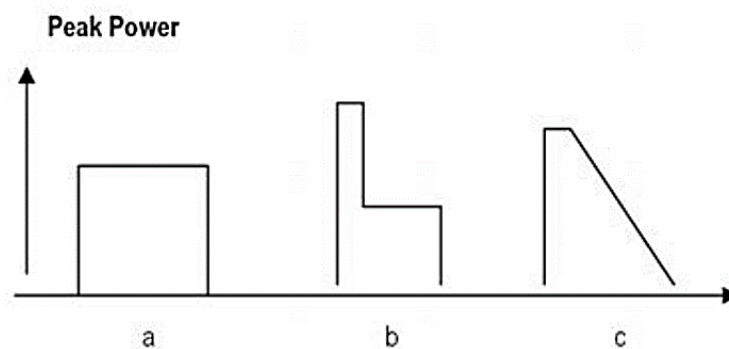


Figure 2.13 - Most common pulse shapes used in pulsed laser welding, such as (a) square, (b) spike, (c) downward ramp [34].

2.5.5 Optimizing Peak Power and Pulse Width

For pulsed welding, the peak power and pulse width are the key parameters to optimize [34]. The peak power is the main parameter for the weld, and is used to control penetration, while pulse width is a fine-tuning parameter that is used to adjust to penetration and weld width [34], Figure 2.14.

Welds made with high peak powers exhibit narrow deep welds that exert a high thermal cycle on the weld material [34]. To increase weld width, reduce the thermal cycling, and minimize depth variation, the pulse width can be increased to introduce a more conduction-based welding mechanism [34].

Another important parameter is the pulse repetition rate or pulse frequency which controls the heat into the part and thermal heat cycle for a seam weld [34].

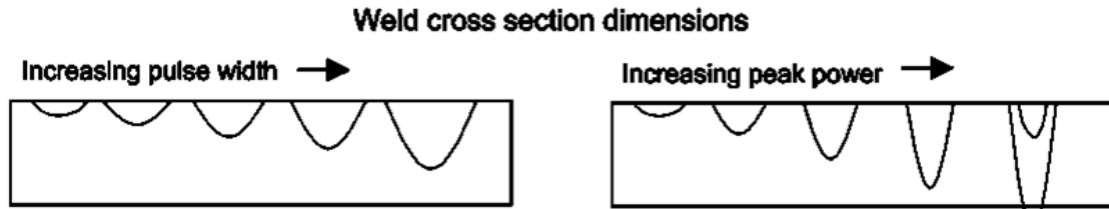


Figure 2.14 - Effect on weld dimensions of increasing pulse width and peak power on weld dimensions [33].

2.5.6 Pulsed Laser Parameters

The weld created by each pulse is determined by the peak power density and duration of that pulse [33]. The number of pulses per second, pulse overlap, and the welding speed additionally defines a seam weld [33]. These laser parameters are defined as follows, Figure 2.15 [33]:

- **Peak power** (P_{peak}): this is a direct parameter that can be selected on the laser. It controls the maximum power of each pulse and is expressed in Watts (W).
- **Pulse width** (t_{pulse}): the pulse width is the duration of the laser pulse in milliseconds (ms).
- **Pulse energy** (E_{pulse}): for a square-shaped pulse, the pulse energy is the energy contained within a pulse and is product of peak power and pulse width, as shown in Equation 2.2.

$$E_{pulse} = P_{peak} * t_{pulse} \quad [J] \quad \text{Equation 2.2}$$

- **Pulse repetition rate** (f): the pulse repetition rate equates to the number of flash lamp pulses per second in Hertz (Hz).
- **Average power** (P_{avg}): this applies when more than one pulse is used for welding. It represents the power averaged over the period of the pulse, and is the product of the pulse energy and the pulse repetition rate (frequency), Equation 2.3.

$$P_{avg} = E_{pulse} * f \quad [W] \quad \text{Equation 2.3}$$

- **Peak Power density** ($P_{peak,d}$): the peak power density is the concentration of the power at the part, and is determined by dividing the peak power by the focus spot size area (A_f) (Equation 2.4).

$$P_{peak,d} = \frac{P_{peak}}{A_f} \quad [W/cm^2] \quad \text{Equation 2.4}$$

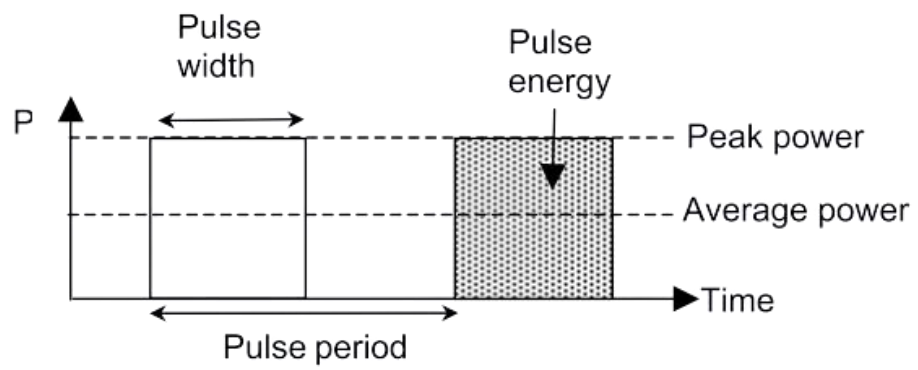


Figure 2.15- Important parameters of pulsed laser welding [33].

2.6 LTW PARAMETERS

2.6.1 Line Energy

The energy input per unit length, also known as line energy (E_L), depends on laser power and travel speed (v), for a constant beam spot area (Equation 2.5), [28].

$$E_L = \frac{P_{avg}}{v} \quad [J/mm] \quad \text{Equation 2.5}$$

A “characteristic curve” of strength versus line energy is commonly used to visualize process behavior and determine the process window location, Figure 2.16 [35]. At low levels of line energy (Figure 2.16 - 1), only light adhesion occurs [35]. From that point on, weld strength increases with line energy until an optimum value (Figure 2.16 - 2), beyond which, the material begins to decompose (Figure 2.16 - 3,4) [35].

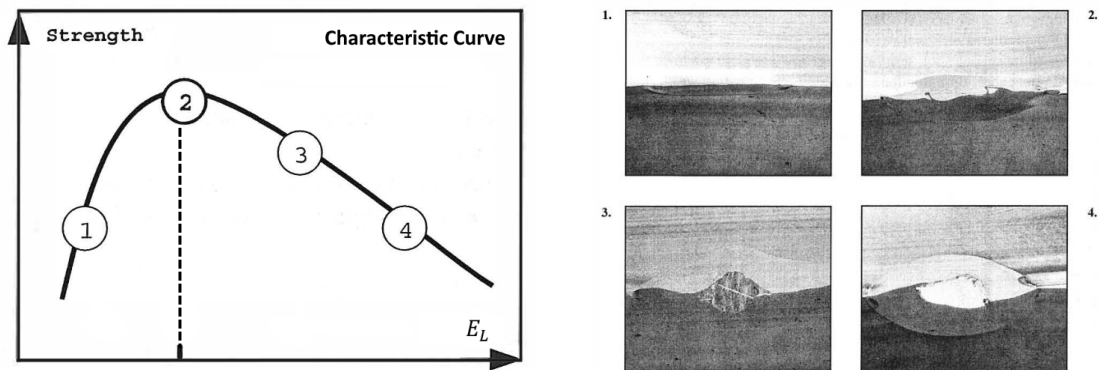


Figure 2.16 - Characteristic curve of an LTWed polymer (left) and microtome cuts of welded PP samples (right) [35].

Acherjee et al. [36] investigated the effects of process parameters on the lap-shear strength for LTW of acrylic using a diode laser system. The results show that, for each power level, there is a threshold line energy value at which the lap-shear strength reaches maximum, Figure 2.17 [36]. Furthermore, the threshold line energy and maximum weld strength values increase with the power [36].

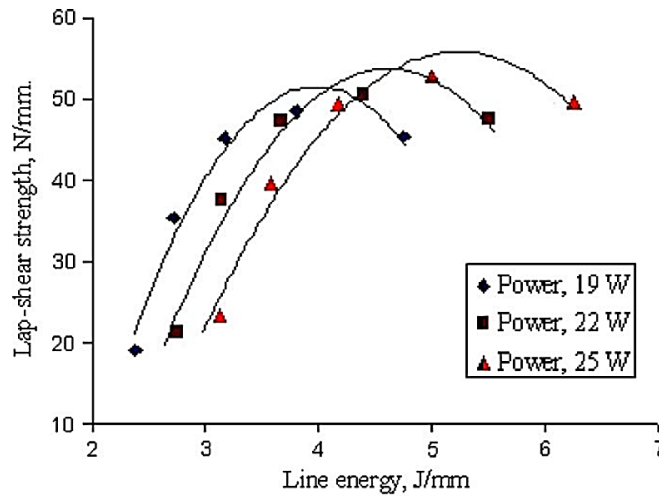


Figure 2.17 - Effect of line energy on the lap-shear strength for different power levels [36].

2.6.2 Laser Power

Increasing laser power causes more base material to melt due to increased laser intensity at the weld interface, resulting in a wider weld seam and thereby higher weld strength [28].

Acherjee et al. [37] investigated the effect of several laser welding parameters on weld strength using RSM (Response Surface Methodology). Regarding laser power, it was observed that weld strength increases with laser power up to a certain level, beyond which it begins to decline, similar to line energy [37]. This can be caused by a lack of fusion at low power levels and material degradation at high power levels [28], [37].

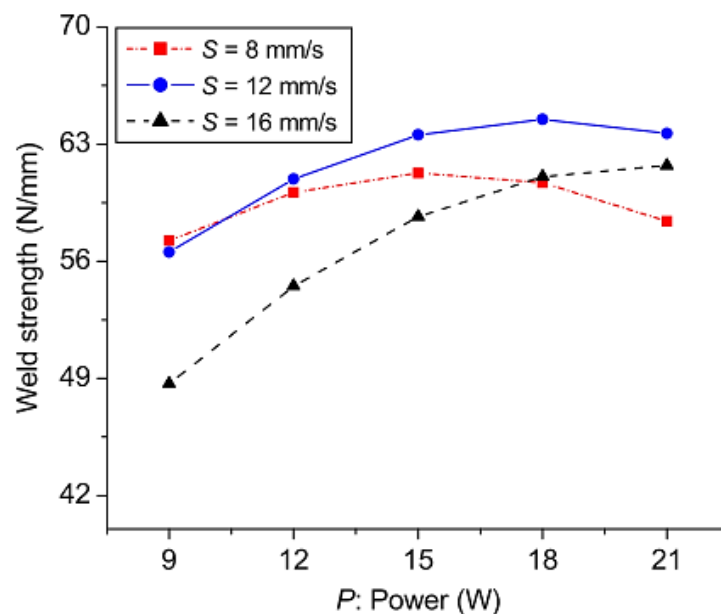


Figure 2.18 – Influence of power on weld strength at different welding speeds [37].

2.6.3 Welding Speed

Maximum weld strength is achieved at low welding speeds [28]. Amanat et al. [38] attempted to determine the influence of scan speed along with other parameters on the lap-joint strength of PEEK (Polyether ether ketone) joined using LTW. The authors observed that the mean lap-shear strength increased with a reduction in the scan speed, Figure 2.19 [38].

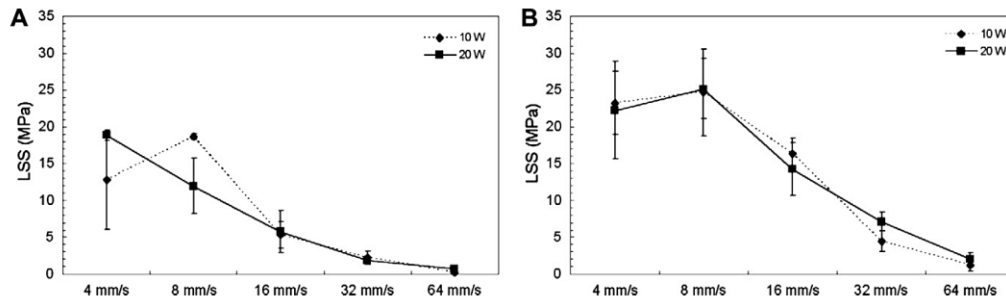


Figure 2.19 - Lap-shear strength (MPa) with varying scanning speed for amorphous (left) and semi-crystalline (right) polymers [38].

Berger et al. [2] observed that the maximum seam strength of 432 N/cm of the lap joints is achieved using the lowest investigated feeding rate of 5 mm/s, Figure 2.20.

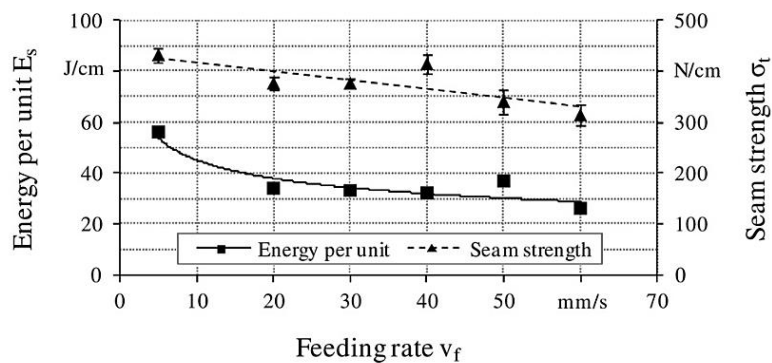


Figure 2.20 - Tensile shear strength of lap joints and required energy per unit length as a function of welding speed [5].

2.6.4 Laser Beam Diameter

Laser beam diameter is the parameter that is used to vary the beam spot area, which governs the power density at the irradiation region [28].

Acherjee et al. [39] varied the beam spot area by changing the focal distance to the beam and noticed a proportional increase in weld strength with this distance, up to 9 mm; beyond this point, weld strength starts to decrease, as the lower power density results in lack of fusion [39].

Jansson et al. [40] investigated diode laser welding of polymers used in electronic devices. The results show that an increase in the weld area of 40% leads to an increase in the maximum weld strength of about 20% [40].

2.6.5 Clamp Pressure

In order to achieve a good weld, among other factors, there must be good enough contact with the melt for the transparent material to be heated by conduction [41]. This can be achieved by applying clamp pressure to the polymer parts [41]. Clamp pressure in the range of 0.5–2.5 MPa is sufficient to ensure good contact at weld interface during welding of soft or hard plastic parts [28].

Prabhakaran et al. [42] studied the effect of contour laser welding parameters on T-joint weld strength and meltdown of PA6 GF30. For the range of weld pressures studied [0.7 MPa to 4.5 MPa], weld strength decreased with increasing weld pressure, Figure 2.21 [42].

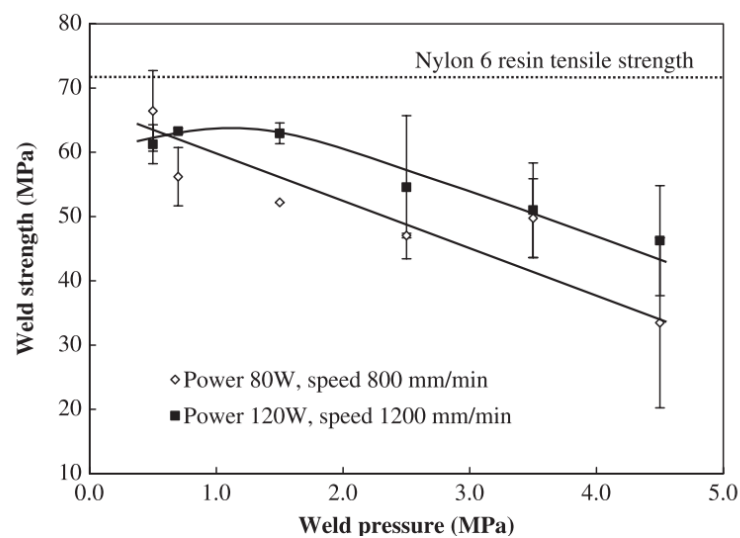


Figure 2.21 - Weld strength as a function of weld pressure for different power/speed combinations [42].

2.6.6 Laser Wavelength

The optical properties of polymers, depend strongly on the laser wavelength [28], as shown in Figure 2.22.

Mingareev et al. [12] calculated laser light absorption in the spectral range $\lambda=0.5\text{--}2.5\ \mu\text{m}$, from measured transmission and reflection of polymer samples. All the investigated polymers showed a higher absorption around $\lambda=2\ \mu\text{m}$ compared to the absorption in the wavelength range $\lambda=0.8\text{--}1\ \mu\text{m}$, where the most common diode and fiber laser systems operate, Figure 2.22 [12]. This opens new opportunities for laser welding without adding any IR-light (Infrared light) absorbers, known as absorber-free welding [12].

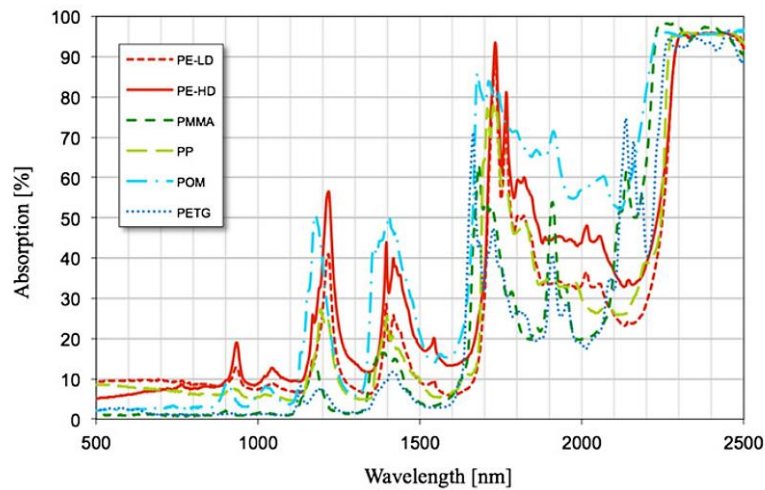


Figure 2.22 - Absorption spectra of different polymer samples with the thickness $d=1.6$ mm [12].

Oliveira et al. [43], conducted NIR spectroscopy to two amorphous materials: PC and PMMA. This study showed a transparency of nearly 90% in all NIR spectra (Figure 2.23), which allowed the authors to conclude that these two materials do not have the capability to absorb laser light in the NIR range [43].

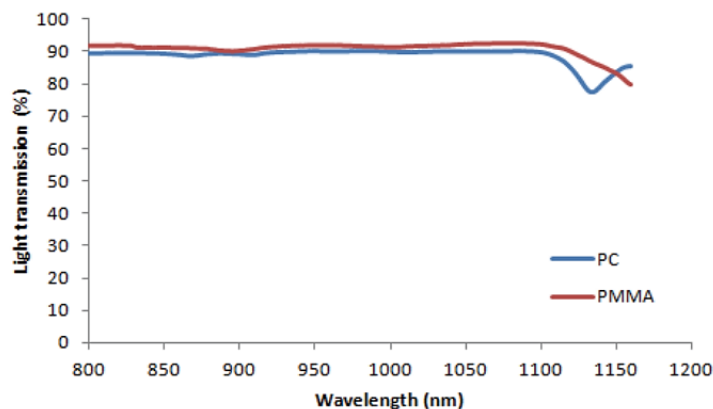


Figure 2.23 - Comparison between PC and PMMA spectroscopy [43].

Kagan et al. [44] evaluated the influence of a wide range of the infrared wavelengths on the optical properties of welded thermoplastics. Over the near-infrared range of interest for diode and Nd:YAG lasers (from 800 to 1100 nm) a maximum of 20% of the laser energy was absorbed by uncolored (natural state) PA, Figure 2.24 [44]. Low absorption, however, does not guarantee high transmission, as a considerable amount of scattering of laser energy occurs in crystalline polymers [28].

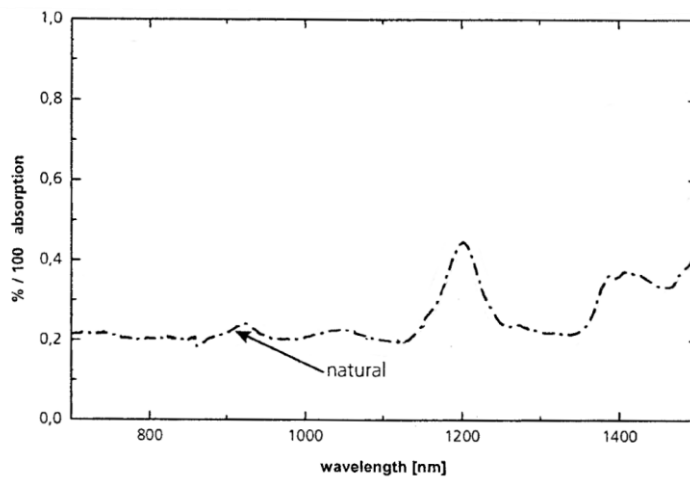


Figure 2.24 - Influence of wavelength on absorption properties for natural PA [44].

2.7 WELD QUALITY

2.7.1 Weld Strength

The welded joint strength can be measured either as breaking load (N) of joint, as weld strength per unit length of the weld (N/m) or as shear or tensile strength of the weld (MPa) [28]. The lap joint is the preferred and the most commonly used joint configuration in LTW and its weld strength is determined by the lap shear test [28].

2.7.2 Failure Modes

In LTW, there can be three main types of failure modes: interfacial, substrate and mixed [38]. Interfacial failure (Figure 2.25-a) occurs when the joint fails at the bond and the base material remains intact, whereas, substrate failure is defined by the opposite situation, where the base material will fail first [38]. Finally, mixed failure mode implies that both elements failed partially [38].

Substrate failure, as well as mixed modes can be further classified into two categories: type I and type II. The following are detailed in the next section [38].

Types of failure modes [38]:

1. **Substrate (Type I, Figure 2.25-b):** the substrate failed away from the interface.
2. **Substrate (Type II, Figure 2.25-c):** the bond remained intact, but the substrate failed close to the interfacial region.
3. **Mixed (Type I, Figure 2.25-d):** failure partially within substrate and at the bond interface.
4. **Mixed (Type II, Figure 2.25-e):** failure mostly interfacial, but with some substrate failure.

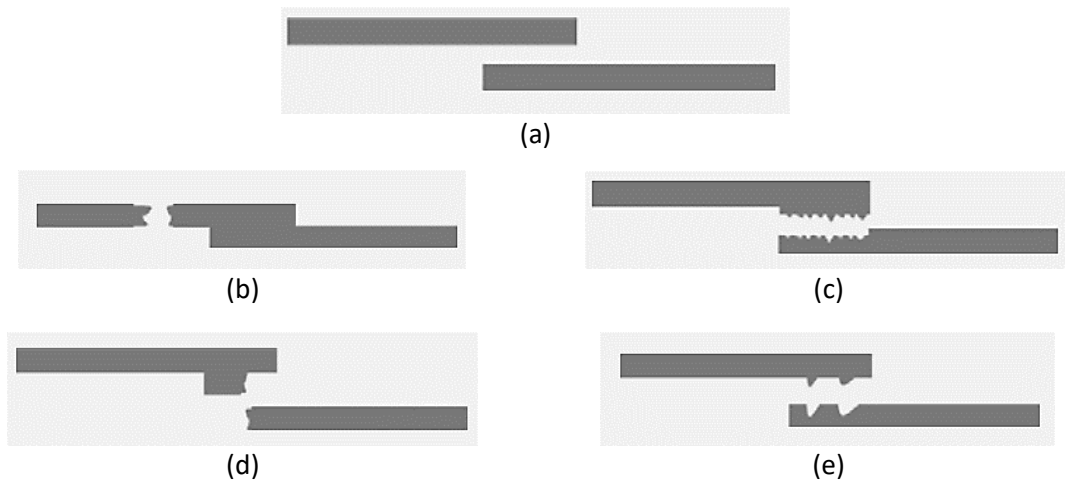


Figure 2.25 - Main types of failure modes in LTW, more specifically, (a) interfacial, (b) substrate type-I, (c) substrate type-II, (d) mixed type-I, (e) mixed type-II. [38].

2.7.3 Weld Pool Dimensions

Weld pool dimensions in LTWed specimens are defined by the weld width (WW), the depth of penetration in the transparent (DT) polymer parts, and the depth of penetration in the absorbing polymer part (DA), measured in mm or μm , Figure 2.26 [28].

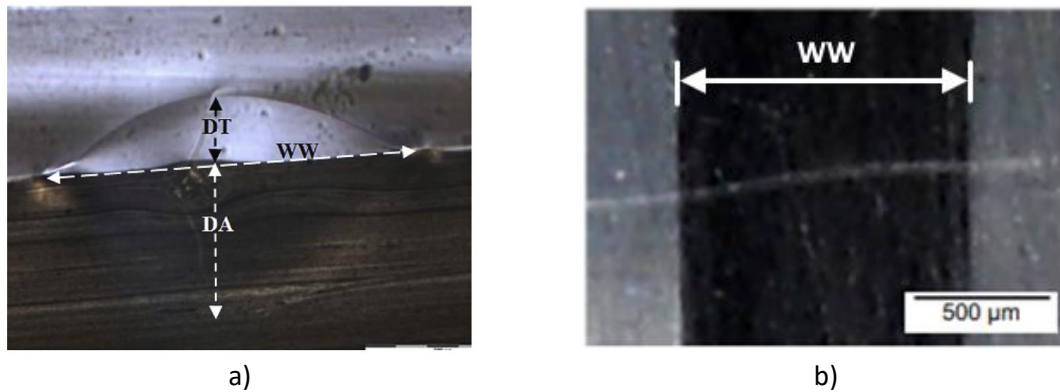


Figure 2.26 - a) cross-sectional view of the weld pool, where WW= weld width, DT = depth of penetration (LT), DA = depth of penetration (LA) [28]; b) Top view of the weld pool [45].

According to Kagan et al. [46], for the calculation of the shear strength of a lap joint it is important to measure the correct width of the weld: w_{HAZ} . The size (diameter) of the focused laser beam at the front of transmitting plastic A (w_{LB}) and the size (width) of heat affected zone (w_{HAZ}) are not the same, Figure 2.27 [46].

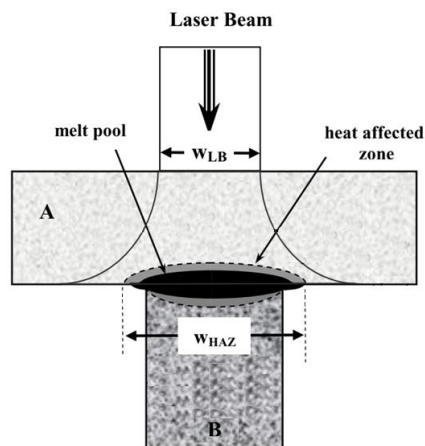


Figure 2.27 - Principles of the T-type butt joint and the formation of the melt pool within the heat affected zone for LTW [46].

Conversely, Amanat et al. [38] believe that the calculation of the LSS (Lap Shear Strength) based on the appearance of the bond area may be misleading, since it is not established whether the interface within the HAZ (Heat Affected Zone) actually bonded. Consequently, the authors assume the contact area to be based on the measured laser diameter at the bond interface [38].

This method is more conservative as it does not consider the HAZ (Figure 2.28). Moreover, by using a theoretical contact area, there will be less variation in the LSS results as it remains constant (for the same beam diameter) throughout the tests, while allowing for a fair comparison with the base material.

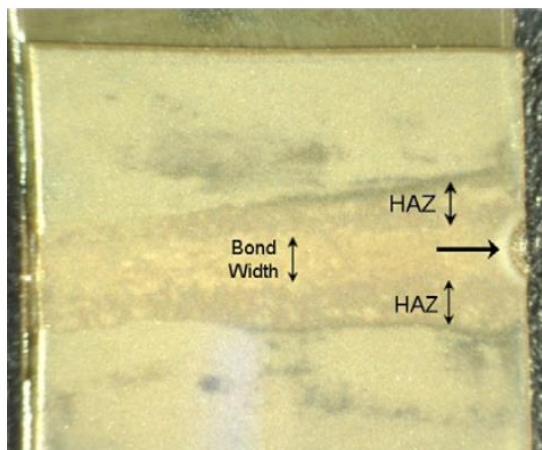


Figure 2.28 - Sample with visible bond width and HAZ [38].

Higher weld strength can be achieved when the weld width is expanded [28]. Acherjee et al. [47] carried out a multivariable optimization of the LTW process. One of the relevant findings in the study was that weld strength increases with weld width, as shown in Figure 2.29 [47].

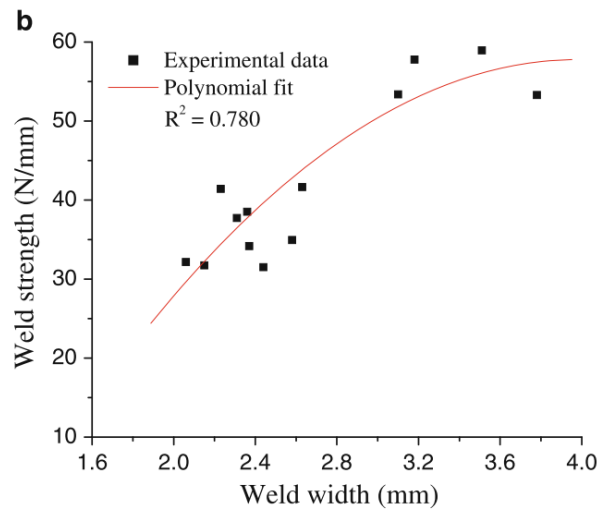


Figure 2.29 - Variation of the weld strength with weld width [47].

2.8 MATERIAL ASPECTS

2.8.1 Polymers

The basic building units of a polymer are chain molecules in which the atoms are held together by covalent bonds, unlike the bonds between chains which are much weaker [48]. These molecular chains are, in turn, composed of numerous identical units called monomers [48].

The amount of cross-linking in molecular chains determines the mechanical properties of a polymer as it restricts relative movement between chains [48]. Polymers can, therefore, be classified according to the level of cross-linkage, in ascending order, as (Figure 2.30) [10], [48], [49]:

- **Thermoplastics:** tough materials; can be melted; can be semi-crystalline or amorphous; soften when heated and harden when cooled, reversibly; can be linear or branched; examples: PE (Polyethylene), PS (Polystyrene), PET (Polyethylene terephthalate), PVC (Polyvinyl chloride).
- **Elastomers:** soft materials; cannot be melted; amorphous; examples: BR (Polybutadiene rubber), SBR (Styrene butadiene rubber), PUR (Polyurethane).
- **Thermosets:** hard materials; cannot be melted; amorphous; network structure; do not soften upon heating; examples: epoxies, PE, etc.

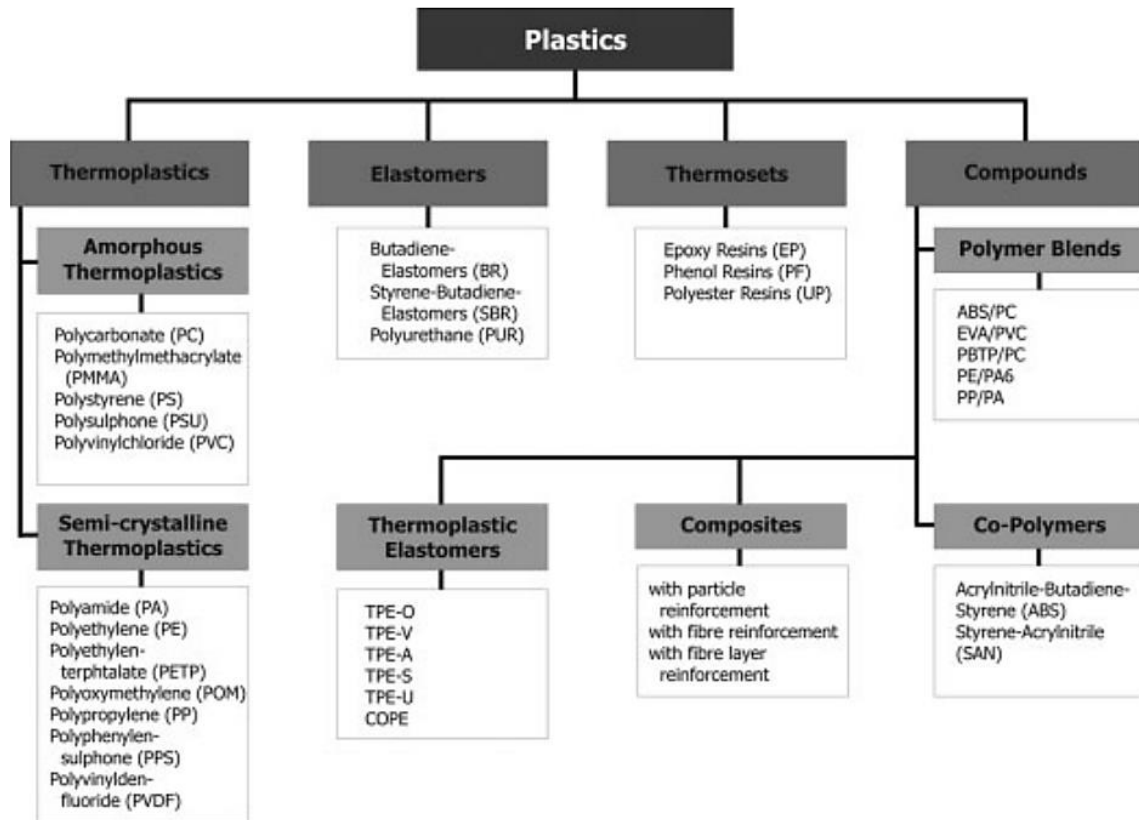


Figure 2.30 - Classification of plastics [10].

2.8.1.1 Polymer Crystallinity

Polymer crystallinity is the packing of molecular chains to create an ordered atomic array [49]. According to the packing density of the molecular chains, molecular substances can be classified as [48], [49], [10]:

- **Crystalline:** composed of only highly ordered, densely packed molecular chains.
- **Semi-crystalline:** contain a mixture of crystalline (spherulites) and amorphous regions.
- **Amorphous:** consist of disordered and misaligned molecular chains.

Due to their size and complexity, polymer molecules are often only partially crystalline (or semicrystalline), where crystalline regions are dispersed within the remaining amorphous material [49].

2.8.1.2 Melting and Glass-Transition Phenomena

In the design and processing of polymeric materials, there are two important phenomena that influence material properties [49]:

- **Melting:** only occurs in crystalline regions and is the transformation of a solid material into a viscous liquid; arises, upon heating, at the melting temperature, T_m .
- **Glass-transition:** only occurs in amorphous regions and is the gradual transformation of a liquid into a rubbery material; arises, upon cooling, at the glass transition temperature, T_g .

2.8.1.3 Melting and Glass Transition Temperatures

Melting and glass transition temperatures are important polymer parameters as they influence fabrication and processing procedures [49]. These represent discontinuous or slope changes in specific volume as can be observed in Figure 2.31 [49].

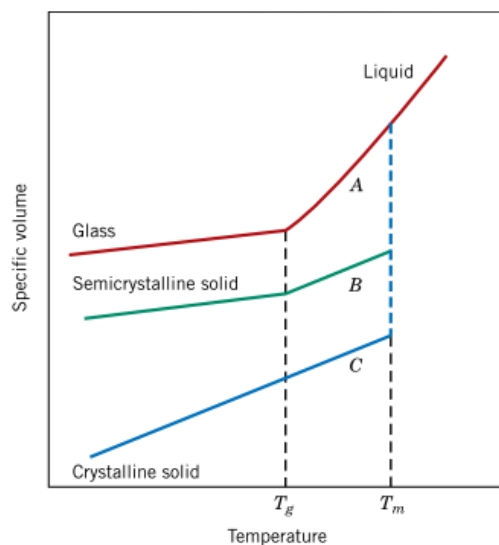


Figure 2.31 - Specific volume versus temperature, upon cooling from the liquid melt, for totally amorphous (curve A), semicrystalline (curve B), and crystalline (curve C) polymers.

2.8.1.4 Thermoplastics

Thermoplastics can be repeatedly melted and resolidified without significant change of mechanical and optical properties [10]. Regarding crystallinity, thermoplastics can be either semi-crystalline or amorphous [10].

2.8.1.4.1 Amorphous Thermoplastics

The temperature state for application of amorphous thermoplastics is the glass condition, below the glass temperature, T_g (Figure 2.32) [10]. Under these circumstances, the polymers are brittle [10]. On exceeding the glass temperature, the mechanical strength will decrease as the resin becomes soft elastic [10]. Typical amorphous thermoplastics are polycarbonate (PC), polymethylmethacrylate (PMMA), polystyrene (PS) or polyvinylchloride (PVC) [10].

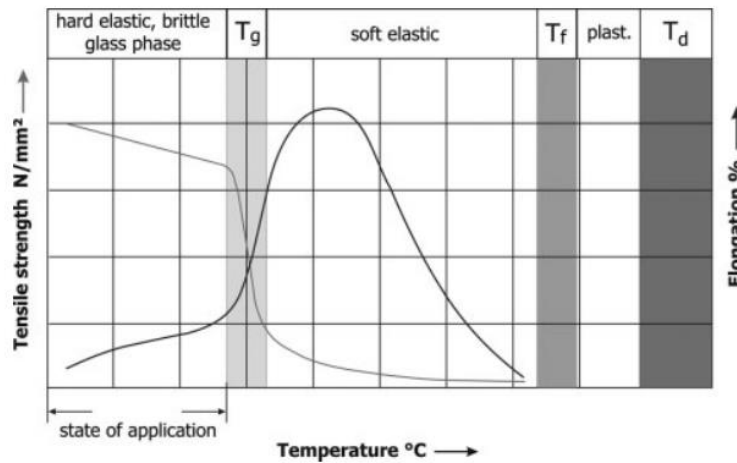


Figure 2.32 - Temperature behavior of amorphous thermoplastics [10].

2.8.1.4.2 Semicrystalline Thermoplastics

Below the glass temperature (T_g) of semicrystalline thermoplastics the material is brittle [10]. Above the glass temperature, usually the state of application, the mechanical behavior of the material is tough elastic to hard [10]. Above the melting temperature (T_m) the material becomes malleable, Figure 2.33 [10]. Typical semicrystalline thermoplastic resins are polyamide (PA), polypropylene (PP) or polyoxymethylene (POM) [10].

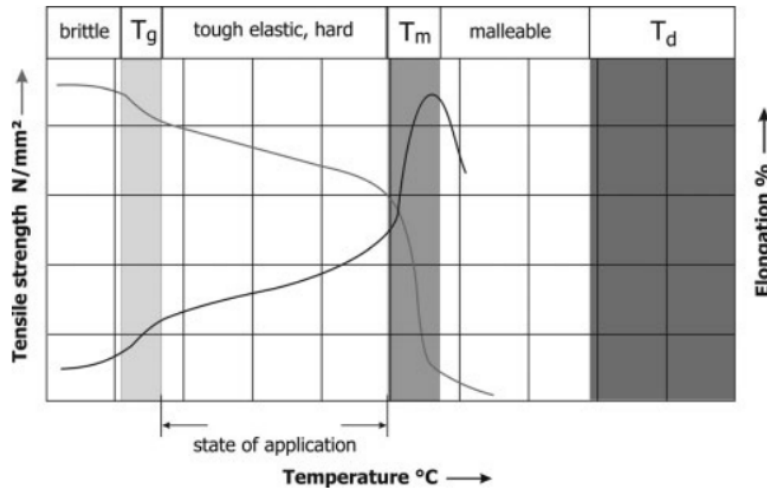


Figure 2.33 - Temperature behavior of semicrystalline thermoplastics [10].

2.8.1.5 Mechanical Behavior of Polymers

Three different types of stress-strain behavior are typically found for polymeric materials (Figure 2.34) [49]:

- **Brittle:** which fractures while deforming elastically.
- **Plastic:** the initial deformation is elastic, which is followed by yielding and a region of plastic deformation.
- **Elastic:** large recoverable strains produced at low stress levels (elastomers).

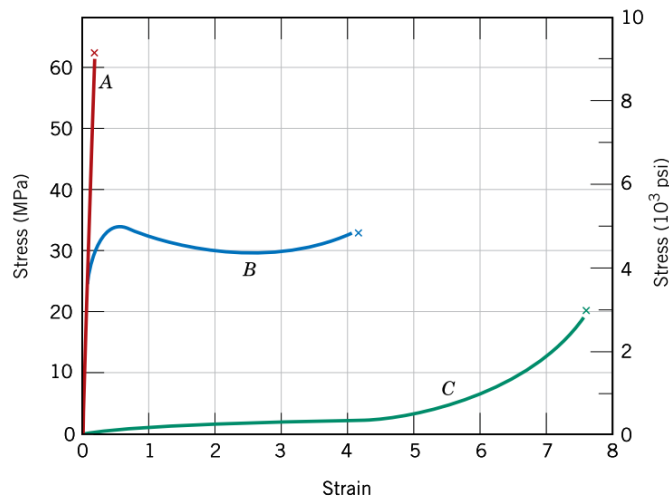


Figure 2.34 - The stress-strain behavior for brittle (curve A), plastic (curve B), and highly elastic (elastomeric) (curve C) polymers [49].

2.8.2 Composites

A composite is a multiphase material whose constituent phases are chemically dissimilar and separated by a distinct interface [49]. Most composites are composed of two phases: the matrix and the dispersed phase [49].

Composites can be classified by the geometry of the reinforcement (particle, flake and fibers) or by the type of matrix (polymer, metal, ceramic and carbon) [50].

2.8.2.1 Fiber-reinforced polymer

Technologically, the most important composites are those in which the dispersed phase is in the form of a fiber, due to their high strength and/or stiffness on a weight basis [49].

Fiber-reinforced polymers consist of a polymer matrix reinforced by fibers [49]. These materials are used in the greatest diversity of composite applications, as well as in the largest quantities, due to their room-temperature properties, ease of fabrication, and cost [49].

2.8.2.2 Fiber Phase

Length wise, fibers can be further classified into continuous (long) or discontinuous (short) [49]. The main advantage of short fibers is their cheaper production and easier manufacturing process, however, long fibers are mechanically superior to shorter ones [48]. Therefore, it is preferable to use fibers as long as possible [48].

Regarding orientation, fibers can be aligned in parallel or randomly oriented [49]. Continuous fibers are usually aligned, whereas discontinuous fibers may be aligned, randomly oriented, or partially oriented, Figure 2.35 [49]. Better overall composite properties are achieved when the fiber distribution is uniform [49].

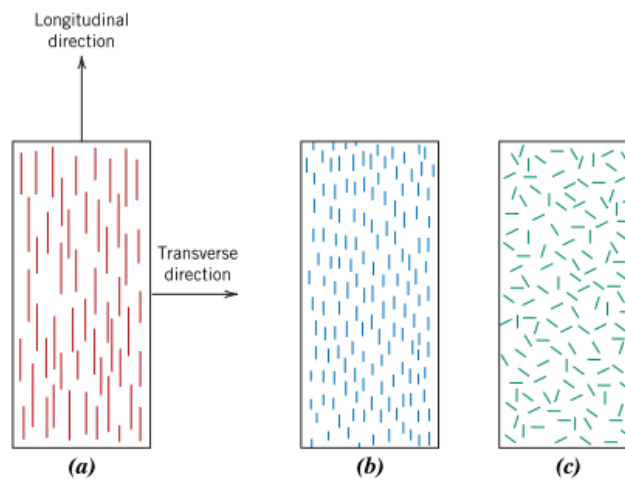


Figure 2.35 – Schematic representations of (a) continuous and aligned, (b) discontinuous and aligned, and (c) discontinuous and randomly oriented fiber–reinforced composites [49].

In terms of material, the most commonly used fiber reinforcements are made of glass, carbon or aramid [49]. Fiberglass is the type of composite produced in the largest quantities, whereas, carbon fiber is a high performance material most commonly used as reinforcement of advanced composites [49].

2.8.3 Laser Weldability of Polymers

Thermoplastic polymers (similar or dissimilar) can be successfully welded using LTW process [28], although, joining dissimilar polymers tends to be more complex and yields weaker welds [10]. Thermosets, on the other hand, cannot be welded without applying an inter-layer material, since they cannot be re-melted [28].

Pereira et al. [51] studied the mechanical properties of PA6 using a pulsed Nd:YAG laser. The authors were able to achieve a maximum of 55% of the base material tensile strength, for the average failure shear stress [51].

Mingareev et al. [12] performed transmission welding with similar and dissimilar polymers, such as PETG (Polyethylene terephthalate), PMMA (Polymethyl methacrylate), PP (Polypropylene) and PE-LD (Low-density polyethylene). According to the authors, LTW of similar polymers resulted

in large-area material intermixing, designated as “material joint” (Figure 2.36-a,b), while, the joining of dissimilar polymers, exhibited no effective material intermixing, which was classified as “form joint”, Figure 2.36-c,d [12]. Regardless of the type of joint obtained, the experiments proved that LTW of similar as well as dissimilar polymers is attainable.

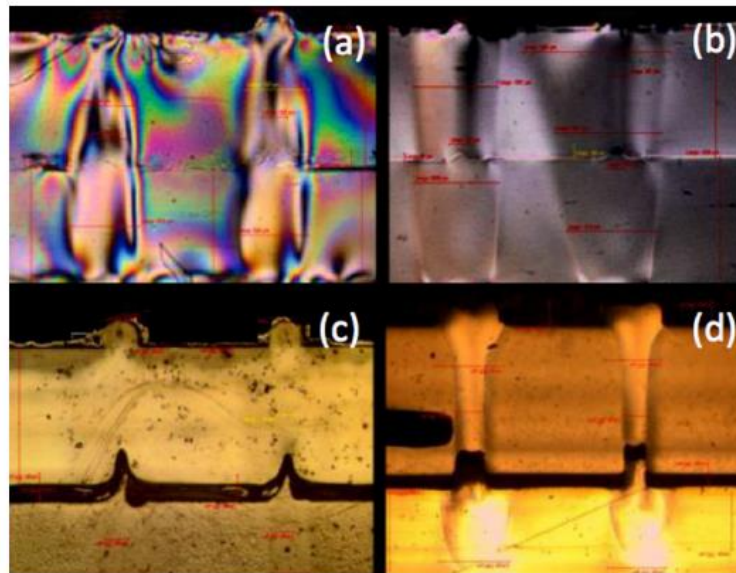


Figure 2.36 - Cross-sections of LTWed polymers: similar polymers, material joint - (a), (b); dissimilar polymers, form joint - (c), (d) [12].

In order to successfully weld dissimilar polymers together, they have to be compatible, more specifically, their molecules must be miscible and their melt temperature ranges should overlap [10].

Thanks to the increasing interest in polymer laser welding in recent years, numerous studies have already been carried in order to evaluate material compatibility. As a consequence, weldability charts (Figure 2.37) are now used to aid in polymer laser welding.

From the analysis of the chart (Figure 2.37), it is possible to conclude that compatibility occurs only between amorphous polymers or blends, while semi-crystalline polymers may mostly only be welded to themselves, with a few exceptions [11]. Moreover, it is not possible to combine incompatible polymers as the molecule chains do not interfuse with each other in molten form, but rather establish distinct phases [11].

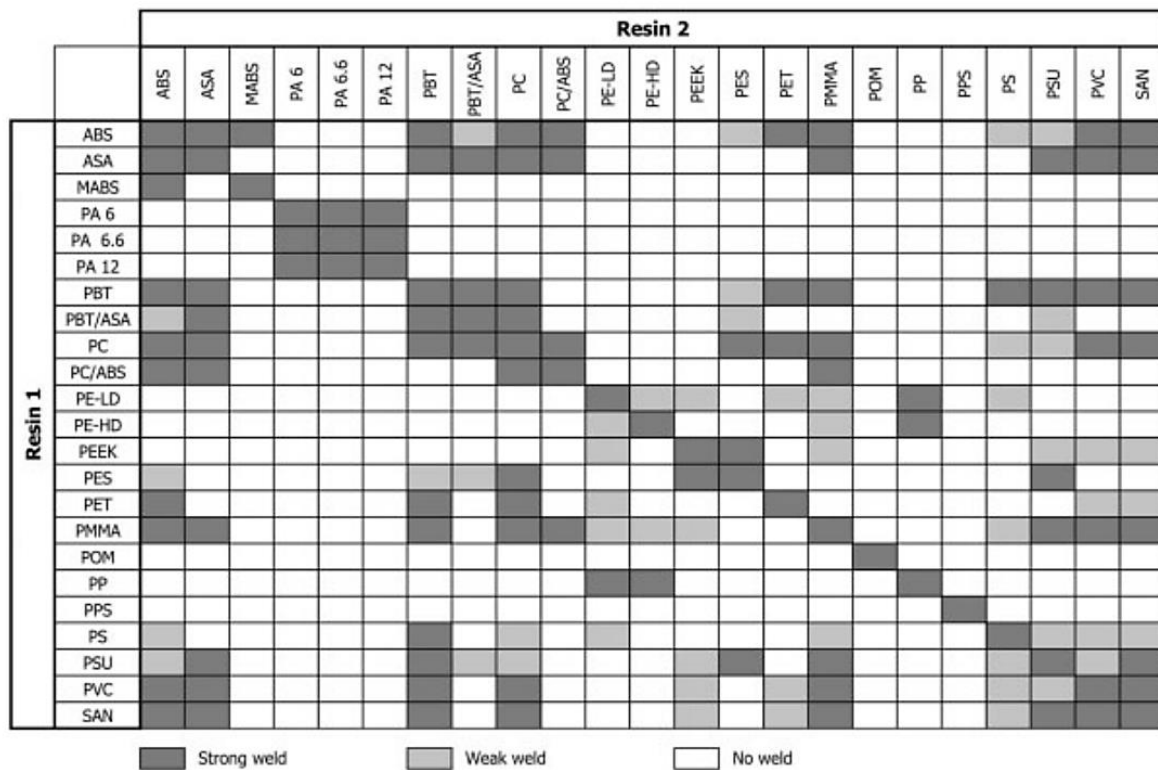


Figure 2.37 - Laser weldability chart for possible polymer combinations [10].

When welding dissimilar polymers, it is appropriate to calculate relative weld strengths rather than weld factors. The relative weld strength can be obtained by dividing the weld strength of a dissimilar pair with the lowest strength of a weld made from each of the two polymers welded to itself [52].

Juhl et al. [52] evaluated the laser weldability of dissimilar polymers. In order to assess weld quality, relative weld strengths were calculated. Out of all the polymers tested, transparent PMMA welded to absorbing PC yielded the highest value for relative weld strength (112%) [52].

2.8.4 Laser Weldability of Composites

Welding of polymer composites containing glass fiber and carbon fiber reinforcements with acceptable weld quality and high strength is performed successfully using LTW process [28].

Prabhakaran et al. [42] used a continuous-wave diode laser, operating at 940 nm to weld PA6 GF30 in a T-weld joint configuration. By optimizing the energy input, the authors were able to achieve a maximum weld strength of 70 MPa, which is comparable to the PA6 unreinforced strength, Figure 2.38 [42].

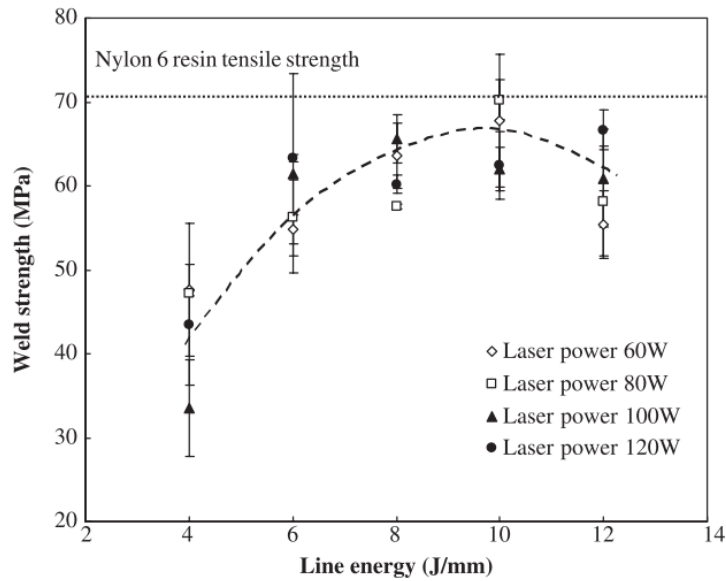


Figure 2.38 - Weld strength as a function of line energy for different laser powers [42].

Kagan et al. [22] evaluated the effect of specific nylon composition factors, such as fiber glass on the NIR transmission characteristics and related these findings to the mechanical performance of the welded joints. For PA6, results show that the tensile strength (MPa) of the weld decreases with increasing wt. % GF [22].

Jaeschke et al [4] compared the weldability of PPS (Polyphenylene sulfide) Natural as LT-partner (Laser Transparent partner) when combined with PPS-CF Natural (LA-partner) versus its combination with PPS-CB unreinforced (LA-partner). From the investigations, the authors concluded that the lap shear strengths are higher for the case where the PPS-CF is the LA (Laser Absorbent) partner [4].



2.9 CONCLUSION

2.9.1 Summary

From this literature review, it can be concluded that LTW is heavily influenced by the laser parameters used, as well as material composition and pre-welding conditions.

Regarding material composition and pre-welding conditions, an increase in colorants (LA), reinforcements, crystallinity, part thickness and surface roughness, generally has a negative impact on transmittance in the LT partner, for semi-crystalline polymers.

Concerning laser parameters (such as power, speed, etc.), they all have, mostly the same influence on weld strength. Initially, the weld strength increases with their increase, up to a threshold, beyond which it begins to decrease. Consequently, one of the main areas of research in LTW is parameter optimization, where an attempt is made to find this threshold under certain conditions.

2.9.2 Literature Gaps

Many studies in LTW focus on welding an LT unfilled material to its LA counterpart filled with CB [2], [13], [51], [36], [38], [39], [42], while studies on welding of dissimilar polymers or even polymers to composites are scarce, due to the comparatively worse results obtained [12], [18], [19], [22]. Moreover, diode [37], [2], [40], [42] and fiber [38], [12] laser systems are frequently used, unlike Nd:YAG pulsed lasers.

Hence, in this study, LTW of PA66N to PA66 GF30, using pulsed Nd:YAG LASER will be investigated, in an effort to expand scientific knowledge in this field.

3 EXPERIMENTAL PROCEDURE

3.1 INTRODUCTION

In order to achieve the set goals, the following steps were taken during the experimental procedure:

1. Material Selection
2. Material Characterization
3. Test Pieces for Welding (preparation & dimensions)
4. Clamping Device
5. Parameter Optimization
6. Lap Shear Tests
7. Diameter Measurement

3.2 MATERIAL SELECTION

Due to reduced availability of compatible composites and thermoplastics, the materials chosen were (Figure 3.1): TECAMID 66 Natural, manufactured by *Ensinger*; ERTALON® 6 SA and ERTALON® 66 GF30, both manufactured by *Mitsubishi Chemical Advanced Materials*.

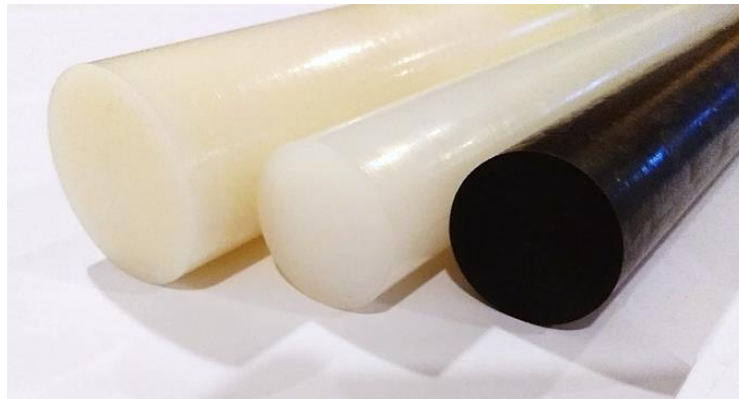


Figure 3.1 - Photograph of the materials used in rod format.

3.2.1 TECAMID 66 Natural

TECAMID 66 Natural² is the trade name for the polyamide 66 manufactured by Ensinger [53]. This semi-crystalline thermoplastic is characterized by its high rigidity, strength and toughness, as well as good weldability [54]. However, this material's propensity to absorb moisture can compromise its dimensional stability [54].

Table 3.1 - Relevant properties of TECAMID 66 Natural [53], [22].

Color	Density [g/cm ³]	Melting Temp. [°C]	Thermal Conductivity ³ [W/(K.m)]	CLTE ⁴ [μm/(m.K)]	Tensile Strength [MPa]	Young's Modulus [MPa]	Transmittance ⁵ (%)
Natural	1.15	258	0.36	110-120	85	3500	72



Figure 3.2 - Examples of applications of Polyamide 66 Natural [55].

² The datasheet of TECAMID 66 Natural can be consulted in appendix A.1.

³ Value obtained at 23 °C.

⁴ Average value between 23–60 °C and 23–100 °C.

⁵ Value obtained at a wavelength of 1064 nm, for a 3.2 mm thick specimen.

3.2.2 ERTALON® 6 SA

ERTALON® 6 SA⁶ is the trade name for the polyamide 6 manufactured by MCAM [56]. This semi-crystalline thermoplastic combines high strength, stiffness and hardness with good creep and wear resistance, heat aging properties and machinability [56]. These properties make ERTALON® 6 SA a "general purpose" grade for mechanical construction and maintenance, Figure 3.3 [57].

Table 3.2 - Relevant properties of ERTALON® 6 SA [22], [56].

Color	Density [g/cm ³]	Melting Temp. [°C]	Thermal Conductivity ⁷ [W/(K.m)]	CLTE ⁸ [μm/(m.K)]	Tensile Strength [MPa]	Young's Modulus [MPa]	Transmittance ⁹ (%)
Natural	1.14	220	0.28	90-105	80	3300	69.32



Figure 3.3 - Examples of applications of ERTALON® 6 SA [58].

⁶ The datasheet of ERTALON 6 SA can be consulted in appendix A.2.

⁷ Value obtained at 23 °C.

⁸ Average value between 23–60 °C and 23–100 °C.

⁹ Value obtained at a wavelength of 1064 nm, for a 3.2 mm thick specimen.

3.2.3 ERTALON® 66 GF30

ERTALON® 66 GF30¹⁰ is the trade name for the 30% short glass-fiber reinforced polyamide 66 manufactured by MCAM [59]. This composite with an ideal balance of strength and toughness is commonly used in applications requiring high compressive strength and rigidity, Figure 3.4 [60]. Due to sharing the same matrix material as the TECAMID 66, dimensional changes can also occur as a consequence of moisture absorption [60].

Table 3.3 - Relevant properties of ERTALON® 66 GF30 [59].

Color	Density [g/cm ³]	Melting Temp. [°C]	Thermal Conductivity ¹¹ [W/(K.m)]	CTE ¹² [μm/(m.K)]	Young's Modulus [MPa] ³	Tensile Strength [MPa]	Elongation at break (%)
Black	1.29	260	0.30	50-60	5000	85	5

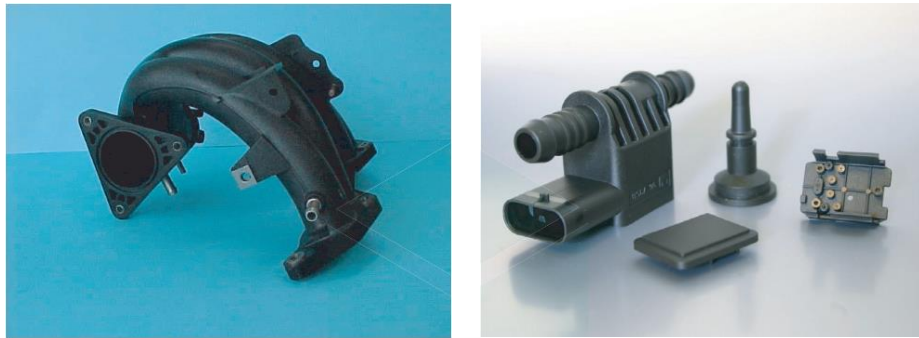


Figure 3.4 - Examples of applications of ERTALON® 66 GF30 [61].

¹⁰ The datasheet of ERTALON 66 GF30 can be consulted in appendix A.3.

¹¹ Value obtained at 23 °C.

¹² Average value between 23–60 °C and 23–100 °C.

3.3 MATERIAL CHARACTERIZATION

In order to calculate the welding efficiency, it was necessary to carry out tensile tests on the base material. For this, specimens with the format shown in Figure 3.5, were used.

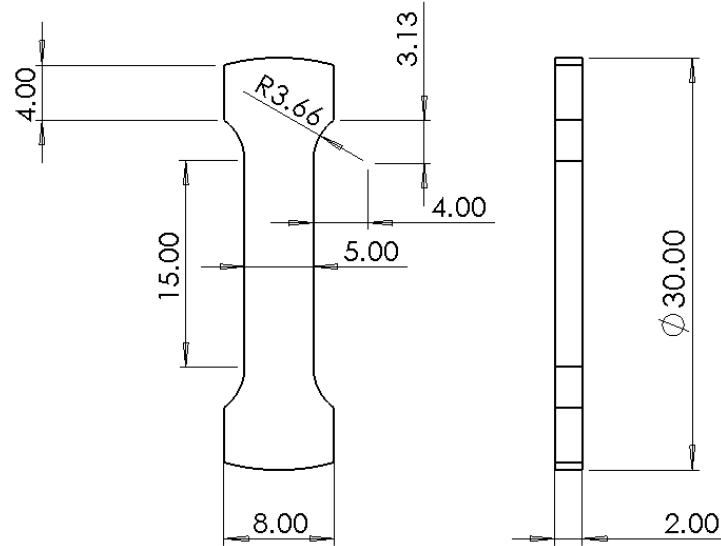


Figure 3.5 - Specimens used in material characterization tests, adapted from [62].

The rods were first lathed into discs and then milled in a CNC machine to achieve the desired shape (Figure 3.6).

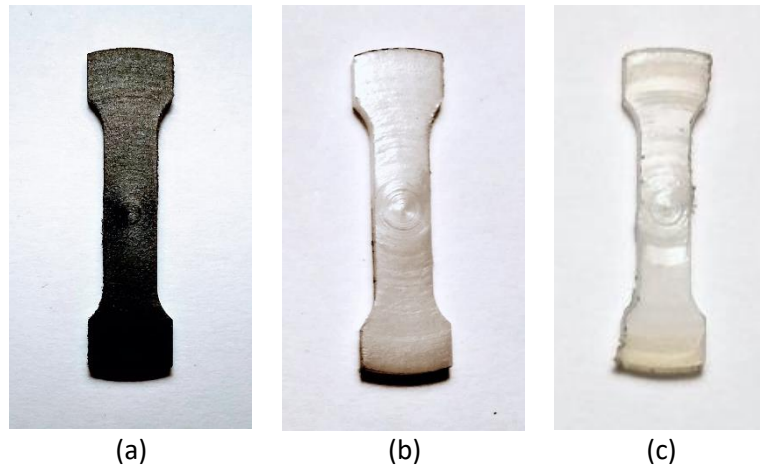


Figure 3.6 - Machined specimens of (a) PA66 GF30, (b) PA66N and (c) PA6N.

3.4 TEST PIECES FOR WELDING

In the following section, the preparation of the test pieces used in the optimization process is described, as well as their final dimensions and joint configuration.

3.4.1 Preparation

The selected materials were acquired in the form of rods, which are shown in Figure 3.7. TECAMID 66 had initial dimensions of $\phi 40 \times 1000$ mm, while ERTALON 66 GF30 had dimensions of $\phi 30 \times 3000$ mm and ERTALON 6 SA has dimensions of $\phi 30 \times 1000$ mm.

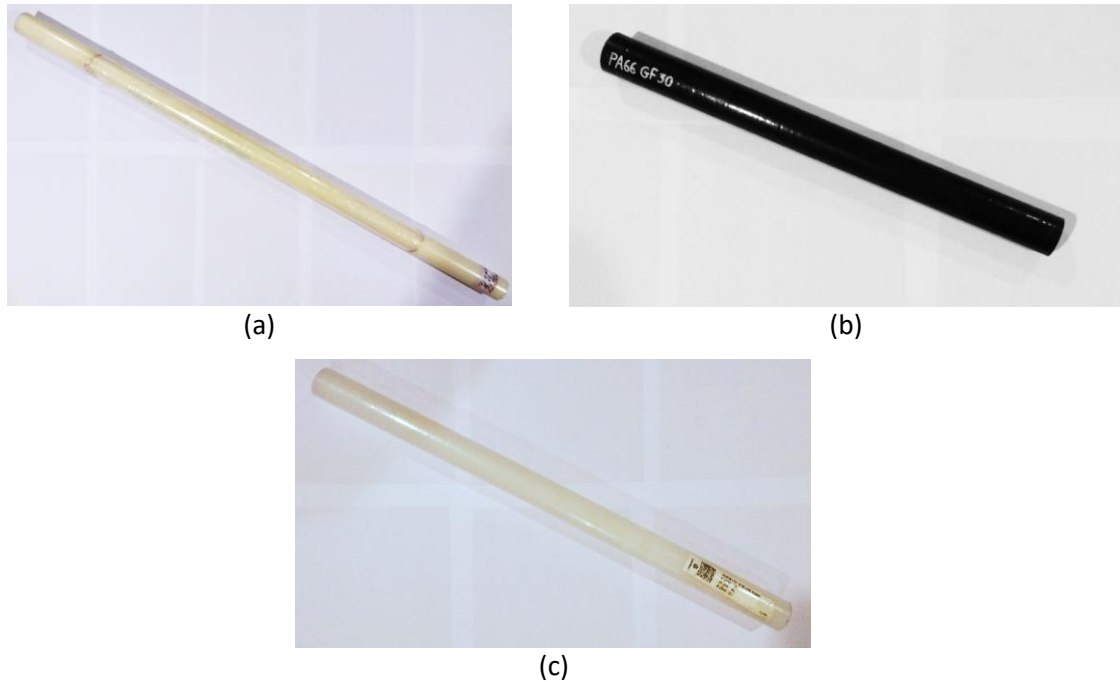


Figure 3.7 - Photograph of the TECAMID 66 rod (a), of an ERTALON 66 GF30 rod section (b) and of an ERTALON 6 SA rod section (c).

From the raw materials, 2 mm thick discs were lathed, Figure 3.8.



Figure 3.8 - (a) Lathing operation to turn the rods into discs and (b) ERTALON 66 GF30 discs.

Subsequently, the discs were sanded, in order to remove the spike in its center. Finally, these were milled (Figure 3.9) so as to arrive at the final shape of the specimens, Figure 3.10.

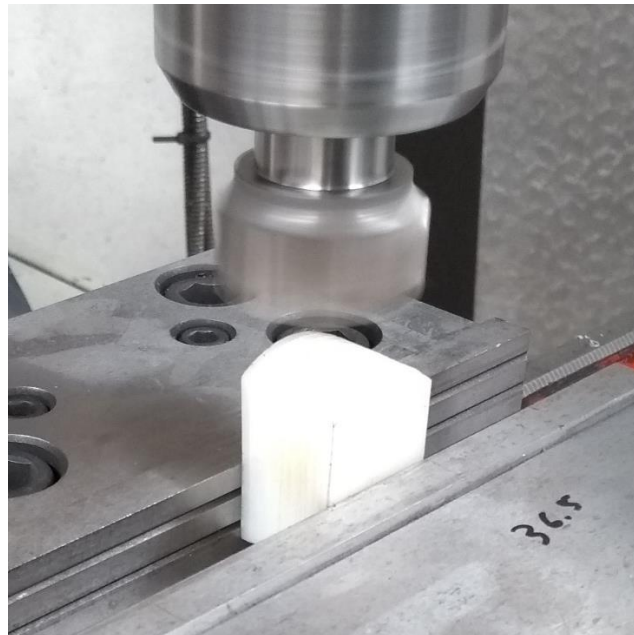


Figure 3.9 – Milling operation of the discs.

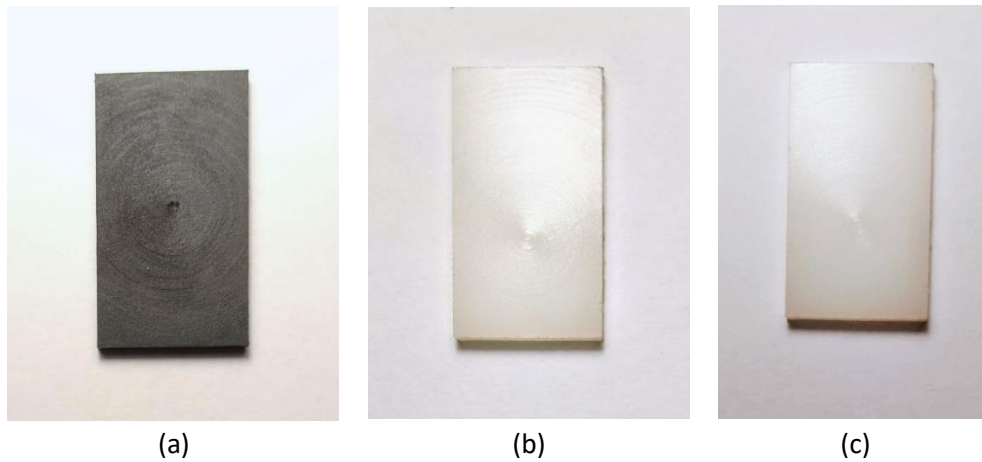


Figure 3.10 - Photographs of the specimen of (a) PA66 GF30, (b) PA66N and (c) PA6N in their final dimensions.

3.4.2 Dimensions

The final dimensions of the test pieces were 26x14.5x2 [mm] and they were welded in a lap joint configuration, as shown in Figure 3.11. Moreover, only one weld bead was performed, in a single scan, located at the center of the overlapping region.

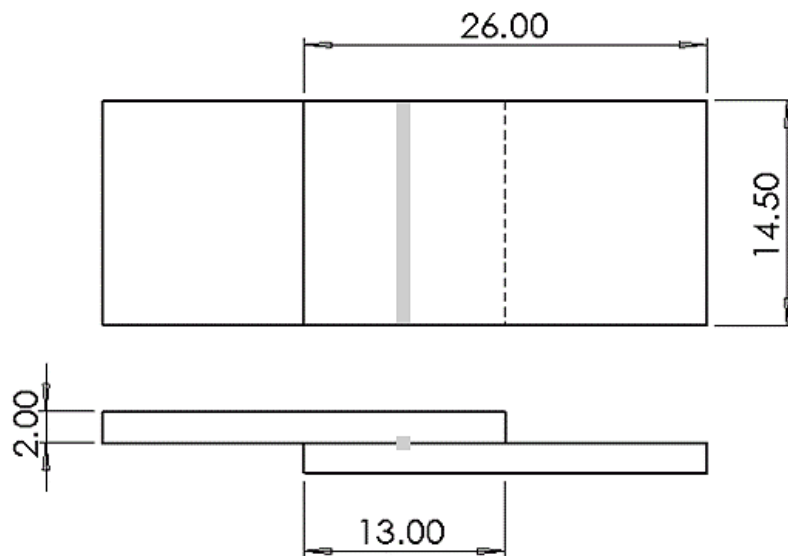


Figure 3.11 – Specimen configuration and final dimensions.

3.5 WORKSTATION

The laser welding machine used in the experimental procedure was the SISMA SWA-300 [63]. This is the more powerful model of the mold maintenance and repairing SWA range designed and manufactured by SISMA [63].



Figure 3.12 - SISMA SWA-300 [63].

The SWA-300 has an Nd:YAG pulsed laser operating at 1064 nm and 300 W of maximum average power [64]. Moreover, the laser is flashlamp-pumped, and the laser beam is transmitted through optical fibers [64]. Table 3.4 summarizes the most important technical specification of the machine.

Table 3.4 - Technical specifications of SISMA-SWA 300 [63].

Model	SWA 300
Average Power	300 W
Peak power	12 kW
Pulse energy	100 J
Pulse frequency	0-50 Hz
Pulse duration	0.2-25 ms
Spot diameter	0.6-2 mm
Laser beam transport	Fiber-coupled
Moving speed	0-20 mm/s

3.5.1 Main Components

3.5.1.1 Operator Panel

3.5.1.1.1 Working Page

This page contains the following functions [64]:

1. **Configuration of the laser parameters:** peak power (%), pulse time (ms), pulse frequency (Hz)/overlap (%), pulse diameter (mm).
2. **Operational features:** overlap, line & fill, path, inclined plane, circumference, engine management.
3. **Indication of energy and average power**
4. **Other functions:** programs, pulse shape, alarms, activate laser, turn on lamp.

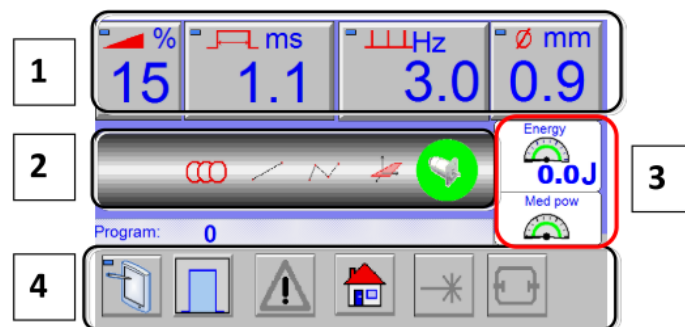


Figure 3.13 - SISMA-SWA 300 working page [64].

3.5.1.2 Console

The console is equipped with [64]:

1. **Joystick:** for manual control of X, Y, Z axes and laser firing.
2. **Quick Keys:** enable quick selection of the laser parameters.
3. **Dial button:** for accurate regulation of the laser parameter values.
4. **Emergency button**



Figure 3.14 - SISMA SWA 300 console [64].

3.6 CLAMPING DEVICE

3.6.1 Components

The clamping device was adapted from ref. [62] and consists of (Figure 3.15):

- A. Two springs - 50 [mm]
- B. One aluminum base - 90x50x3 [mm]
- C. One shim - 50x12.5x2 [mm]
- D. Two metal plates - 35x14x3 [mm]

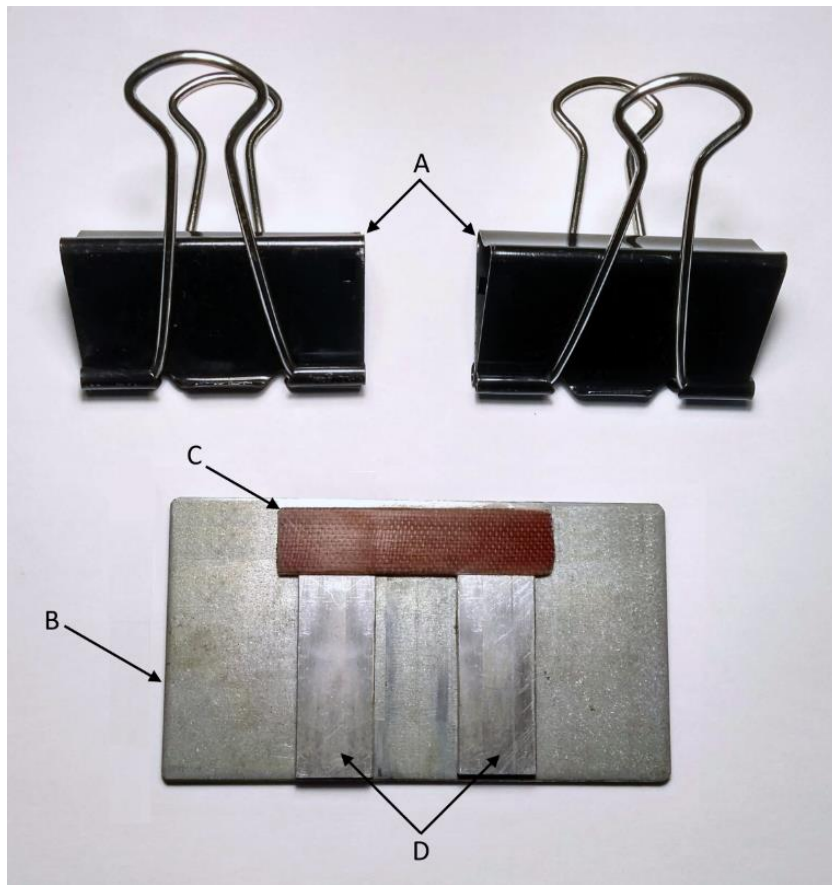


Figure 3.15 – Main components of the clamping device, including (A) two springs, (B) an aluminum base, (C) a shim, (D) two metal plates.

3.6.2 Configuration

The springs press the overlapped test pieces on each side of the base, leaving only a small opening where they will be welded, Figure 3.16 (a). To ensure parallelism between the test pieces, it was also necessary to glue a shim as well as two guiding metal plates to the base, Figure 3.16 (b).

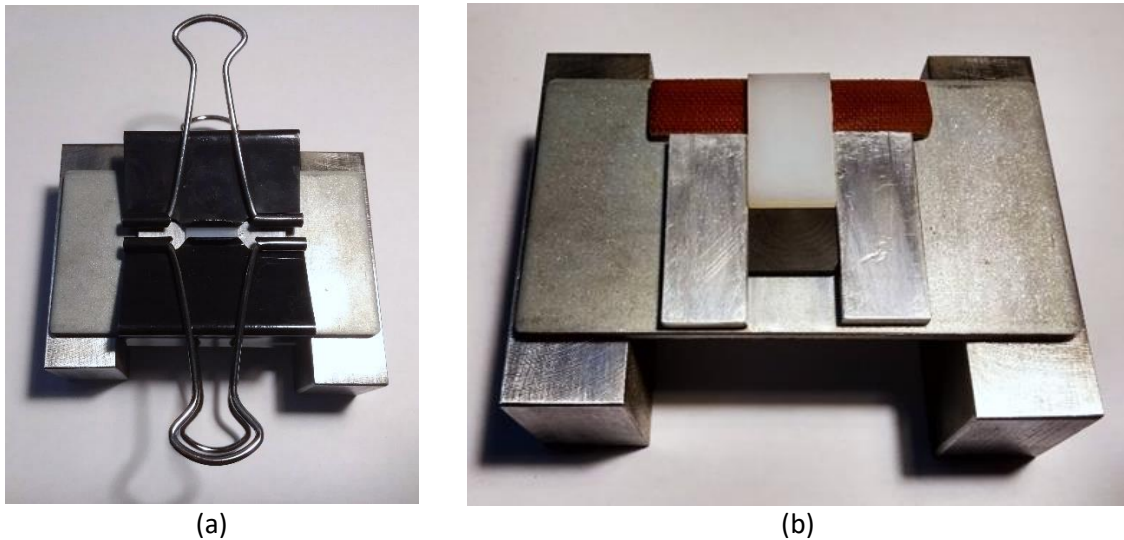


Figure 3.16 - Clamping device in its final configuration (a) and positioning of the specimens (b).

3.6.3 Pressure Calculation

As previously stated, pressure plays a fundamental role in the welding of polymers and composites. Therefore, it is important to calculate the pressure to which the test pieces are subjected during welding. For this purpose, tensile tests were performed to the springs (Figure 3.17).

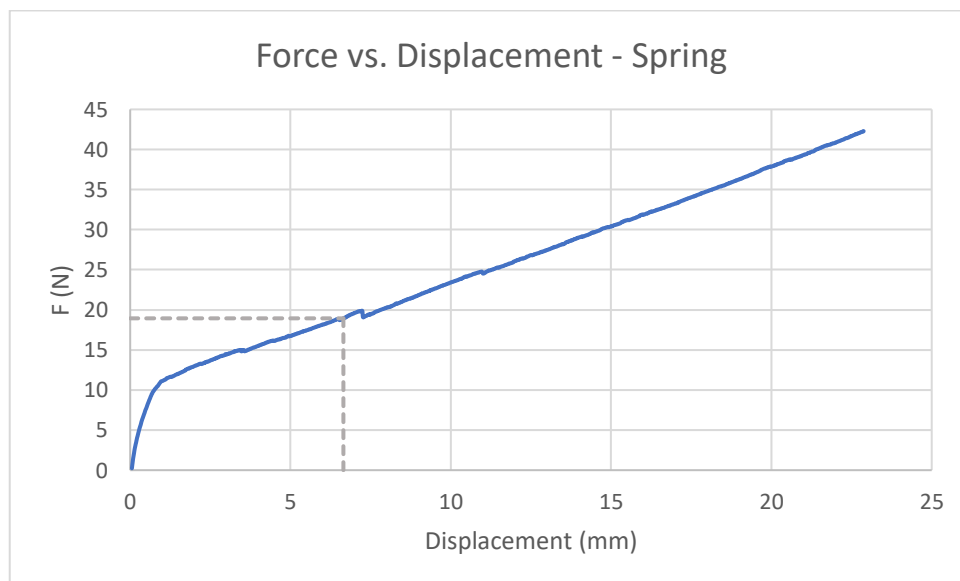




Figure 3.17 – Force vs. displacement curve obtained through the spring tensile test.

Knowing the spring's displacement when pressing the test pieces and the overlapping area (Figure 3.11), it is possible to obtain the force (Figure 3.17) and, consequently, to calculate the pressure (Equation 3.1). Table 3.5 summarizes the data used to calculate the pressure.

Table 3.5 – Pressure calculation data.

Spring displacement	6.65 mm
Force @ d=6.65 mm	18.94 N
Total force (two springs)	37.88 N
Overlap area	188.5 mm ²

$$P = \frac{F@d}{A_{OL}}$$

Equation 3.1

According to Equation 3.1, the pressure to which the test pieces are subjected is 0.2 MPa. This value is below the minimum 0.5 MPa recommended for the welding of polymers [28], however, tests carried out with other more elaborate clamping devices, did not show great variations in the results.

3.7 OPTIMIZATION PROCESS

3.7.1 Introduction

In order to find the optimal parameters, the optimization process was divided into the following phases:

1. Material comparison
2. Process window definition
3. Optimal parameters
4. Comparison to the base material

3.7.2 Material Comparison

Before starting the optimization of the welding parameters, it was necessary to choose a combination of materials that yielded satisfactory results. For this, the welding efficiency of the pairs PA6N/PA66GF30 and PA66N/PA66GF30 was compared (Table 3.6), using as initial parameters the ones recommended in ref. [51].

Table 3.6 - Comparison between PA66N and PA6N when welded with PA66 GF30.

Group H	Material Comparison						
	Test piece	Peak Power ¹³ [%]	Pulse Width [ms]	Overlap [%]	Beam Diameter [mm]	Pulse Energy ¹⁴ [J]	Scan Speed [mm/s]
PA6N/ PA66 GF30	H1	3	10	65	2	7.8	5
PA66N/ PA66 GF30	H2						

3.7.3 Process Window Definition

The experimental procedure of this study is based on the analysis of the influence of critical parameters on the laser welding process. From the results obtained, a process window was determined for each variable, that is, a region in which the results are acceptable. The parameters evaluated were:

- Peak Power (%) – Group A (Table 3.7)
- Pulse Width (ms) – Group B (Table 3.8)
- Overlap (%) – Group C (Table 3.9)
- Laser Beam Diameter (mm) – Group D (Table 3.10)
- Scan Speed (mm/s) – Group F (Table 3.11)

¹³ Peak Power is expressed as a percentage of the maximum Peak Power of 12 kW as shown in Table 3.4.

¹⁴ The pulse energy is specified by the laser welding machine and differs from the results obtained using Equation 2.2

Initial considerations:

- The pulse type (square-shaped) and the distance between the lens and the test piece (156 mm) were kept constant.
- Each test (x_i) was performed three times, from which an average value (\bar{x}) was obtained as well as the corresponding error (Δx): $\Delta x = \max\{d_i\}$, where $d_i = |x_i - \bar{x}|$.

Figure 3.18 showcases a group of specimens used to evaluate the influence of the different parameters on weld strength.

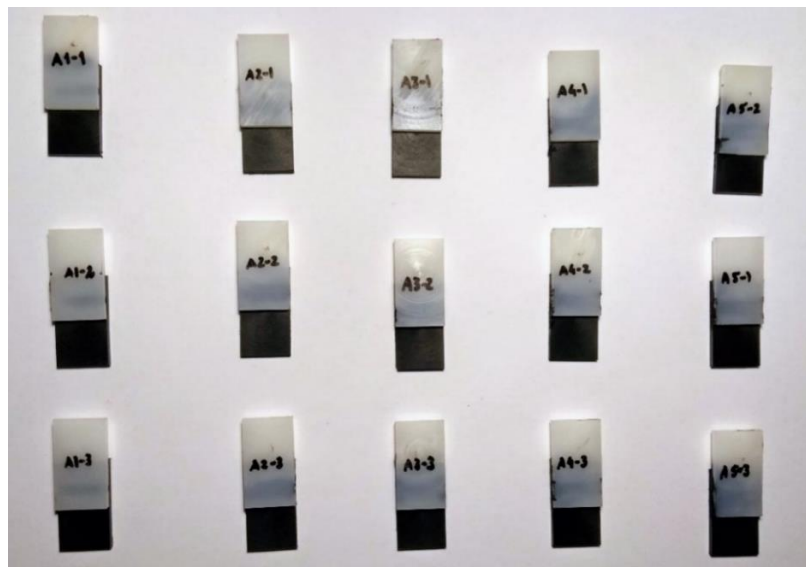


Figure 3.18 - Photograph of the welded specimens of Group A.

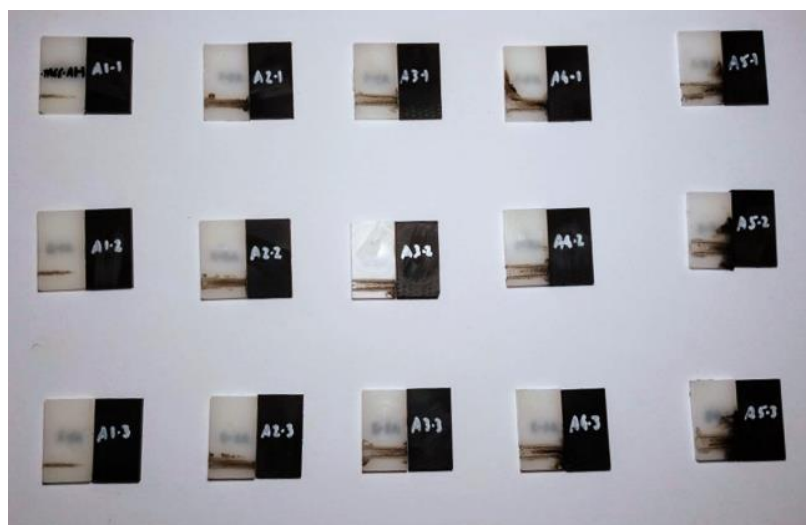


Figure 3.19 - Photograph of the specimens of Group A after the tensile test had been performed.

Bellow, the tables that summarize the values of each parameter throughout the procedure are presented.

Table 3.7 - Evaluation of Peak Power.

Group A	Influence of Peak Power						
	Test piece	Peak Power [%]	Pulse Width [ms]	Overlap [%]	Beam Diameter [mm]	Pulse Energy [J]	Scan Speed [mm/s]
A1	3	10	65	2	7.8	5	
A2	10				12.3		
A3	20				19.2		
A4	30				26.7		
A5	40				34.8		

Table 3.8 - Evaluation of Pulse Width.

Grupo B	Influence of Pulse Width						
	Test piece	Peak Power [%]	Pulse Width [ms]	Overlap [%]	Beam Diameter [mm]	Pulse Energy [J]	Scan Speed [mm/s]
B1	3	10	65	2	7.8	5	
B2		13			10.1		
B3		16			12.4		
B4		20			15.6		
B5		25			19.5		

Table 3.9 - Evaluation of Overlap.

	Influence of Overlap						
	Test piece	Peak Power [%]	Pulse Width [ms]	Overlap [%]	Beam Diameter [mm]	Pulse Energy [J]	Scan Speed [mm/s]
Grupo C	C1	3	10	50	2	7.8	5
	C2			60			
	C3			80			
	C4			90			
	C5			95			

Table 3.10 - Evaluation of Laser Beam Diameter.

	Influence of Laser Beam Diameter						
	Test piece	Peak Power [%]	Pulse Width [ms]	Overlap [%]	Beam Diameter [mm]	Pulse Energy [J]	Scan Speed [mm/s]
Grupo D	D1	3	10	65	0.6	7.8	5
	D2				0.9		
	D3				1.2		
	D4				1.5		
	D5				2		



Table 3.11 - Evaluation of Scan Speed.

	Influence of Scan Speed						
	Test piece	Peak Power [%]	Pulse Width [ms]	Overlap [%]	Beam Diameter [mm]	Pulse Energy [J]	Scan Speed [mm/s]
Grupo F	F1	3	10	65	2	7.8	1
	F4						2.5
	F2						5
	F5						7.5
	F3						10

3.7.4 Optimal Parameters

After obtaining the optimal ranges for each variable, these were combined in final tests (Table 3.12), with the aim of reaching the best set of parameters. More specifically, the objective was to increase the power while the remaining parameters were reduced, to minimize the degradation of the material, thus trying to find a midpoint where a threshold in the welding strength was reached. Conversely, speed was increased with power due to the fact that low speeds benefit the welding strength and, consequently, its increase offsets the power effect.

Table 3.12 - Combination of the optimal parameter ranges.

	Optimal Parameters						
	Test piece	Peak Power [%]	Pulse Width [ms]	Overlap [%]	Beam Diameter [mm]	Pulse Energy [J]	Scan Speed [mm/s]
Grupo X	X1	3	25	80	2	19.5	2.5
	X2	5	24.1	80		21.6	3
	X3	7	23.2	80		23.8	3.5
	X4	8	22.3	75		24.3	4
	X5	10	21.4	75		26.3	4.5
	X6	12	20.5	75		27.8	5
	X7	14	19.6	70		29.2	5.5
	X8	16	18.7	70		30.4	6
	X9	18	17.8	70		31.5	6.5
	X10	20	16.9	70		32.4	7.5

3.8 LAP SHEAR TESTS

The elastic-plastic behavior of materials is frequently described by stress-strain curves, obtained from tensile tests [48]. A tensile test consists of slowly pulling a sample of material at constant speed with a varying axial force (P), until it breaks [48], [65]. The extension and the required force measured during the test can then be transformed into material parameters, such as nominal stress (Equation 3.2) and nominal strain (Equation 3.3) [48], [65]:

$$\sigma = \frac{P}{A_i} \quad \text{Equation 3.2}$$

$$\varepsilon = \frac{\Delta L}{L_i} \quad \text{Equation 3.3}$$

where A_i is the initial cross-sectional area, ΔL is the change in length, and L_i is the initial gauge length [48], [65], as shown in Figure 3.20.

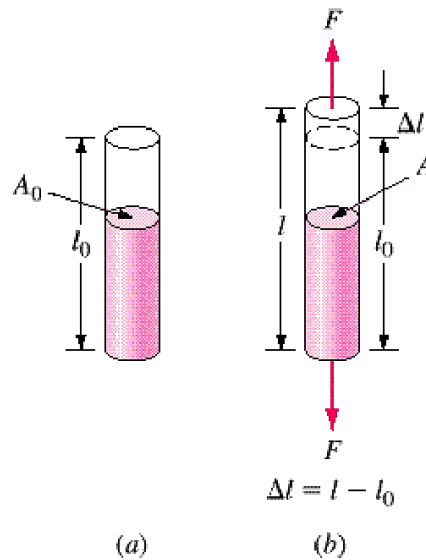


Figure 3.20 - Cylindrical rod before (a) and after (b) being subjected to a uniaxial tensile force 'F' [66].

The results of materials tests are mainly used to obtain values of materials properties such as the strength in tension [65].

The *ultimate tensile strength* is the highest engineering stress reached prior to fracture [65]. If large elongation has occurred upon fracture, the material is designated as ductile (Figure 2.34 - curve C), otherwise, it is labelled as brittle (Figure 2.34- curve A) [48]. In this case, the highest stress occurs at the point of fracture [65]. However, in ductile materials, the force and hence the engineering stress, reaches a maximum and then decreases prior to fracture [65].

In either case, the maximum force (P_{max}) reached at any point during the test is used to obtain the ultimate tensile strength (σ_{UTS}), by dividing by the original cross-sectional area [65]:

$$\sigma_{UTS} = \frac{P_{max}}{A_i} \quad \text{Equation 3.4}$$

However, in the case of a lap shear test, the weld seam is under a load parallel to its surface area, hence it is a shear load and therefore produces a shear stress. The average shear stress can be calculated by dividing the shear force (S) by the area of the cross-section (A_i)¹⁵, according to Equation 3.5 [66], while the shear strain is defined by the shear displacement (a) divided by the distance (h)¹⁶ (Equation 3.6), as shown in Figure 3.21 [66]:

$$\tau_{avg} = \frac{S}{A_i} \quad \text{Equation 3.5}$$

$$\gamma = \frac{a}{h} \quad \text{Equation 3.6}$$

Consequently, the *ultimate shear strength* then is defined by Equation 3.7 :

$$\tau_{UTS} = \frac{S_{max}}{A_i} \quad \text{Equation 3.7}$$

¹⁵ In this case, the area A_i is calculated by multiplying the weld bead width by the weld bead length.

¹⁶ The distance h , in this case, corresponds to the penetration depth (DA), which was assumed to be constant and equal to 0.5 mm as it does not influence the shear strength calculation.

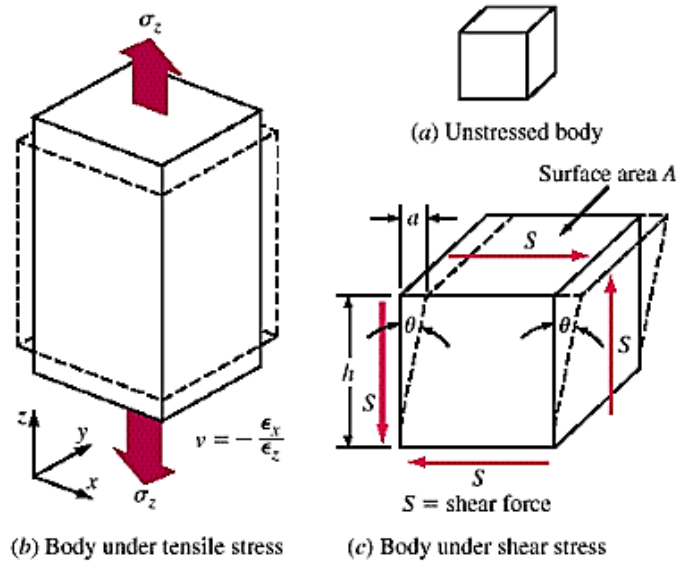


Figure 3.21 - (a) Unstressed body; (b) Body subjected to tensile stress; (c) Body subjected to pure shear forces 'S' acting over surface areas 'A' [66].

In LTW, besides the shear strength (MPa), the weld strength (Equation 3.8) - (N/mm) is also commonly used to evaluate the welding quality. During this experimental procedure, when analyzing parameter variation, weld strength was calculated. However, when comparing the results to the base material, shear strength is more appropriate and was used instead.

For a quantitative comparison, two types of weld efficiency were obtained, due to the different nature of the stress states that occur during lap shear tests and tensile tests. The first type (Equation 3.9), is a joint efficiency (η_j) that does not consider the weld bead stress state, aiming to simply compare the tensile strengths. The second type (η_{wb} - Equation 3.10), on the other hand, is a weld bead efficiency which considers the stress state of the weld bead and compares it to the shear strength of the base material.

$$w_s = \frac{S_{max}}{L_{seam}} \quad \text{Equation 3.8}$$

$$\eta_j = \frac{\sigma_{UTS,j}}{\sigma_{UTS,b}} * 100 \quad \text{Equation 3.9}$$

$$\eta_{wb} = \frac{\tau_{UTS,wb}}{\tau_{UTS,b}} * 100 \quad \text{Equation 3.10}$$

Where:

- L_{seam} is the seam length;
- $\sigma_{UTS,j}$ is the tensile strength of the welded joint, calculated using the test piece cross-sectional area (14.5x2) mm²;
- $\sigma_{UTS,b}$ is the tensile strength of the weakest base material;
- $\tau_{UTS,wb}$ is the shear strength of the weld bead, calculated using the area of the weld bead¹⁵;
- $\tau_{UTS,b}$ is the shear strength of the weakest base material, obtained using Equation 3.11 [67];

$$\tau_{UTS,b} = 0.75 * \sigma_{UTS,b}$$

Equation 3.11

The tensile tests were performed in the universal testing machine Shimadzu AGS-X (10kN), Figure 3.22. The welded specimens were tested at a constant speed of 1 mm/min, due to their reduced dimensions. Regarding the material characterization tests, the PA6 and PA66 specimens were tested at a speed of 5 mm/min, while the PA66 GF30 was tested at a speed of 2 mm/min.

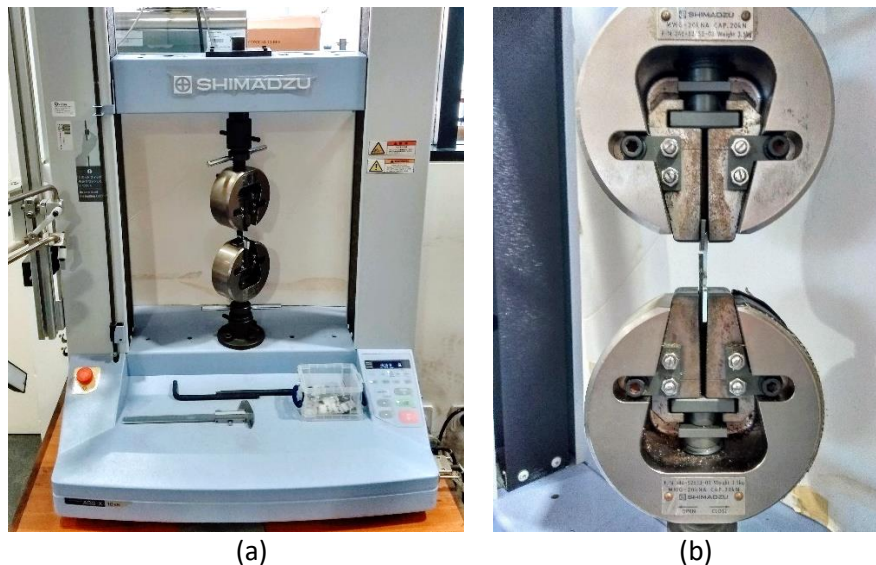


Figure 3.22 – (a) Universal testing machine Shimadzu AGS-X (10 kN); (b) close-up of the test fixtures.

During the lap shear test, it was necessary to add shims on each side of the test piece to minimize bending moments and subsequent flexure, as shown in Figure 3.23.

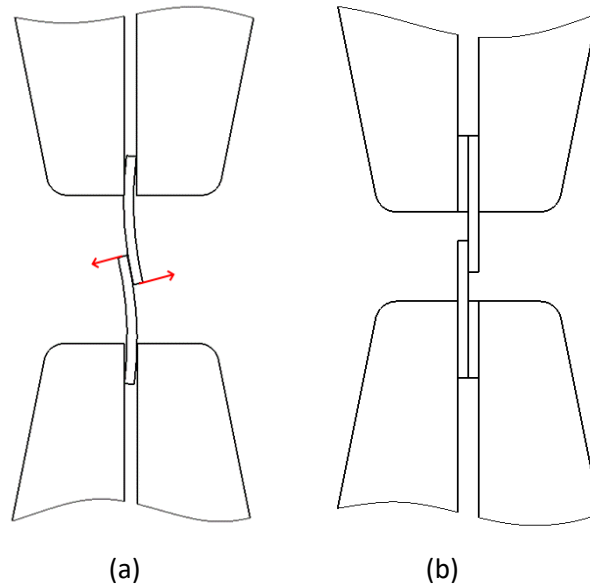


Figure 3.23 - a) Schematic representation of a lap shear test in which flexure of the parts occurs due to bending moments; b) Schematic representation of a lap shear test where shims were added to reduce flexure.

3.9 DIAMETER MEASUREMENT

In order to calculate the shear strength, it was first necessary to measure the weld seam width. However, due to difficulty in measuring this value accurately as well as the variability it generates in the results, a theoretical width was obtained based on the observed diameter at the interface, during spot welding (Figure 3.24), as proposed in ref. [38]. The interior circle was considered for the measurement, whereas the exterior perimeter was assumed to correspond to the HAZ.

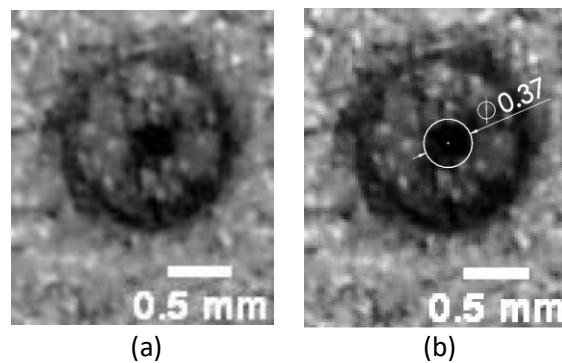
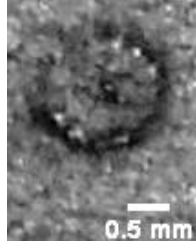
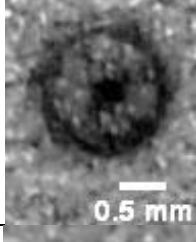
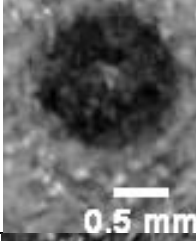
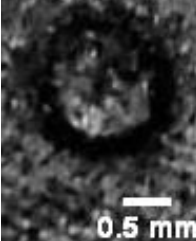
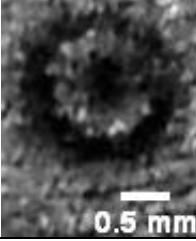


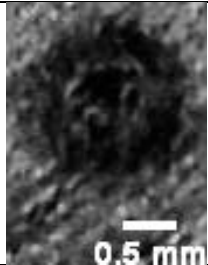
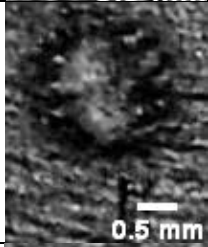
Figure 3.24 - Photograph of the welding spot corresponding to the sample N1-2 (a) and of the measuring process (b).

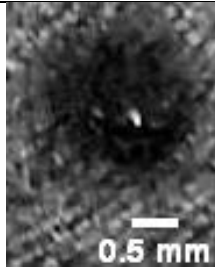
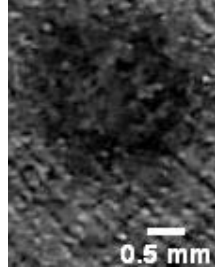
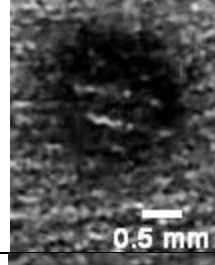
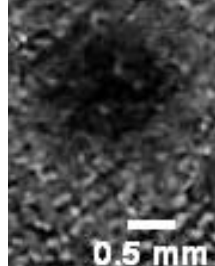
In Table 3.13, the results from these measurements are presented along with photographs of the spots, for PA66N¹⁷.

Table 3.13 - Measurements of the spot diameter generated in the laser absorbing part for the PA66N/PA66 GF30 pair.

Material	Group	Sample	Theoretical Beam Diameter [mm]	Photograph of the spot	Measured diameter [mm]	Average measured Diameter [mm]
PA66N	N	N1-1	0.6		0.37	0.37 ± 0.01
		N1-2			0.37	
		N1-3			0.36	
	O	O1-1	0.9		0.43	0.43 ± 0.01
		O1-2			0.42	

¹⁷ Diameter measurements for PA6N/PA66 GF30 can be consulted on appendix B.1.

		O1-3			0.43	
p	1.2	P1-1		0.66	0.64 ± 0.02	
		P1-2		0.64		
		P1-3		0.61		
		Q		1.5		Q1-1
Q1-2	0.75					

		Q1-3			0.70	
	R	R1-1	2		0.99	0.98 ± 0.01
		R1-2			0.97	
		R1-3			0.98	

According to Table 3.13, the diameters specified by the laser welding machine do not correspond to the actual weld spot diameter. This is caused by scattering, which is more prevalent in semi-crystalline polymers such as PA6 and PA66 [23].

In this case, for PA66N, the reduction in diameter is between [39-53] %, as shown in Table 3.13, while for PA6N, the reduction is within [18-50] %, as shown in Appendix B.1, and corroborated by the findings in ref. [51]. The slightly higher percent reduction observed in PA66N is to be expected, as PA66 has lower transmittance when compared to PA6, due to its higher level of crystallinity [11], as mentioned previously.



4 RESULTS AND DISCUSSION



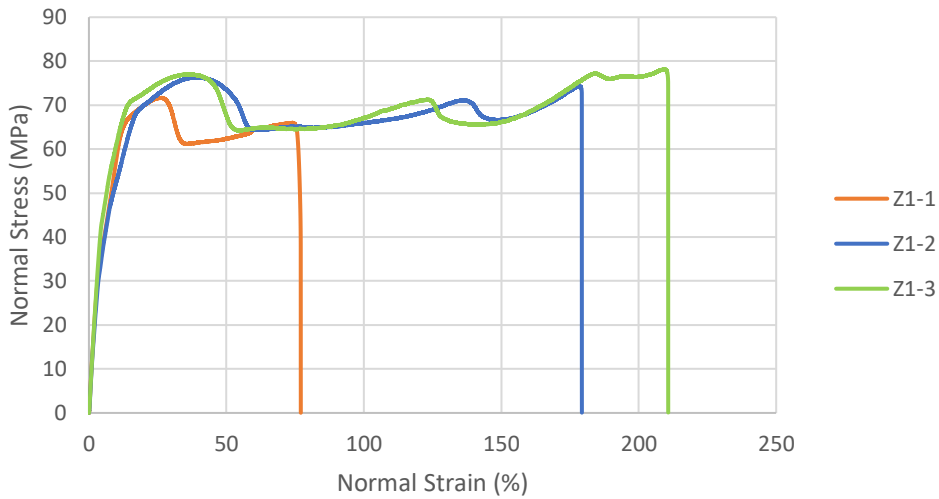
4.1 MATERIAL CHARACTERIZATION

The tables below summarize the results obtained in the tensile tests performed to characterize the three different materials used.

From the analysis of those results it is evident that PA66N and PA6N both show higher toughness and ductility when compared to PA66 GF30. Additionally, PA66N (75.36 MPa) has the highest tensile strength, while PA66 GF30 has the lowest (51.73 MPa). PA66N generally possesses higher mechanical strength relative to PA6N [55], however, the tensile strength obtained with PA66 GF30 is underwhelming. This can be caused either by material defects or machining direction.

When compared to the tensile strength indicated by the manufacturers [53], [58], [61], all of the results obtained are inferior, however, as stated in ISO 527-2 [68], results obtained from small specimens are not comparable those obtained from regular size standard specimens.

Table 4.1 - Summary of the tensile test results for PA66N.

PA66 Natural	
A_i (mm ²)	L_i (mm)
10	15
P_{max} (N)	
753.58 ± 37.17	
PA66N Sample	
	
Tensile stress-strain curves ¹⁸	
	
σ_{UTS} (MPa)	
75.36 ± 3.72	

¹⁸ The test Z1-1 should be repeated as the specimen fractured at a strain of 77%, well below the other tests.

Table 4.2 - Summary of the tensile test results for PA6N.



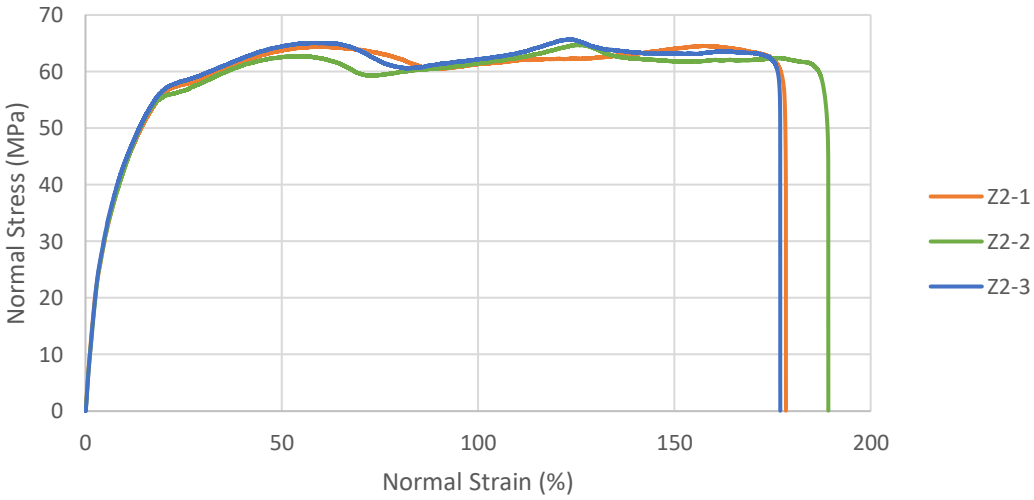


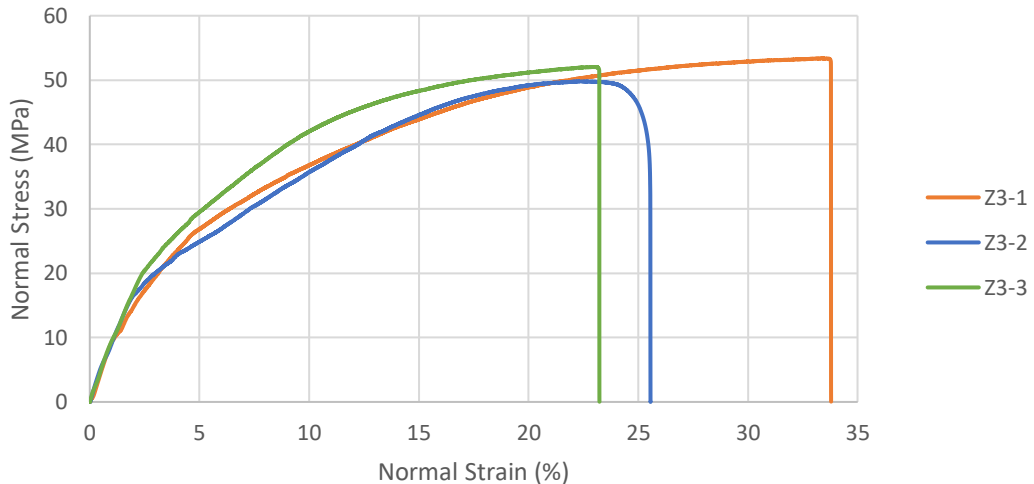
PA6 Natural	
A_i (mm ²)	L_i (mm)
10	15
P_{max} (N)	
649.34 ± 7.02	
PA6N Sample	
	
Tensile stress-strain curves	
	
σ_{UTS} (MPa)	
64.93 ± 0.70	

Table 4.3 - Summary of the tensile test results for PA66 GF30.

PA66 GF30 Black	
A_i (mm ²)	L_i (mm)
10	15
P_{max} (N)	
517.32 ± 19.38	
PA66 GF30 Black Sample	
	
Tensile stress-strain curves	
	
σ_{UTS} (MPa)	
51.73 ± 1.94	

4.2 MATERIAL COMPARISON

From observation of Figure 4.1, it is evident that the pair PA66N/PA66GF30 yields considerably better results, reaching a weld bead efficiency of almost 87% (42% higher than the pair PA6N/PA66GF30) and surpassing 33 MPa of weld bead shear strength, even though, the failure mode remained interfacial.

Additionally, the weld joint strength of PA66N/PA66GF30 was equally superior, reaching a weld joint efficiency of 35% (53% higher than PA6N/PA66GF30), although the overall results were low (Figure 4.2). This is due to the existence of only one weld bead, which naturally yields low joint strengths, as the area considered is the test piece cross-sectional area.

The results obtained were expected, since most materials are more compatible with themselves than with any other material. Accordingly, PA66N/PA66 GF30 was the combination chosen to use in the parameter optimization process.

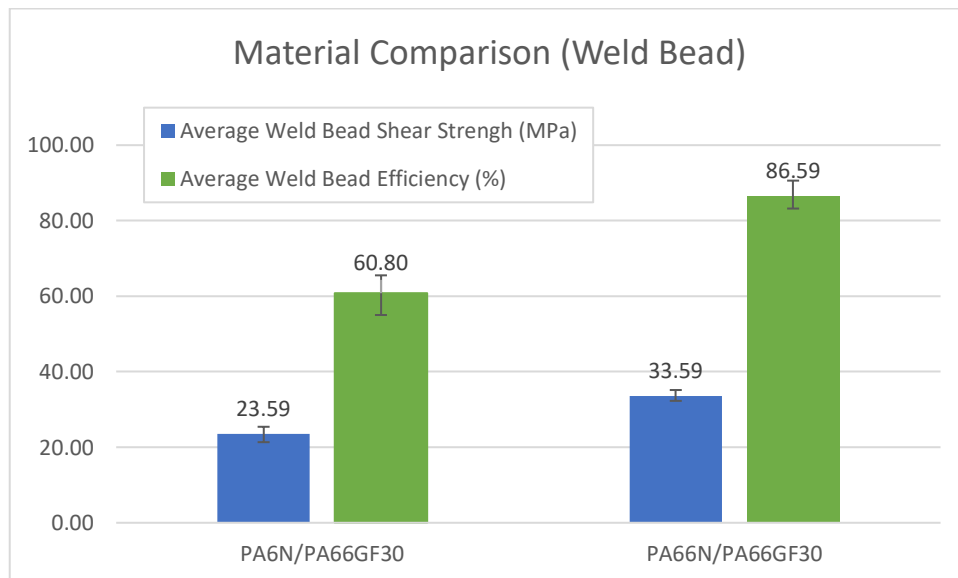


Figure 4.1 - Bar chart comparing the Weld Bead Shear Strength and Efficiency of PA6 and PA66N (Group H)^{19,20}.

¹⁹ The error bars used in the graphs throughout this study represent the maximum and minimum values obtained from the lap shear tests.

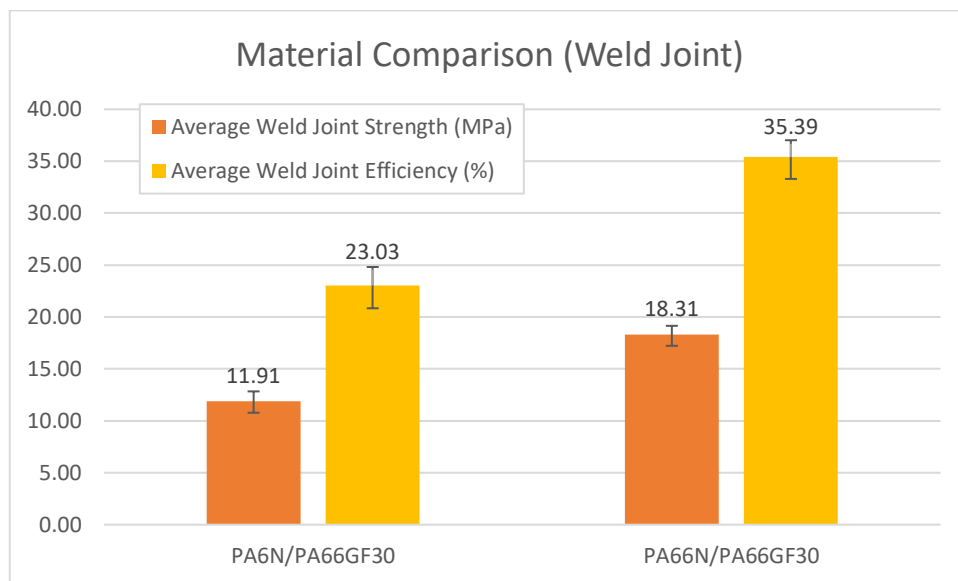


Figure 4.2 - Bar chart comparing the Weld Joint Strength and Efficiency of PA6 and PA66N (Group H)²⁰.

²⁰ The stress-strain curves corresponding to the material comparison can be found in appendix C.1.

4.3 PROCESS WINDOW DEFINITION

In this section, the results obtained from the evaluation of single parameter influence on the laser welding process will be presented and discussed.

4.3.1 Evaluation of Peak Power

In Figure 4.3, it is possible to observe that the weld strength increases with peak power, as concluded in [37], but only up to, approximately, 27.5%, with a process window between 22.5-32.5%. This may be due to material degradation caused by excessive power.

Moreover, this range of values of peak power are unusually high for polymers, and there is no sufficient variation across the results. Furthermore, in terms of shear strength, the results do not surpass 22 MPa, which is rather low. This may be due to the presence of grease or dirt in the test piece surface due to improper cleaning or surface roughness.

Due to the factors mentioned previously, lower values of power range (3-20%) will be considered in the final tests.

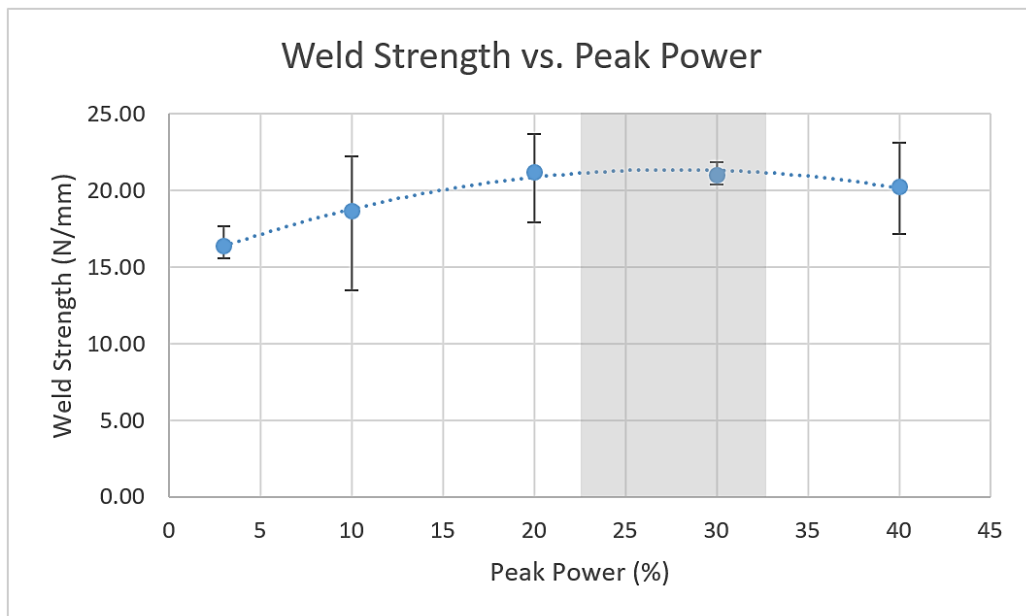


Figure 4.3 - Effect of Peak Power on Weld Strength (Group A)²¹.

²¹ The stress-strain curves corresponding to Group A can be found in appendix C.2.

4.3.2 Evaluation of Pulse Width

According to Figure 4.4, the weld strength reaches a maximum at a pulse width of 20 ms, thereby yielding a process window between 15-25 ms. Even though, the pulse width is considered to be a fine-tuning parameter [34], in this case, there is a noticeable increase in the weld strength when varying this parameter.

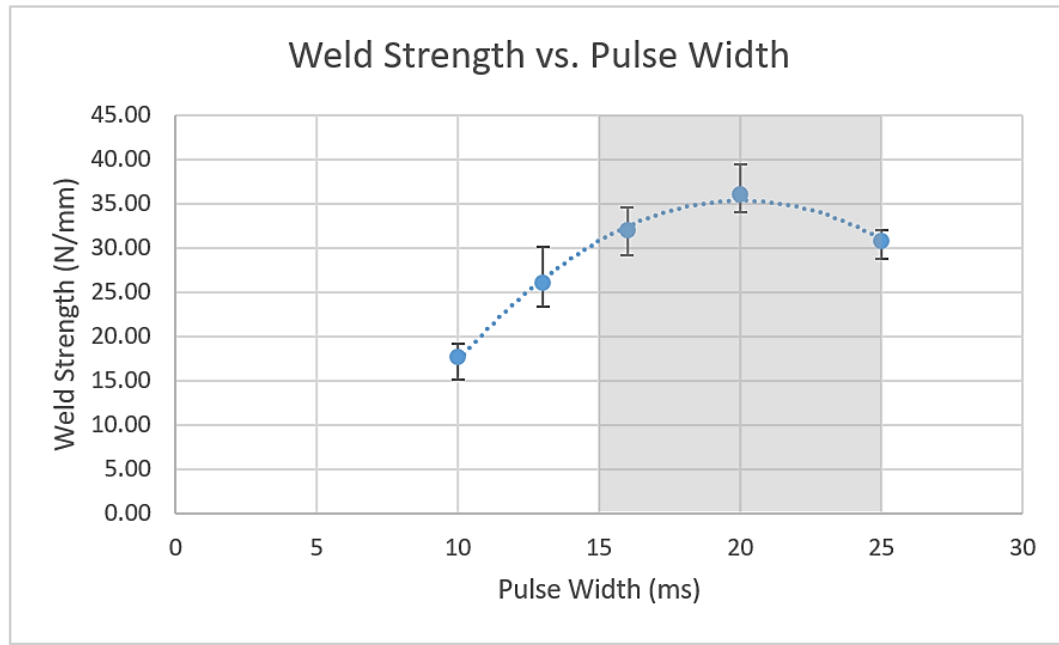


Figure 4.4 - Effect of Pulse Width on Weld Strength (Group B)²².

²² The stress-strain curves corresponding to Group B can be found in appendix C.3.

4.3.3 Evaluation of Overlap

The effective penetration increases with increasing weld spot overlap [34]. Penetration depth does not benefit the welding quality in LTW, as it reduces conduction between the parts at the interface. Therefore, weld strength should decrease with increasing overlap. As Figure 4.5 shows, weld strength increased with overlap instead, up to 80% of overlap. This likely occurs due to the fact that an increase in overlap also increases average power, which has more influence on weld strength than a possible detrimental effect of penetration depth, up to 80%. Beyond this point, material damage becomes significant.

Upon observation of Figure 4.5, a process window was defined between 70-90%.

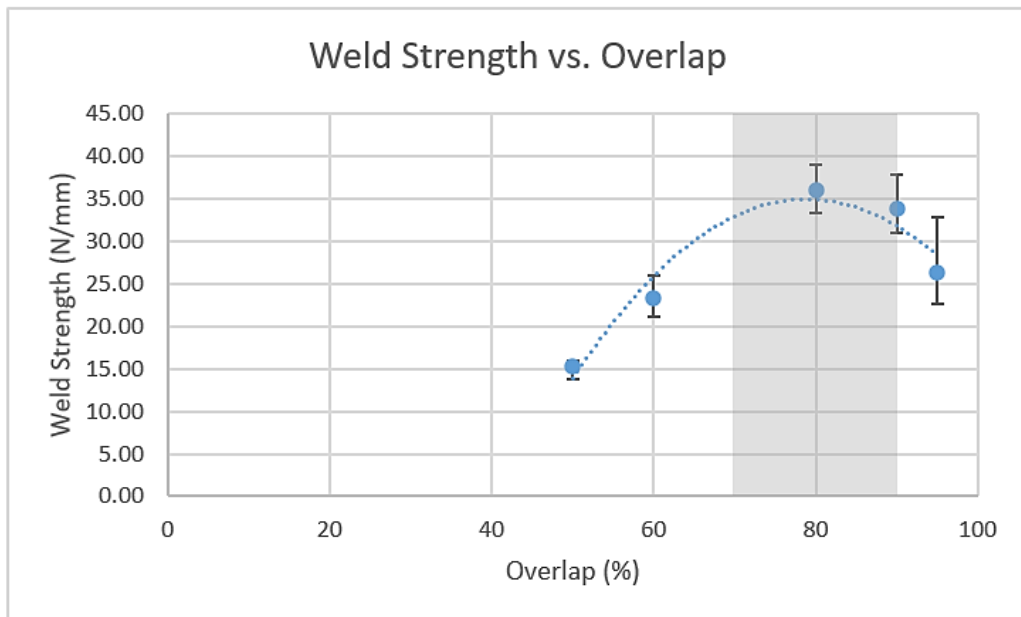


Figure 4.5 - Effect of Overlap on Weld Strength (Group C)²³.

²³ The stress-strain curves corresponding to Group C can be found in appendix C.4.

4.3.4 Evaluation of Laser Beam Diameter

As Figure 4.6 indicates, the weld strength increases with increasing laser beam diameter up to $\phi 1.5$ mm, decreasing slightly beyond this point, although more tests should be performed. More specifically, sample D3 ($\phi 1.2$ mm) should be repeated, as it is seemingly an outlier, thus having a negative impact on the shape of the trendline. Notwithstanding, the process window is defined in the range 1.25-1.75 mm.

This results from the wider weld seam created by a bigger weld spot, which benefits the weld strength [28]. However, when the diameter is further increased beyond the threshold, the weld strength is begins to decline, due to loss of power density, which results in lack of fusion [39].

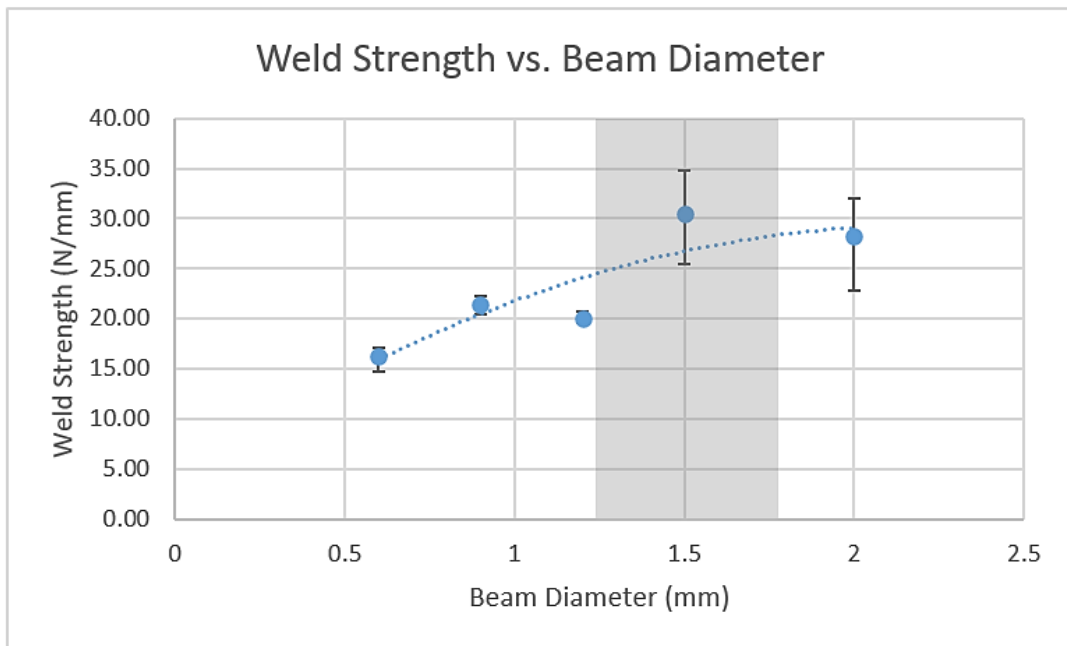


Figure 4.6 - Effect of the Laser Beam Diameter on Weld Strength (Group D)²⁴.

²⁴ The stress-strain curves corresponding to Group D can be found in appendix C.5.

4.3.5 Evaluation of Scan Speed

From previous studies [38], [5], it is known that higher values of weld strength are achieved at low welding speeds. In this case (Figure 4.7), that decrease only begins after 5 mm/s, which shows that below this value, the scan speeds are excessively low, allowing for cooling in the welding seam. Consequently, for the scan speed, the process window was chosen in the 3-7 mm/s range.

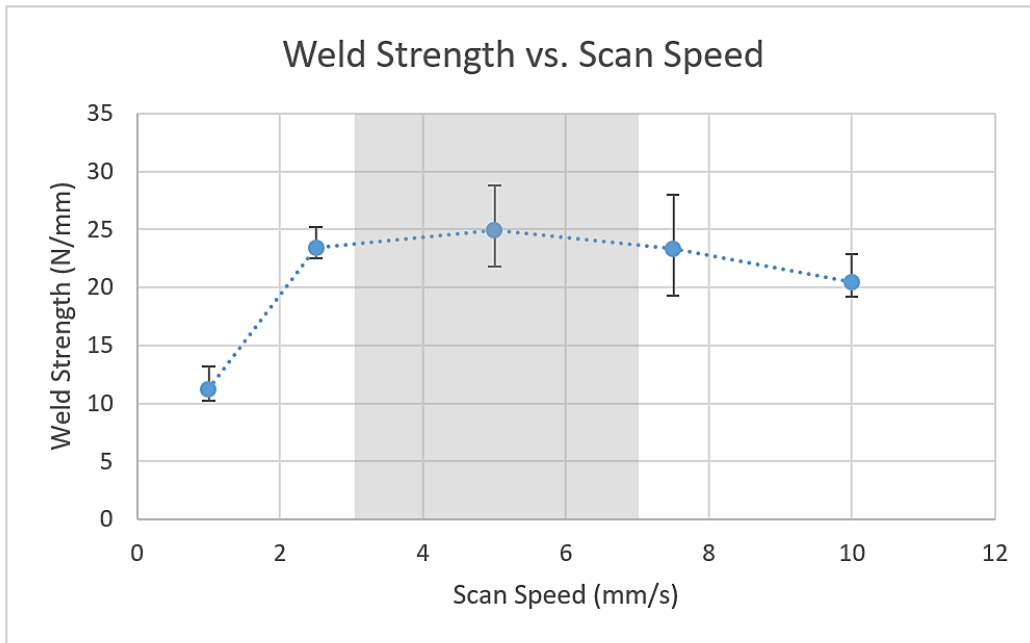


Figure 4.7 - Effect of the Scan Speed on Weld Strength (Group F)²⁵.

²⁵ The stress-strain curves corresponding to Group F can be found in appendix C.6

4.4 OPTIMAL PARAMETERS

Figure 4.8 shows that the sample X1 with weld strength of 23.51 N/mm corresponds to the parameter set that yielded the best results. This suggests that lower values of peak power improve the weld strength, meaning that the subsequent parameter sets were excessive.

Moreover, the previous remark highlights one of the limitations of this experimental procedure. By evaluating one parameter at a time, the process window is dependent on the remaining parameters that were kept constant. This means that increasing a parameter while the rest have low values is not the same as combining the optimum values of each parameter together.

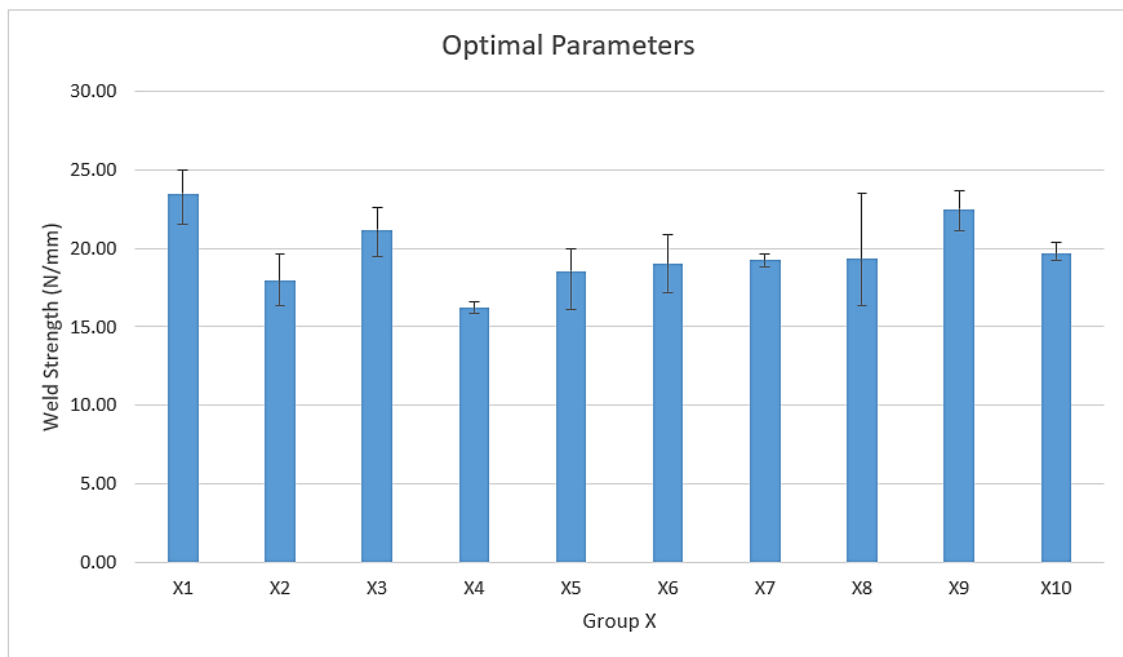


Figure 4.8 - Bar Graph comparing the weld strength obtained for the samples of the optimal parameters (Group X)²⁶.

²⁶ The stress-strain curves corresponding to Group X can be found in appendix C.7.

4.5 GLOBAL RESULTS

Due to the limitations of the optimization approach used, it is pertinent to compare the results globally to assess if any of the parameter combinations used are, in fact, better than the optimal parameters used.

As Figure 4.9 shows, the sample C3 resulted in the highest weld strength (36.07 N/mm). The parameters used during the test are summarized in Table 4.4. This confirms that the optimal sample is not within Group X and, therefore, more tests should be carried out with parameters closer to these ones.

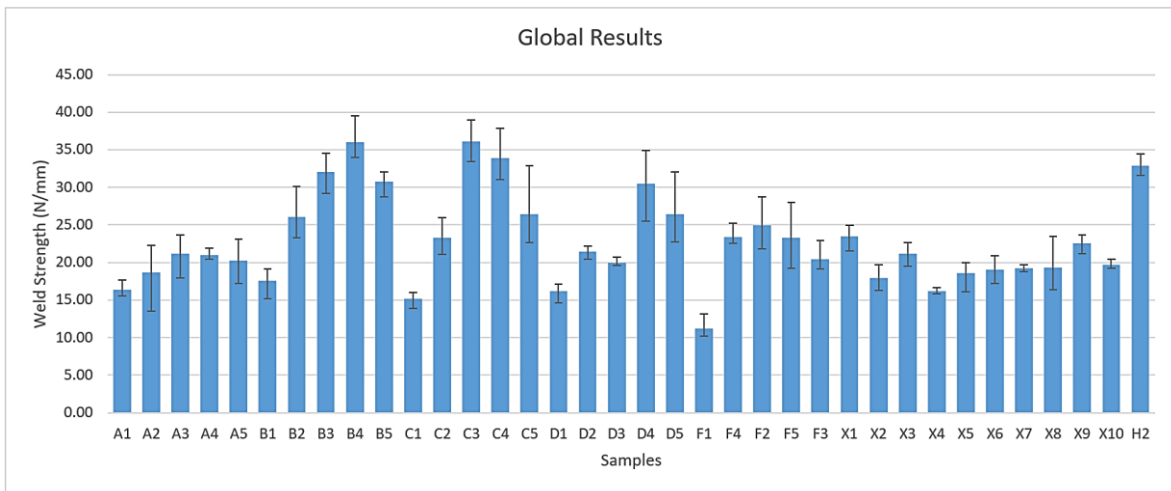


Figure 4.9 - Bar chart comparing all the samples welded during the experimental procedure.

Table 4.4 - Parameter set corresponding to the sample C3.

Test piece	Peak Power [%]	Pulse Width [ms]	Overlap [%]	Beam Diameter [mm]	Pulse Energy [J]	Scan Speed [mm/s]
C3	3	10	80	2	7.8	5

4.6 COMPARISON TO THE BASE MATERIAL

In order to gauge the significance of the results obtained, the weld bead shear strength as well as the weld bead efficiency were calculated for the sample that yielded the highest weld strength. As indicated in Figure 4.10, a maximum of 36.81 MPa of shear strength was achieved, corresponding to more than 94% of shear strength of the weakest base material (PA66 GF30, $\tau_{UTS,b} = 38.80$ MPa).

Concerning the weld joint strength (Figure 4.11), a value of 18 MPa was obtained, corresponding to a weld joint efficiency of over 34% (relative to PA66 GF30, $\sigma_{UTS,b} = 51.73$ MPa). As mentioned previously, these values are low, but foreseeable.

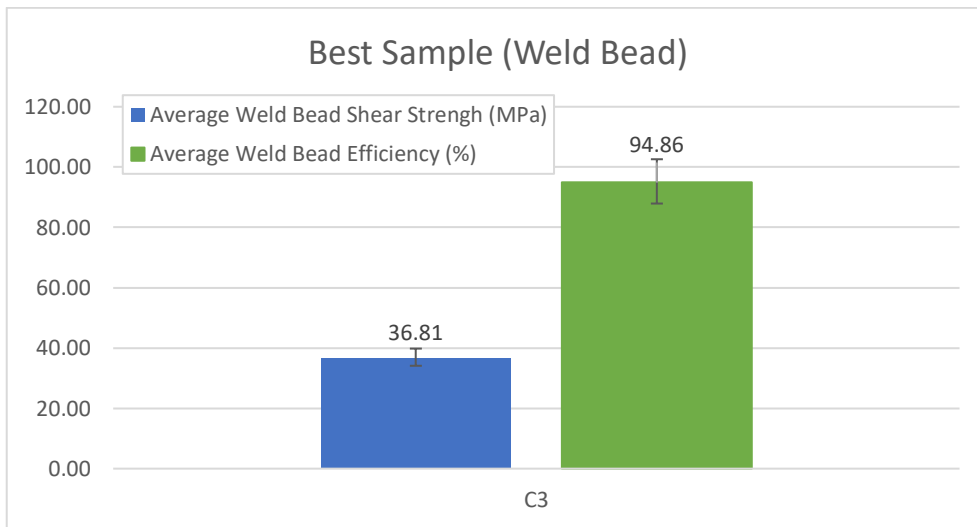


Figure 4.10 - Average Weld Bead Strength and Efficiency obtained in the sample C3²⁷.

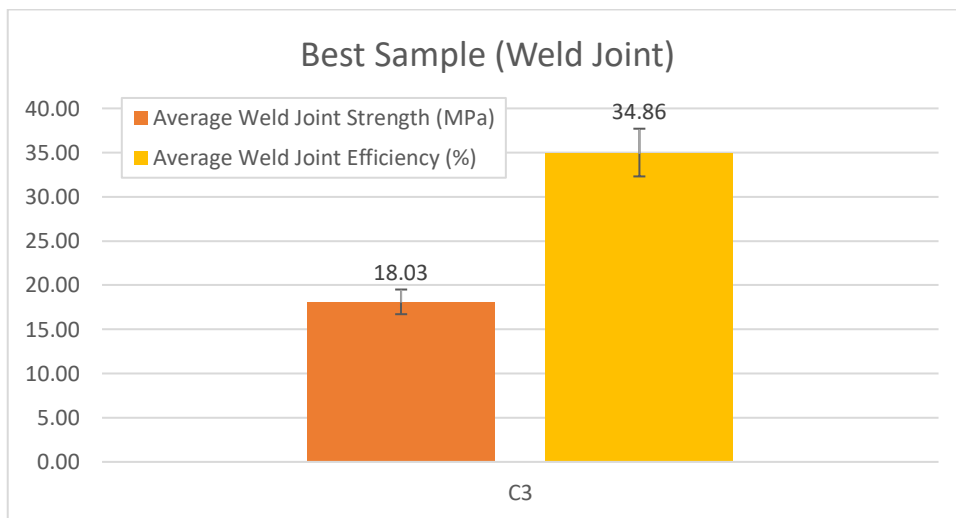


Figure 4.11 - Average Weld Joint Strength and Efficiency obtained in the sample C3²⁷.

²⁷ The stress-strain curves corresponding to the best sample can be found in appendix C.8.



5 CONCLUSIONS

This study aimed to find the best parameters for pulsed Nd:YAG LASER welding of thermoplastic polymers to thermoplastic matrix composites. To this end, after selecting the most suitable material, each parameter was varied individually, in order to obtain the process windows. Lastly, final tests were carried out in which the best parameters were combined, based on the results obtained previously.

After completing the investigation, it is possible to draw the following conclusions:

- I. In LTW, a polymer will generally be more compatible with itself, than with dissimilar polymers, as shown in Figure 4.1 and Figure 4.3. This finding is supported by the weldability chart shown in Figure 2.37;
- II. Clamp pressure is not a crucial parameter in LTW of polymers, even though, a small amount pressure (at least 0.2MPa) must be applied when welding;
- III. Weld strength increases with peak power (Figure 4.3), pulse width (Figure 4.4), overlap (Figure 4.5) and beam diameter (Figure 4.6), up to a threshold. Beyond this point, material degradation and excessive penetration limit the conduction and bonding between parts;
- IV. Although, the pulse width is considered to be a fine-tuning parameter [6], there was a noticeable increase in the weld strength when varying this parameter, unlike peak power;
- V. The overlap impacts the weld strength significantly. Below 70% of overlap, the weld strength decreases quickly;
- VI. As the literature suggests (Figure 2.19), the weld strength increases with decreasing scan speed (Figure 4.7), except for excessively small values;
- VII. The experimental procedure applied revealed itself to be inadequate and the optimal set of parameters was obtained outside of Group X;
- VIII. The highest weld efficiency was obtained in sample C3 (95% weld bead efficiency and 35% weld joint efficiency) with low values of peak power, but high overlap.
- IX. At the interface between the LT (Laser Transparent) and LA (Laser Absorbent) partners, a diameter reduction occurs for both PA6N and PA66N, caused by scattering. The percent reduction is higher for PA66N due to its higher level of crystallinity and consequent lower transmittance.



6 FUTURE WORK

This study focused on the optimization of laser parameters such as peak power, pulse width, scan speed, etc. However, more research is needed in many other areas related to LTW, specifically:

- Innovative welding approaches:
 - LTW using filler material (i.e., monofilament);
 - LTW using Inter-layer material (i.e., films);
- Evaluation of the influence of other parameters such as:
 - Weight percent of colorants and reinforcements;
 - Surface finish;
 - Crystallinity;
 - Part thickness;
 - Air gap;
- Perform near-infrared spectroscopy to evaluate material properties such as transmittance and reflectance;
- Perform shear tests on the selected materials, to obtain a more accurate value for the shear strength of the base material ($\tau_{UTS,b}$);
- Welding of thermoplastics to composites with a dissimilar matrix;
- Welding of natural color composites;
- Selection of amorphous thermoplastics more suitable for LTW, such as PC/PMMA;
- Evaluation of the influence of the pulse shape on weld strength;
- Application of an alternative optimization process consisting of determining the process “characteristic curve” by plotting weld strength vs. line energy. Using the optimal line energy, different values of laser power and scan speed can be combined to assess its impact on weld strength.



REFERENCES

- [1] N. Amanat, N.L. James, D.R. McKenzie, Welding methods for joining thermoplastic polymers for the hermetic enclosure of medical devices, *Med. Eng. Phys.* 32 (2010) 690–699. <https://doi.org/10.1016/j.medengphy.2010.04.011>.
- [2] S. Berger, F. Oefele, M. Schmidt, Laser transmission welding of carbon fiber reinforced thermoplastic using filler material—A fundamental study, *J. Laser Appl.* 27 (2015) S29009. <https://doi.org/10.2351/1.4906391>.
- [3] K. van der Straeten, C. Engelmann, A. Olowinsky, A. Gillner, Laser transmission welding of long glass fiber reinforced thermoplastics, *High-Power Laser Mater. Process. Lasers, Beam Deliv. Diagnostics, Appl. IV.* 9356 (2015) 93560H. <https://doi.org/10.1117/12.2079566>.
- [4] P. Jaeschke, D. Herzog, H. Haferkamp, C. Peters, A.S. Herrmann, Laser transmission welding of high-performance polymers and reinforced composites - A fundamental study, *J. Reinf. Plast. Compos.* 29 (2010) 3083–3094. <https://doi.org/10.1177/0731684410365365>.
- [5] P. Jaeschke, V. Wippo, O. Suttman, L. Overmeyer, Advanced laser welding of high-performance thermoplastic composites, *J. Laser Appl.* 27 (2015) S29004. <https://doi.org/10.2351/1.4906379>.
- [6] H. Liu, Y. Jiang, W. Tan, X. Wang, Enhancement of the laser transmission weldability between polyethylene and polyoxymethylene by plasma surface treatment, *Materials (Basel)*. 11 (2017). <https://doi.org/10.3390/ma11010029>.
- [7] B. Acherjee, State-of-art review of laser irradiation strategies applied to laser transmission welding of polymers, *Opt. Laser Technol.* 137 (2021) 106737. <https://doi.org/10.1016/j.optlastec.2020.106737>.
- [8] L.F.M. da Silva, M.S. El-Zein, P. Martins, *Advanced Joining Processes: Welding, Plastic Deformation, and Adhesion*, Elsevier, 2020.
- [9] V.A. Kagan, Innovations in laser welding of thermoplastics: This advanced technology is ready to be commercialized, *SAE Tech. Pap.* (2002). <https://doi.org/10.4271/2002-01-2011>.
- [10] R. Klein, *Laser welding of plastics: materials, processes and industrial applications*, John Wiley & Sons, 2012.
- [11] B. Acherjee, Laser transmission welding of polymers – A review on process fundamentals, material attributes, weldability, and welding techniques, *J. Manuf. Process.* 60 (2020) 227–246. <https://doi.org/10.1016/j.jmapro.2020.10.017>.
- [12] I. Mingareev, F. Weirauch, A. Olowinsky, L. Shah, P. Kadwani, M. Richardson, Welding of polymers using a 2 μm thulium fiber laser, *Opt. Laser Technol.* 44 (2012) 2095–2099. <https://doi.org/10.1016/j.optlastec.2012.03.020>.
- [13] S. Berger, M. Schmidt, Laser transmission welding of CFRTP using filler material, *Phys. Procedia.* 56 (2014) 1182–1190. <https://doi.org/10.1016/j.phpro.2014.08.033>.
- [14] BASF, *Laser Welding of Engineering Plastics*, (2013) 1–8.
- [15] M.J. Troughton, *Handbook of plastics joining: a practical guide*, William Andrew, 2008.
- [16] C. Hopmann, M. Weber, New concepts for laser transmission welding of dissimilar



- thermoplastics, *Prog. Rubber, Plast. Recycl. Technol.* 28 (2012) 157–172. <https://doi.org/10.1177/147776061202800402>.
- [17] X. Wang, X. Zhong, W. Liu, B. Liu, H. Liu, Investigation on enhancement of weld strength between PMMA and PBT in laser transmission welding—Using intermediate material, *J. Appl. Polym. Sci.* 133 (2016) 1–14. <https://doi.org/10.1002/app.44167>.
- [18] H. Liu, Y. Jiang, W. Tan, G. Chen, W. Liu, X. Wang, The study of laser transmission joining PA66 and PVC with large compatibility difference, *J. Manuf. Process.* 26 (2017) 252–261. <https://doi.org/10.1016/j.jmapro.2017.02.024>.
- [19] H. Liu, G. Chen, H. Jiang, D. Guo, Z. Yan, X. Wu, P. Li, X. Wang, Performance and mechanism of laser transmission joining between glass fiber-reinforced PA66 and PC, *J. Appl. Polym. Sci.* 133 (2016) 1–8. <https://doi.org/10.1002/app.43068>.
- [20] V. Kagan, A. Chambers, R. Bray, Forward to better understanding of optical characterization and development of colored polyamides for the infra-red/laser welding, Part II - Family of colored polyamides, *J. Reinf. Plast. Compos.* 22 (2003) 593–602. <https://doi.org/10.1177/073168403023284>.
- [21] M. Chen, G. Zak, P.J. Bates, Effect of carbon black on light transmission in laser welding of thermoplastics, *J. Mater. Process. Technol.* 211 (2011) 43–47. <https://doi.org/10.1016/j.jmatprotec.2010.08.017>.
- [22] V. Kagan, R.G. Bray, Advantages and limitations of laser welding technology for semi-crystalline reinforced plastics, *1218 (2018) 1218–1227*. <https://doi.org/10.2351/1.5059784>.
- [23] E. Azhikannickal, P.J. Bates, G. Zak, Use of thermal imaging to characterize laser light reflection from thermoplastics as a function of thickness, laser incidence angle and surface roughness, *Opt. Laser Technol.* 44 (2012) 1491–1496. <https://doi.org/10.1016/j.optlastec.2011.12.013>.
- [24] X.F. Xu, P.J. Bates, G. Zak, Effect of glass fiber and crystallinity on light transmission during laser transmission welding of thermoplastics, *Opt. Laser Technol.* 69 (2015) 133–139. <https://doi.org/10.1016/j.optlastec.2014.12.025>.
- [25] C.Y. Wang, P.J. Bates, G. Zak, Optical properties characterization of thermoplastics used in laser transmission welding: Scattering and absorbance, *Adv. Mater. Res.* 97–101 (2010) 3836–3841. <https://doi.org/10.4028/www.scientific.net/AMR.97-101.3836>.
- [26] M. Rhew, A. Mokhtarzadeh, A. Benatar, Diode laser characterization and measurement of optical properties of polycarbonate and high-density polyethylene, *Annu. Tech. Conf. - ANTEC, Conf. Proc.* 1 (2003) 1056–1060.
- [27] F.G. Bachmann, U.A. Russek, Laser welding of polymers using high-power diode lasers, *Laser Process. Adv. Mater. Laser Microtechnologies.* 5121 (2003) 385. <https://doi.org/10.1117/12.515630>.
- [28] B. Acherjee, Laser transmission welding of polymers – A review on welding parameters, quality attributes, process monitoring, and applications, *J. Manuf. Process.* 64 (2021) 421–443. <https://doi.org/10.1016/j.jmapro.2021.01.022>.
- [29] A. Jansson, S. Kouvo, V. Kujanpää, Preliminary investigations of laser welding of plastics in massproduction (504), *ICALEO 2004 - 23rd Int. Congr. Appl. Laser Electro-Optics, Congr.*



- Proc. 504 (2004). <https://doi.org/10.2351/1.5060280>.
- [30] J.D. Van De Ven, A.G. Erdman, Bridging gaps in laser transmission welding of thermoplastics, *J. Manuf. Sci. Eng. Trans. ASME*. 129 (2007) 1011–1018. <https://doi.org/10.1115/1.2769731>.
- [31] U.A. Russek, H. Staub, A. Palmen, H. Kind, Simultaneous laser beam welding of thermoplastics - Innovations and challenges, *ICALEO 2003 - 22nd Int. Congr. Appl. Laser Electro-Optics, Congr. Proc.* 604 (2003). <https://doi.org/10.2351/1.5060068>.
- [32] N. Ahmed, *New developments in advanced welding*, Elsevier, 2005.
- [33] U.M. CORPORATION, *Nd: YAG laser welding*, 2003.
- [34] A. Miyachi America Inc, *Laser Welding Fundamentals*, (2016) 42. www.amadamiyachi.com.
- [35] U.-A. Russek, Laser beam welding of polymers with high power diode lasers joining innovation for micro and macro technologies, 483 (2018) 483–491. <https://doi.org/10.2351/1.5059900>.
- [36] B. Acherjee, D. Misra, D. Bose, K. Venkadeshwaran, Prediction of weld strength and seam width for laser transmission welding of thermoplastic using response surface methodology, *Opt. Laser Technol.* 41 (2009) 956–967. <https://doi.org/10.1016/j.optlastec.2009.04.007>.
- [37] B. Acherjee, A.S. Kuar, S. Mitra, D. Misra, S. Acharyya, Experimental investigation on laser transmission welding of PMMA to ABS via response surface modeling, *Opt. Laser Technol.* 44 (2012) 1372–1383. <https://doi.org/10.1016/j.optlastec.2011.12.029>.
- [38] N. Amanat, C. Chaminade, J. Grace, D.R. McKenzie, N.L. James, Transmission laser welding of amorphous and semi-crystalline poly-ether-ether-ketone for applications in the medical device industry, *Mater. Des.* 31 (2010) 4823–4830. <https://doi.org/10.1016/j.matdes.2010.04.051>.
- [39] B. Acherjee, A.S. Kuar, S. Mitra, D. Misra, Selection of process parameters for optimizing the weld strength in laser transmission welding of acrylics, *Proc. Inst. Mech. Eng. Part B J. Eng. Manuf.* 224 (2010) 1529–1536. <https://doi.org/10.1243/09544054JEM1854>.
- [40] A. Jansson, S. Kouvo, A. Salminen, V. Kujanpää, The effect of parameters on laser transmission welding of polymers, *ICALEO 2003 - 22nd Int. Congr. Appl. Laser Electro-Optics, Congr. Proc.* 609 (2003). <https://doi.org/10.2351/1.5060071>.
- [41] B. Baylis, Y.P. Huang, D. Watt, Welding thermoplastic elastomers to polypropylene with a diode laser, *ICALEO 2002 - 21st Int. Congr. Appl. Laser Electro-Optics, Congr. Proc.* 171828 (2002). <https://doi.org/10.2351/1.5066211>.
- [42] B.K. Prabhakaran, R., Kontopoulou, M., Zak, G., Bates, P. J., & Baylis, Contour laser - Laser-transmission welding of glass reinforced nylon 6, *J. Thermoplast. Compos. Mater.* 19 (2006) 427–439. <https://doi.org/10.1177/0892705706062200>.
- [43] N. Oliveira, A.J. Pontes, In mold laser welding for high precision polymer based optical components, *AIP Conf. Proc.* 1593 (2014) 204–208. <https://doi.org/10.1063/1.4873764>.
- [44] V. Kagan, A. Chambers, R. Bray, A. Chambers, Forward to better understanding of optical characterization and development of colored polyamides for the infra-red/laser welding: Part I - Efficiency of polyamides for infra-red welding, *J. Reinf. Plast. Compos.* 22 (2003) 533–547. <https://doi.org/10.1106/073168403023283>.



- [45] B. Acherjee, 3-D FE heat transfer simulation of quasi-simultaneous laser transmission welding of thermoplastics, *J. Brazilian Soc. Mech. Sci. Eng.* 41 (2019) 1–13. <https://doi.org/10.1007/s40430-019-1969-3>.
- [46] V.A. Kagan, G.P. Pinho, Laser Transmission Welding of Semicrystalline Thermoplastics - Part II: Analysis of Mechanical Performance of Welded Nylon, *J. Reinf. Plast. Compos.* 23 (2004) 95–107. <https://doi.org/10.1177/0731684404029360>.
- [47] B. Acherjee, A.S. Kuar, S. Mitra, D. Misra, Application of grey-based Taguchi method for simultaneous optimization of multiple quality characteristics in laser transmission welding process of thermoplastics, *Int. J. Adv. Manuf. Technol.* 56 (2011) 995–1006. <https://doi.org/10.1007/s00170-011-3224-7>.
- [48] J. Rösler, H. Harders, M. Bäke, *Mechanical Behaviour of Engineering Materials*, 2007. <https://doi.org/10.1007/978-3-540-73448-2>.
- [49] J. WILLIAM D. CALLISTER, D.G. RETHWISCH, *Materials Science and Engineering*, Wiley, 2013.
- [50] A.K. Kaw, *Mechanics of Composite Materials*, 2013. <https://doi.org/10.1016/C2011-0-05224-9>.
- [51] A.B. Pereira, F.A.O. Fernandes, A.B. de Morais, J. Quintão, Mechanical strength of thermoplastic polyamide welded by Nd:YAG laser, *Polymers (Basel)*. 11 (2019) 1–9. <https://doi.org/10.3390/polym11091381>.
- [52] T.B. Juhl, D. Bach, R.G. Larson, J.D. Christiansen, E.A. Jensen, Predicting the laser weldability of dissimilar polymers, *Polymer (Guildf)*. 54 (2013) 3891–3897. <https://doi.org/10.1016/j.polymer.2013.05.053>.
- [53] Ensinger, TECAMID 66 natural - Data Sheet, (n.d.). https://www.ensinger-online.com/modules/public/sheet/createsheet.php?SID=792&FL=0&FILENAME=TECAMID_66_natural_0.PDF&ZOOM=1.2.
- [54] Ensinger, TECAMID 66 natural, (n.d.). <https://www.ensingerplastics.com/en/shapes/products/pa66-tecamid-66-natural> (accessed May 20, 2021).
- [55] POLY LANEMA®, ERTALON® 66 SA Technical Data Sheet, (n.d.). https://www.polylanema.pt/client/files/0000000001/ertalon-66sa-datasheet_1723.pdf (accessed May 4, 2021).
- [56] Mitsubishi Chemical Advanced Materials, ERTALON® 6 SA Technical Data Sheet, (n.d.) 66. https://media.mcam.com/fileadmin/quadrant/documents/QEPP/EU/Product_Data_Sheets_PDF/GEP/Ertalon_6_SA_PDS_E_01042019.pdf.
- [57] Mitsubishi Chemical Advanced Materials, ERTALON® 6 SA, (n.d.). <https://www.mcam.com/eu-en/products/engineering-plastics/engineering-80-160-c/ertalonr-and-nylatronr-products/ertalonr-6-sa/>.
- [58] POLY LANEMA®, ERTALON® 6 SA Technical Data Sheet, (n.d.). https://www.polylanema.pt/client/files/0000000001/ertalon-6sa-datasheet_1400.pdf.
- [59] Mitsubishi Chemical Advanced Materials, Ertalon® GF30 PA66 - Data Sheet, (n.d.). <https://camsad.mcam.com/api/datasheet/single?productId=17&language=en-US>.



- [60] Mitsubishi Chemical Advanced Materials, Ertalon® 66 GF30, (n.d.). <https://www.mcam.com/en/products/engineering-plastics/engineering-80-160/extruded-cast-nylons/ertalonr-66-gf30/> (accessed May 20, 2021).
- [61] POLY LANEMA®, ERTALON® 66 GF30 Technical Data Sheet, (n.d.). https://www.polylanema.pt/client/files/0000000001/ertalon-66gf30-datasheet_1724.pdf (accessed May 4, 2021).
- [62] C.M. Costa, Soldadura Laser Termoplástico-Metal, Universidade de Aveiro, 2021.
- [63] LaserMaq, SISMA SWA Catalog, (n.d.). <https://www.lasermaq.pt/wp-content/uploads/2017/01/catalogo-swa-lm-d-open.pdf> (accessed May 4, 2021).
- [64] SISMA S.p.A., INSTRUCTION MANUAL OF USE AND MAINTENANCE, (2017).
- [65] N.E. Dowling, Mechanical Behavior of Materials, Fourth Edi, Pearson Education, 2013. <http://marefateadyan.nashriyat.ir/node/150>.
- [66] W. Smith, Foundations of Material Science and Engineering, Third, The McGraw-Hill Companies, 2004.
- [67] P.A. Tres, Designing Plastic Parts for Assembly, 2017. <https://doi.org/10.3139/9781569906699.fm>.
- [68] ISO 527-2: Plastics - Determination of tensile properties - Part 2: Test conditions for moulding and extrusion plastics, Int. Organ. Stand. (1993).



APPENDIX A

A.1 TECAMID 66 NATURAL DATASHEET



TECAMID 66 natural - Stock Shapes (rods, plates, tubes)

Chemical Designation

PA 66 (Polyamide 66)

Colour

ivory opaque

Density

1.15 g/cm³

Data generated directly after machining (standard climate Germany).

Main features

- good slide and wear properties
- electrically insulating
- good wear properties
- high strength
- good weldable and bondable
- resistant to many oils, greases and fuels
- high toughness

Target Industries

- mechanical engineering
- aircraft and aerospace technology
- electronics
- food technology
- automotive industry

Mechanical properties	parameter	value	unit	norm	comment
Tensile strength	50mm/min	85	MPa	DIN EN ISO 527-2	(1) For tensile test: specimen type 1b
Modulus of elasticity (tensile test)	1mm/min	3500	MPa	DIN EN ISO 527-2	(2) For flexural test: support span 64mm, norm specimen.
Tensile strength at yield	50mm/min	84	MPa	DIN EN ISO 527-2	(3) Specimen 10x10x10mm
Elongation at yield	50mm/min	7	%	DIN EN ISO 527-2	(4) Specimen 10x10x50mm, modulus range between 0.5 and 1% compression.
Elongation at break (tensile test)	50mm/min	70	%	DIN EN ISO 527-2	(5) For Charpy test: support span 64mm, norm specimen.
Flexural strength	2mm/min, 10 N	110	MPa	DIN EN ISO 178	(2) n.b. = not broken
Modulus of elasticity (flexural test)	2mm/min, 10 N	3100	MPa	DIN EN ISO 178	(6) Specimen in 4mm thickness
Compression strength	1% / 2% / 5% 5mm/min, 10 N	20/35/81	MPa	EN ISO 604	(3)
Compression modulus	5mm/min, 10 N	2700	MPa	EN ISO 604	(4)
Impact strength (Charpy)	max. 7,5J	n.b.	kJ/m ²	DIN EN ISO 179-1eU	(5)
Notched impact strength (Charpy)	max. 7,5J	5	kJ/m ²	DIN EN ISO 179-1eA	
Ball indentation hardness		175	MPa	ISO 2039-1	(6)
Thermal properties	parameter	value	unit	norm	comment
Glass transition temperature		47	°C	DIN EN ISO 11357	(1) Found in public sources.
Melting temperature		258	°C	DIN EN ISO 11357	(2) Found in public sources.
Service temperature	short term	170	°C		Individual testing regarding application conditions is mandatory.
Service temperature	long term	100	°C		
Thermal expansion (CLTE)	23-60°C, long.	11	10 ⁻⁵ K ⁻¹	DIN EN ISO 11359-1;2	
Thermal expansion (CLTE)	23-100°C, long.	12	10 ⁻⁵ K ⁻¹	DIN EN ISO 11359-1;2	
Specific heat		1.5	J/(g*K)	ISO 22007-4:2008	
Thermal conductivity		0.36	W/(K*m)	ISO 22007-4:2008	
Electrical properties	parameter	value	unit	norm	comment
surface resistivity		10 ¹⁴	Ω	DIN IEC 60093	
volume resistivity		10 ¹⁴	Ω*cm	DIN IEC 60093	
Other properties	parameter	value	unit	norm	comment
Water absorption	24h / 96h (23°C)	0.2 / 0.4	%	DIN EN ISO 62	(1) Ø ca. 50mm, h=13mm
Resistance to hot water/ bases		(+)	-	-	(2) (+) limited resistance
Resistance to weathering		-	-	-	(3) - poor resistance
Flammability (UL94)	corresponding to	HB	-	DIN IEC 60695-11-10;	(4) Corresponding means no listing at UL (yellow card). The information might be taken from resin, stock shape or estimation. Individual testing regarding application conditions is mandatory.

Our information and statements reflect the current state of our knowledge and shall inform about our products and their applications. They do not assure or guarantee chemical resistance, quality of products and their merchantability in a legally binding way. Our products are not defined for use in medical or dental implants. Existing commercial patents have to be observed. The corresponding values and information are no minimum or maximum values, but guideline values that can be used primarily for comparison purposes for material selection. These values are within the normal tolerance range of product properties and do not represent guaranteed property values. Therefore they shall not be used for specification purposes. Unless otherwise noted, these values were determined by tests at reference dimensions (typically rods with diameter 40-60 mm according to DIN EN 15860) on extruded and machined specimen. As the properties depend on the dimensions of the semi-finished products and the orientation in the component (esp. in reinforced grades), the material may not be used without a separate testing under individual circumstances. The customer is solely responsible for the quality and suitability of products for the application and has to test usage and processing prior to use. Data sheet values are subject to periodic review, the most recent update can be found at www.ensingerplastics.com. Technical changes reserved.



A.2 ERTALON 6 SA DATASHEET

Polyamide

Ertalon® 6 SA

**MITSUBISHI CHEMICAL
ADVANCED MATERIALS**

PRODUCT DATA SHEET

Physical properties (indicative values [■])

PROPERTIES			
Colour	-	-	White, Black
Density	ISO 1183-1	g/cm ³	1.14
Water absorption:			
- after 24 immersion in water of 23 °C (1)	ISO 62	%	1.28
- at saturation in water of 23 °C	-	%	9
Thermal Properties (2)			
Melting temperature (DSC, 10 °C/min)	ISO 11357-1/-3	°C	220
Glass transition temperature (DSC, 20 °C/min) - (3)	ISO 11357-1/-2	°C	
Thermal conductivity at 23 °C	-	W/(K.m)	0.28
Coefficient of linear thermal expansion:			
- average value between 23 and 60 °C	-	mV/(m.K)	90 x 10 ⁻⁶
- average value between 23 and 100 °C	-	mV/(m.K)	105 x 10 ⁻⁶
Temperature of deflection under load:			
- method A: 1.8 MPa	ISO 75-1/-2	°C	70
Max. allowable service temperature in air:			
- continuously : for min. 20,000 h (4)	-	°C	70
Min. service temperature (5)	-	°C	-40
Flammability (6):			
- according to UL 94 (3 mm thickness)	-	-	HB
Mechanical Properties at 23 °C (7)			
Tension test (8):			
- tensile strength (9)	ISO 527-1/-2	MPa	80
- tensile strain at yield(9)	ISO 527-1/-2	%	4
- tensile strain at break (9)	ISO 527-1/-2	%	50
- tensile modulus of elasticity (10)	ISO 527-1/-2	MPa	3300
Compression test (11):			
- compressive stress at 1 / 2 / 5 % nominal strain (10)	ISO 604	MPa	31 / 59 / 87
Flexural test (12):			
- flexural strength	ISO 178	MPa	
- flexural modulus of elasticity	ISO 178	MPa	
Charpy impact strength - unnotched (13)	ISO 179-1/1eU	kJ/m ²	no break
Charpy impact strength - notched	ISO 179-1/1eA	kJ/m ²	5.5
Rockwell M-hardness (14)	ISO 2039-2	-	88
Dynamic Coefficient of Friction (-)	ISO 7148-2 (15)	-	0.4-0.6
Wear rate	ISO 7148-2 (15)	µm/km	19
Electrical Properties at 23 °C			
Electric strength (16)	IEC 60243-1	kV/mm	25
Volume resistivity	IEC 60093	Ohm.cm	>10E 14
Surface resistivity	ANSI/ESD STM 11.11	Ohm/sq.	>10E13
Relative permittivity ε _r : - at 1 MHz	IEC 60250	-	3.30
Dielectric dissipation factor tan δ: - at 1 MHz	IEC 60250	-	0.021

Note: 1 g/cm³ = 1,000 kg/m³; 1 MPa = 1 N/mm²; 1 kV/mm = 1 MV/m.

Ertalon® is a registered trademark of Mitsubishi Chemical Advanced Materials.

A.3 ERTALON PA66 GF30 DATASHEET

PRODUCT DATA SHEET

Ertalon® 66 GF30 PA66 / Nylatron® GF30 PA66



Polyamide

Nylatron® GF30 Polyamide PA66 / Ertalon® 66 GF30 Polyamide PA66 is a 30% glass fiber-reinforced grade that offers increased strength, stiffness, creep resistance, and dimensional stability, while also maintaining its excellent wear resistance properties. Due to these characteristics, Nylatron® GF30 PA66 / Ertalon® 66 GF30 PA66 components are often favored as solutions for sleeve and slide bearings, wear pads, rollers, pulleys, scrapers, gear wheels, sprockets, star wheels, and insulators.

	ISO*			ASTM*			
	Test methods	Units	Indicative Values	Test methods	Units	Indicative Values	
Thermal Properties (1)	Melting temperature (DSC, 10°C (50°F) / min)	ISO 11357-1/-3	°C	260	ASTM D3418	°F	500
	Glass transition temperature (DSC, 20°C (68°F) / min) (2)	ISO 11357-1/-2	°C	-	ASTM D3418	°F	-
	Thermal conductivity at 23°C (73°F)	-	W/(K.m)	0.3	-	BTU in./hr.ft.°F)	1.7
	Coefficient of linear thermal expansion (-40 to 150 °C) (-40 to 300°F)	-	-	-	ASTM E-831 (TMA)	µin./in.°F	20
	Coefficient of linear thermal expansion (23 to 60°C) (73°F to 140°F)	-	µm/(m.K)	50	-	-	-
	Coefficient of linear thermal expansion (23 to 100°C) (73°F to 210°F)	-	µm/(m.K)	60	-	-	-
	Heat Deflection Temperature: method A: 1.8 MPa (264 PSI)	ISO 75-1/-2	°C	150	ASTM D648	°F	400
	Continuous allowable service temperature in air (20,000 hrs) (3)	-	°C	110	-	°F	220
	Min. service temperature (4)	-	°C	-20	-	°F	-
	Flammability: UL 94 (3 mm (1/8 in.)) (5)	-	-	V-2	-	-	V-2
Flammability: Oxygen Index	ISO 4589-1/-2	%	-	-	-	-	
Mechanical Properties (6)	Tensile strength	ISO 527-1/-2 (7)	MPa	85	ASTM D638 (8)	PSI	13500
	Tensile strain (elongation) at yield	ISO 527-1/-2 (7)	%	-	-	-	-
	Tensile strain (elongation) at break	ISO 527-1/-2 (7)	%	5	ASTM D638 (8)	%	5
	Tensile modulus of elasticity	ISO 527-1/-2 (9)	MPa	5000	ASTM D638 (8)	KSI	675
	Shear Strength	ASTM D732	MPa	69	ASTM D732	PSI	10000
	Compressive stress at 1 / 2 / 5 % nominal strain	ISO 604 (10)	MPa	43 / 77 / 112	-	-	-
	Compressive strength	-	-	-	ASTM D695 (11)	PSI	18000
	Charpy impact strength - unnotched	ISO 179-1/1eU	kJ/m²	50.0	-	-	-
	Charpy impact strength - notched	ISO 179-1/1eA	kJ/m²	6.0	-	-	-
	Izod impact notched	-	-	-	ASTM D256	ft.Lb./in	-
	Flexural strength	ISO 178 (12)	MPa	-	ASTM D790 (13)	PSI	21000
	Flexural modulus of elasticity	ISO 178 (12)	MPa	-	ASTM D790	KSI	650
	Rockwell M hardness (14)	ISO 2039-2	-	76	ASTM D785	-	75
Shore hardness D (14)	ISO 868	-	80	ASTM D2240	-	-	
Electrical Properties	Electric strength	IEC 60243-1 (15)	kV/mm	27	ASTM D149	Volts/mil	350
	Volume resistivity	IEC 62631-3-1	Ohm.cm	10E13	IEC 62631-3-1	Ohm.cm	-
	Surface resistivity	ANSI/ESD STM 11.11	Ohm.sq.	10E12	ANSI/ESD STM 11.11	Ohm.sq.	10E12
	Dielectric constant at 1 MHz	IEC 62631-2-1	-	3.60	ASTM D150	-	-
	Dissipation factor at 1 MHz	IEC 62631-2-1	-	0.0140	ASTM D150	-	-
Miscellaneous	Colour	-	-	Black	-	-	Black
	Density	ISO 1183-1	g/cm³	1.29	-	-	-
	Specific Gravity	-	-	-	ASTM D792	-	1.29
	Water absorption after 24h immersion in water of 23°C (73°F)	ISO 62 (16)	%	0.39	ASTM D570 (17)	%	0.30
	Water absorption at saturation in water of 23 °C (73°F)	-	%	5.5	ASTM D570 (17)	%	5.5
	Wear rate	ISO 7148-2 (18)	µm/km	11	QTM 55010 (19)	mm³/m³.km	-
	Dynamic Coefficient of Friction (-)	ISO 7148-2 (18)	-	0.25-0.4	QTM 55007 (20)	-	-
	Limiting PV at 100 FPM	-	-	-	QTM 55007 (21)	ft.lbs/in².min	-
	Limiting PV at 0.1 / 1 m/s cylindrical sleeve bearings	-	Mpa.m/s	0.18 / 0.12	-	-	-
	Chemical Resistance	https://www.mcom.com/ntsupp/chemical-resistance-information/			https://www.mcom.com/ntsupp/chemical-resistance-information/		

Note: 1 g/cm³ = 1,000 kg/m³; 1 MPa = 1 N/mm²; 1 kV/mm = 1 MV/m

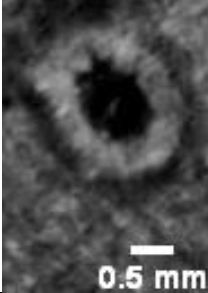
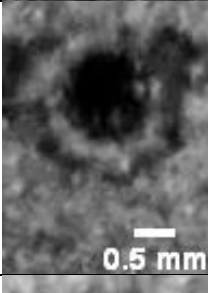
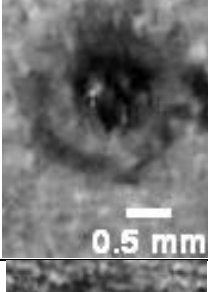
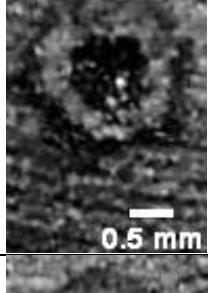
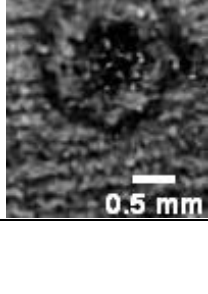
NYP: there is no yield point

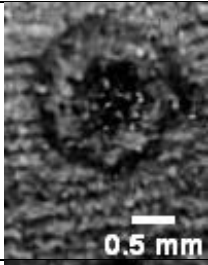
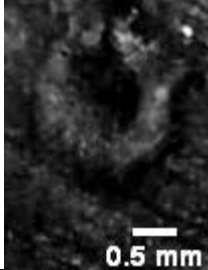
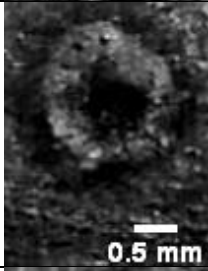
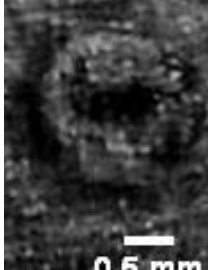

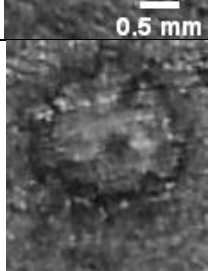
This table, mainly to be used for comparison purposes, is a valuable help in the choice of a material. The data listed here fall within the normal range of product properties of dry material. However, they are not guaranteed and they should not be used to establish material specification limits nor used alone as the basis of design. See the remaining notes on the next page.


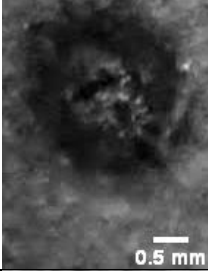
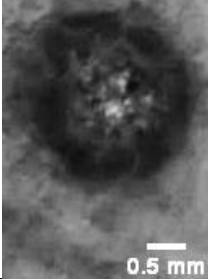
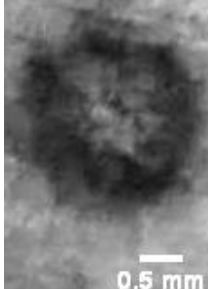
Ertalon® 66 GF30 PA66 / Nylatron® GF30 PA66 is a registered trademark of Mitsubishi Chemical Advanced Materials

APPENDIX B

B.1 DIAMETER MEASUREMENTS FOR PA6N/PA66 GF30

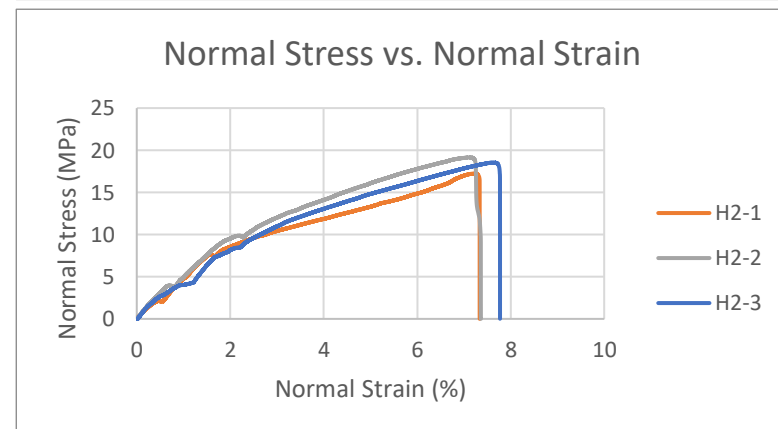
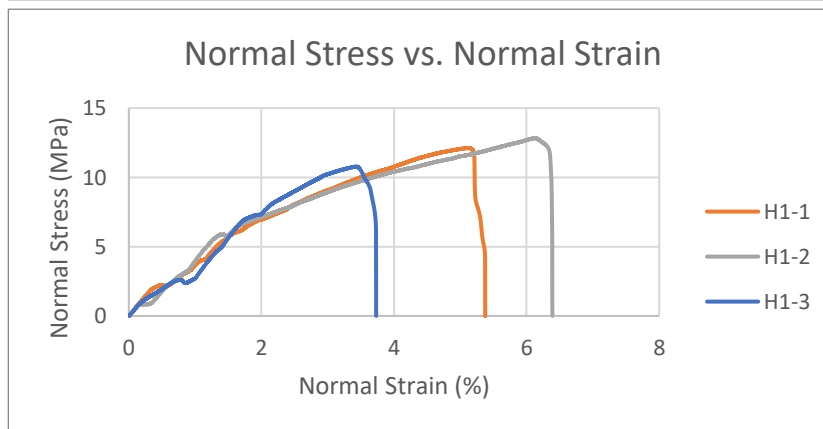
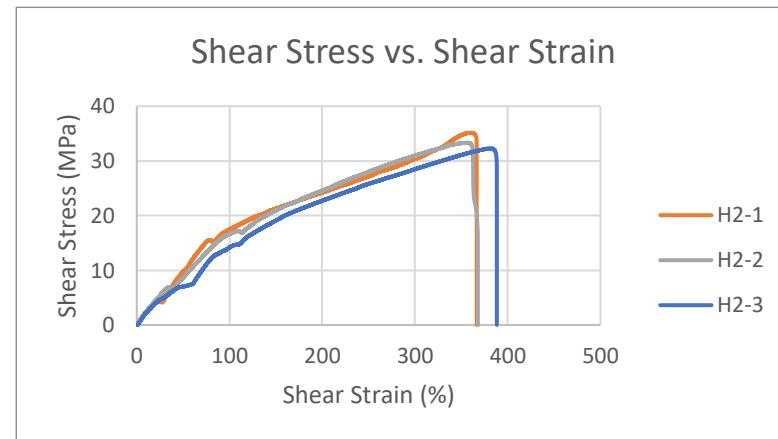
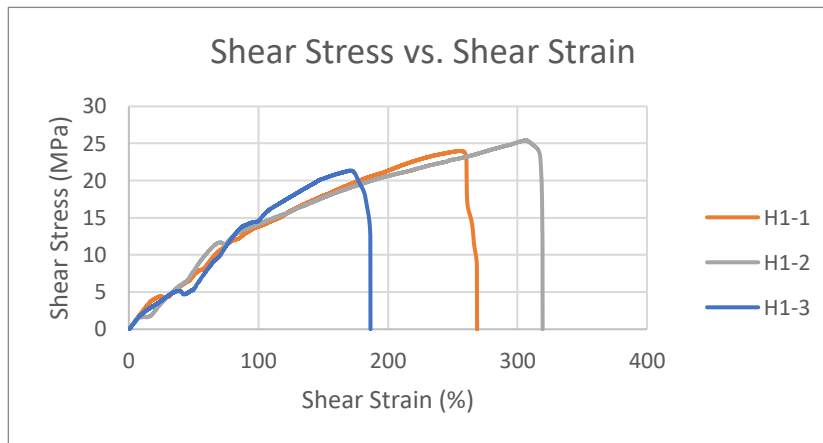
Material	Group	Sample	Theoretical Beam Diameter [mm]	Photograph of the spot	Measured diameter [mm]	Average measured Diameter [mm]
PA6N	S	S1-1	0.6		0.50	0.49±0.01
		S1-2			0.48	
		S1-3			0.50	
	T	T1-1	0.9		0.56	0.58±0.02
		T1-2			0.59	

		T1-3			0.57	
	U	U1-1	1.2		0.68	0.67±0.02
		U1-2			0.67	
		U1-3			0.65	
		V1-1		1.5		
	V1-2		0.77		0.76±0.02	

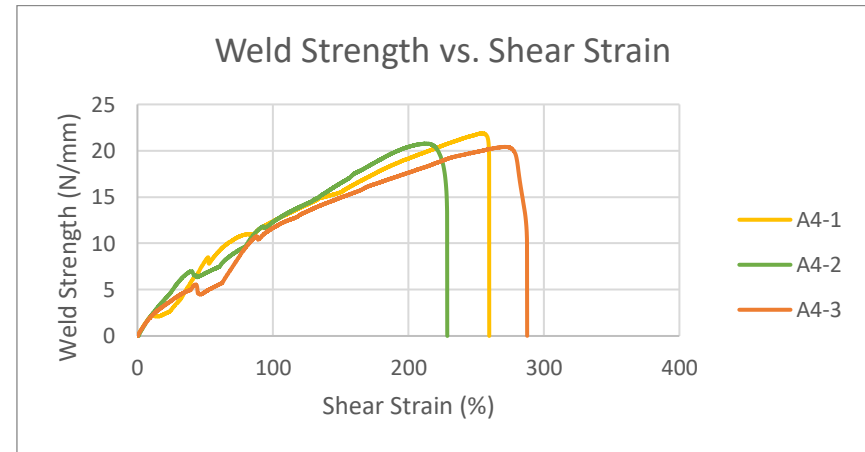
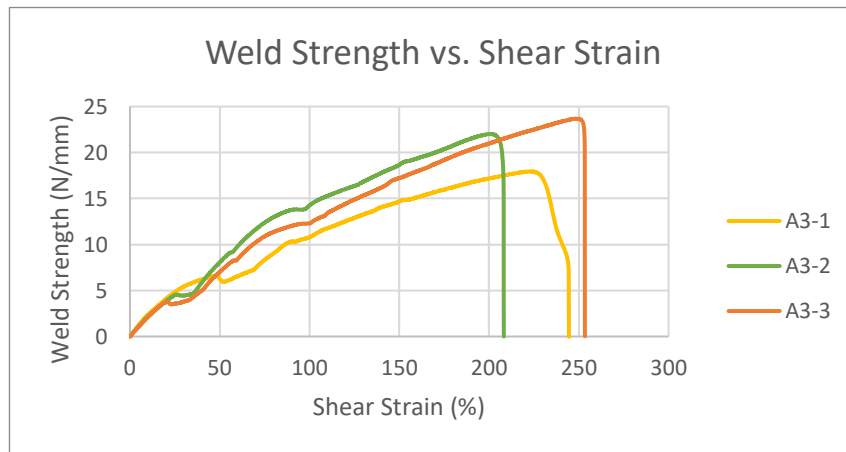
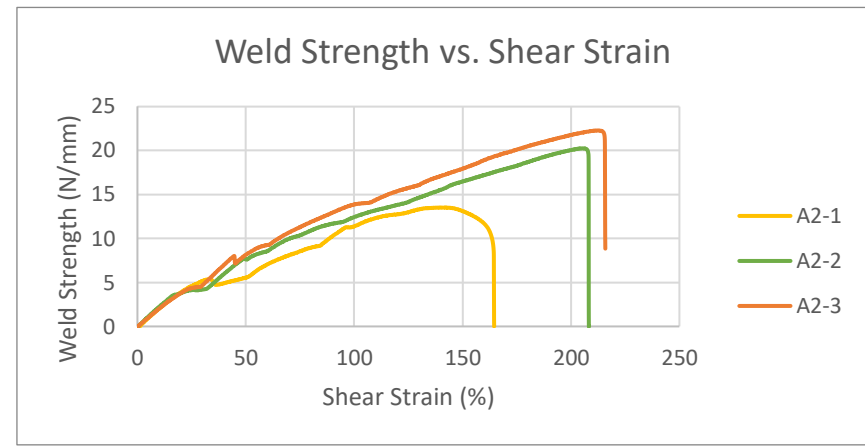
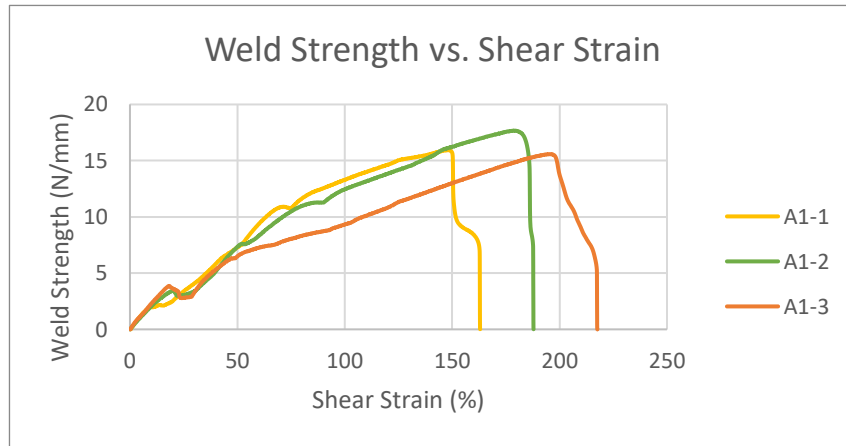
		V1-3			0.74	
W	W	W1-1	2		1.02	1.01±0.01
		W1-2			1.01	
		W1-3			1.00	

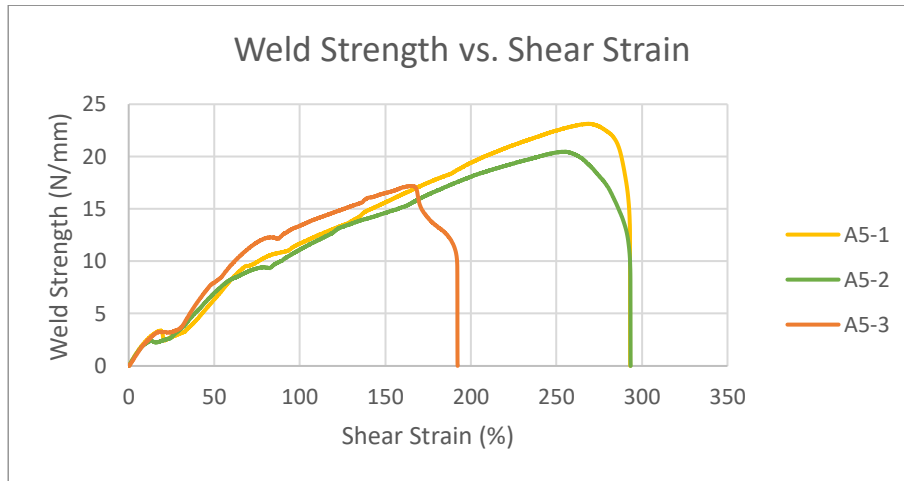
APPENDIX C

C.1 STRESS-STRAIN CURVES (GROUP H)

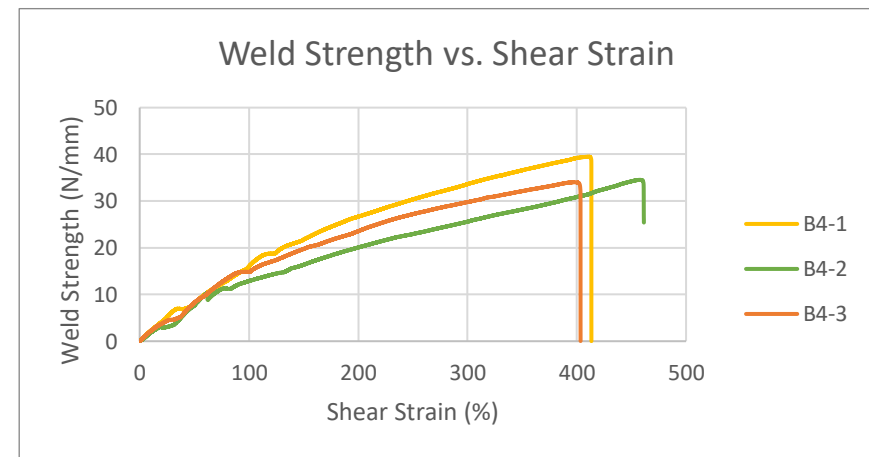
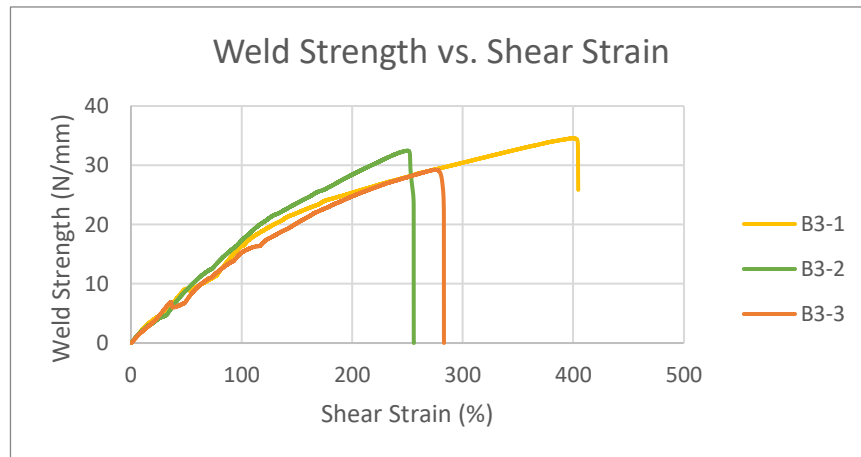
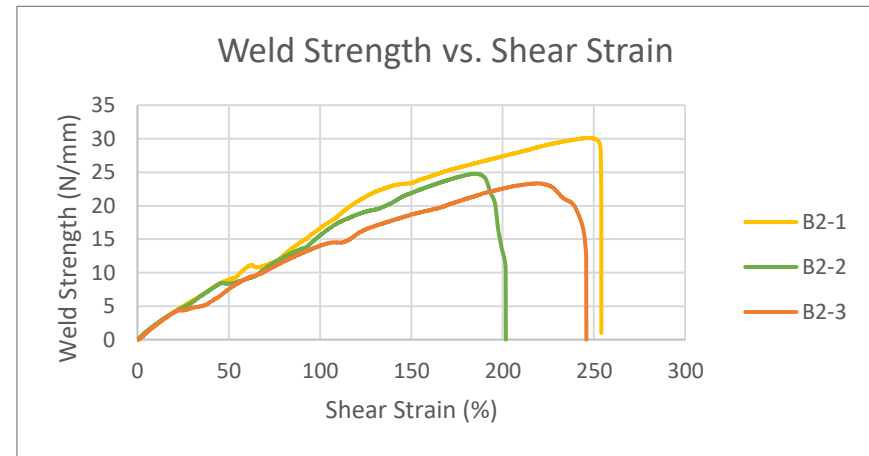
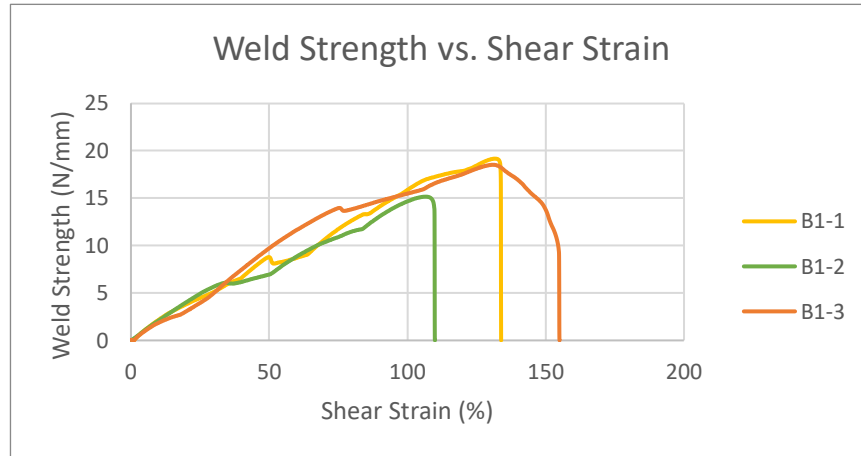


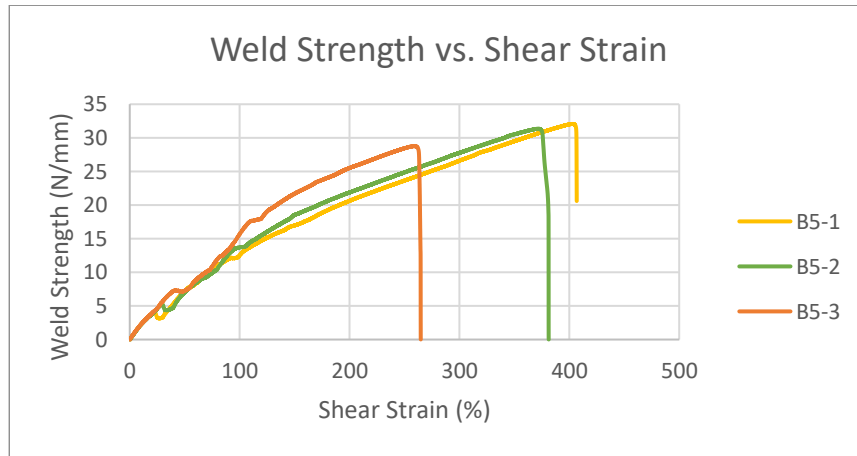
C.2 WELD STRENGTH-STRAIN CURVES (GROUP A)



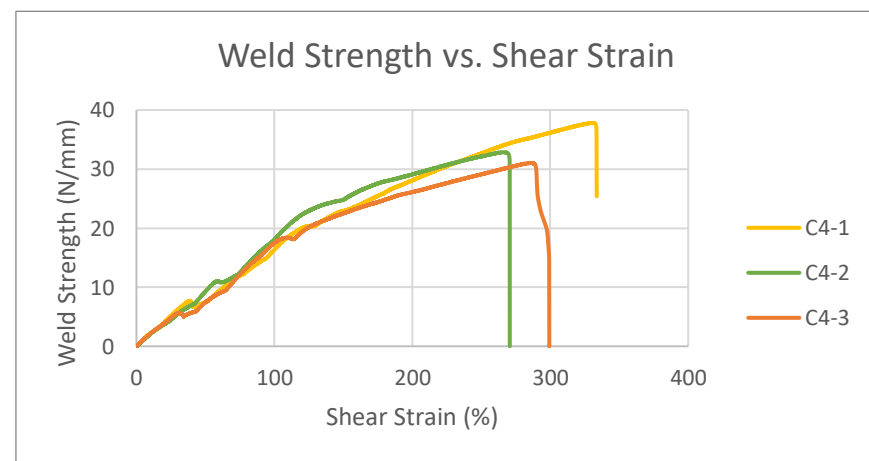
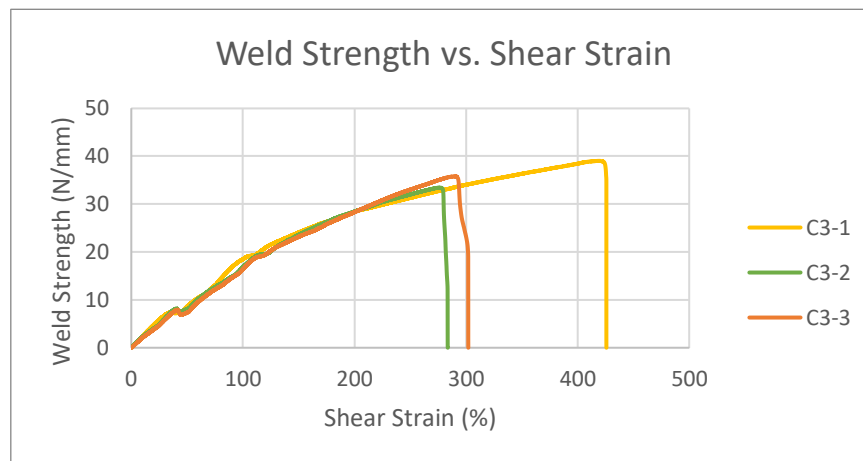
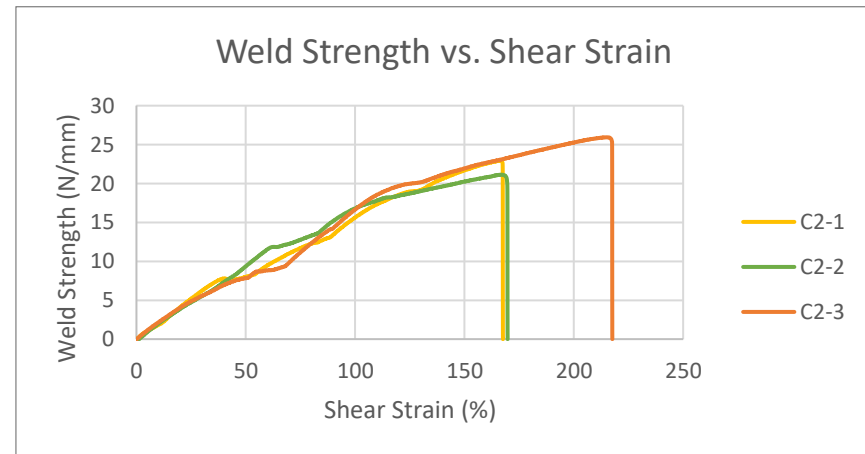
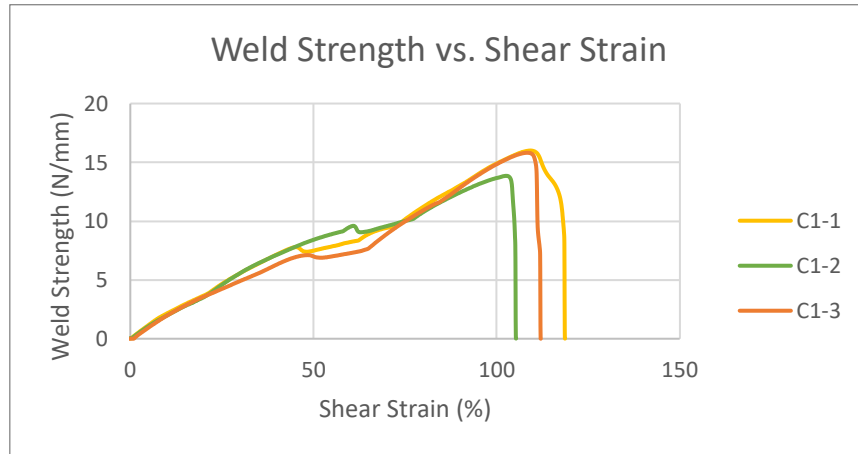


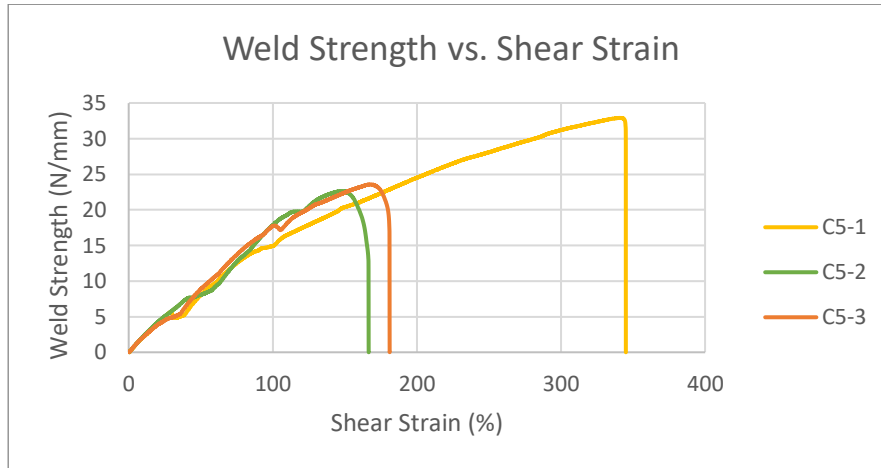
C.3 WELD STRENGTH-STRAIN CURVES (GROUP B)



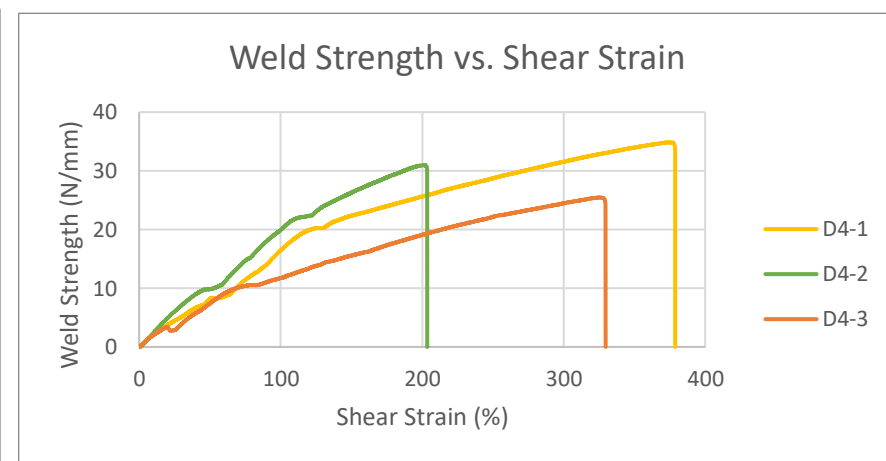
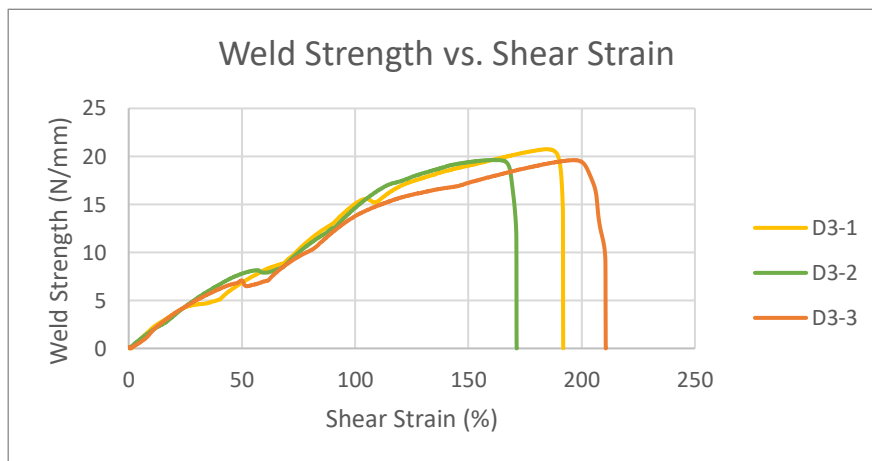
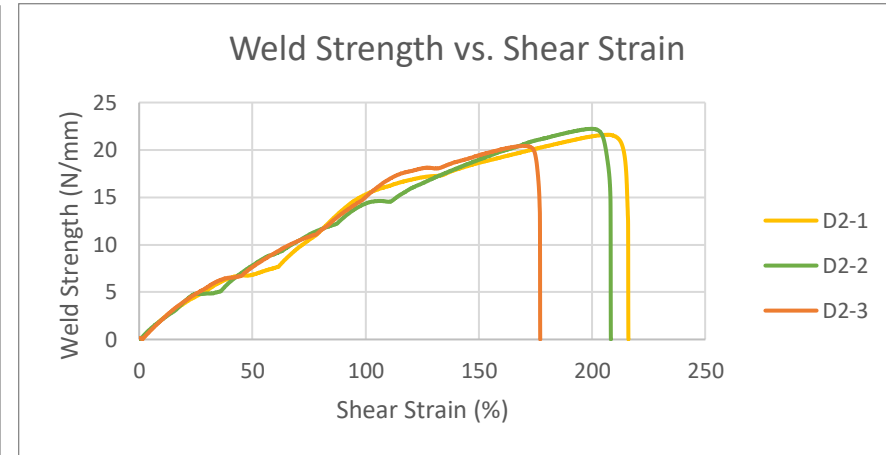
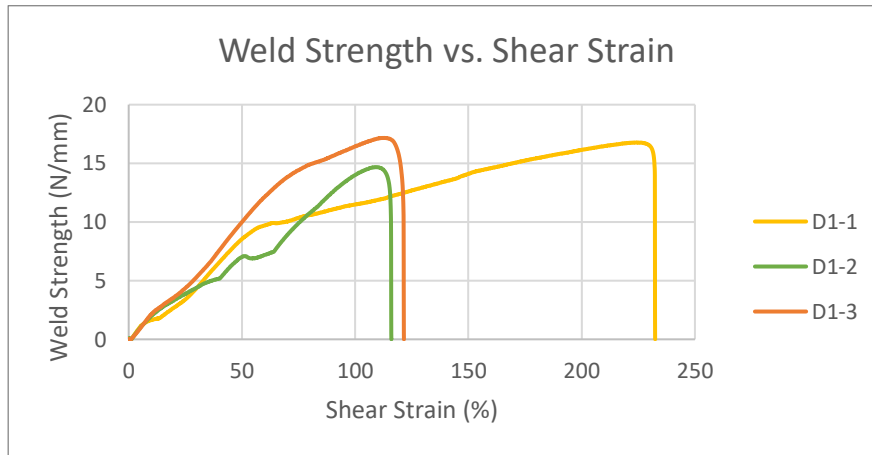


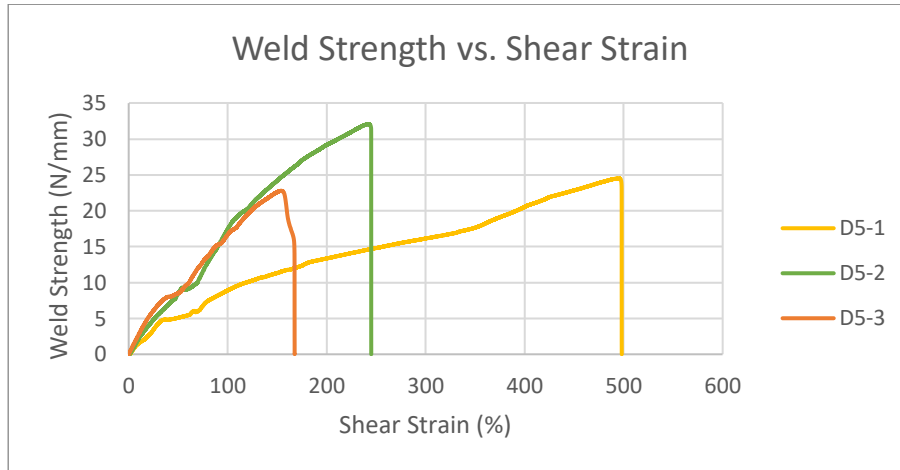
C.4 WELD STRENGTH-STRAIN CURVES (GROUP C)



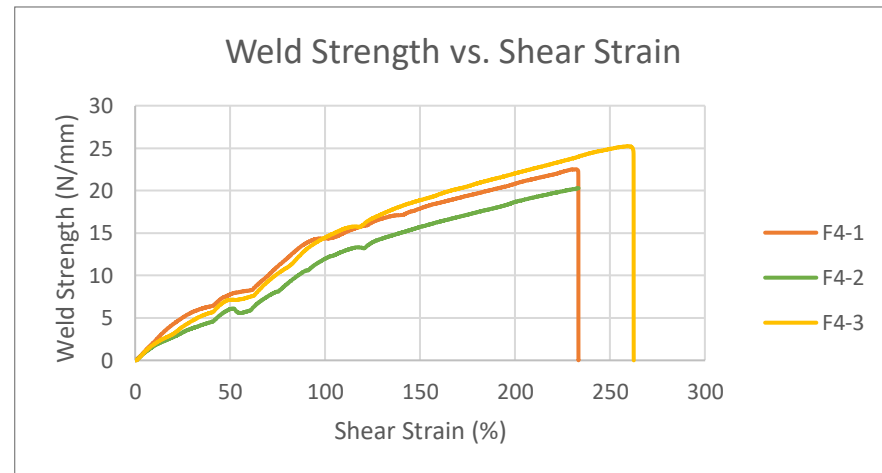
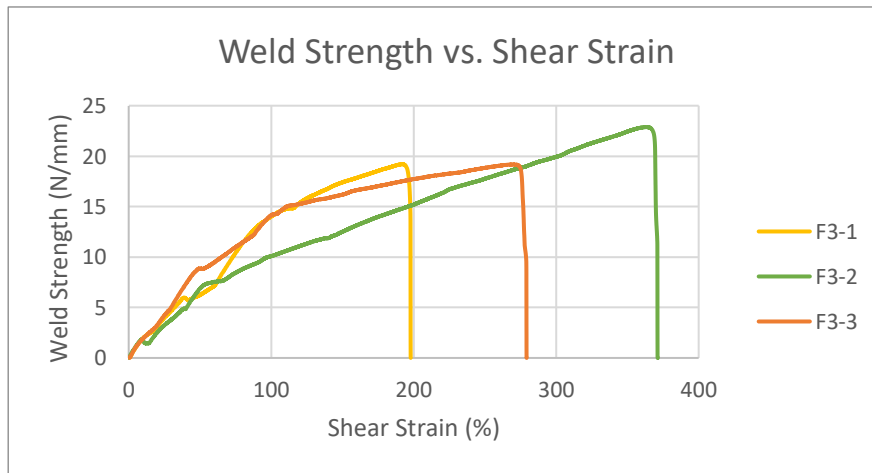
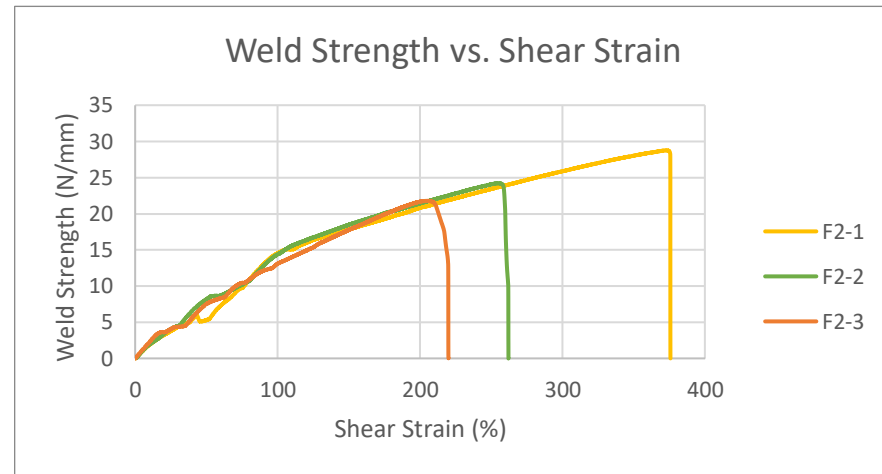
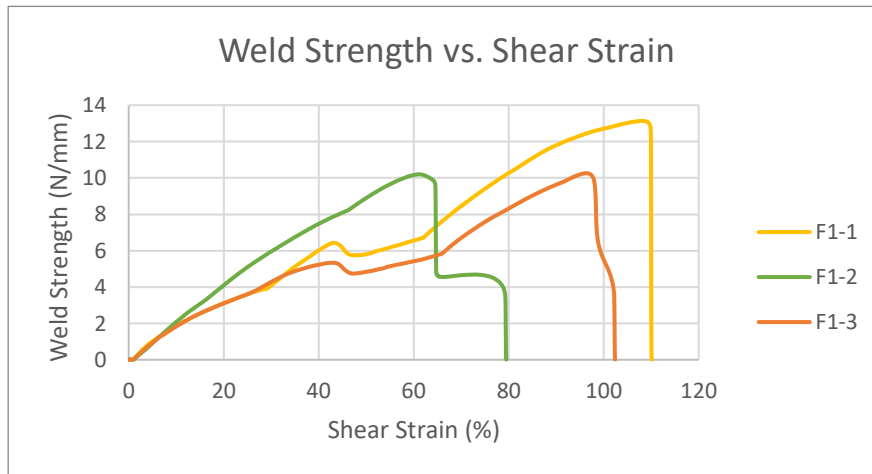


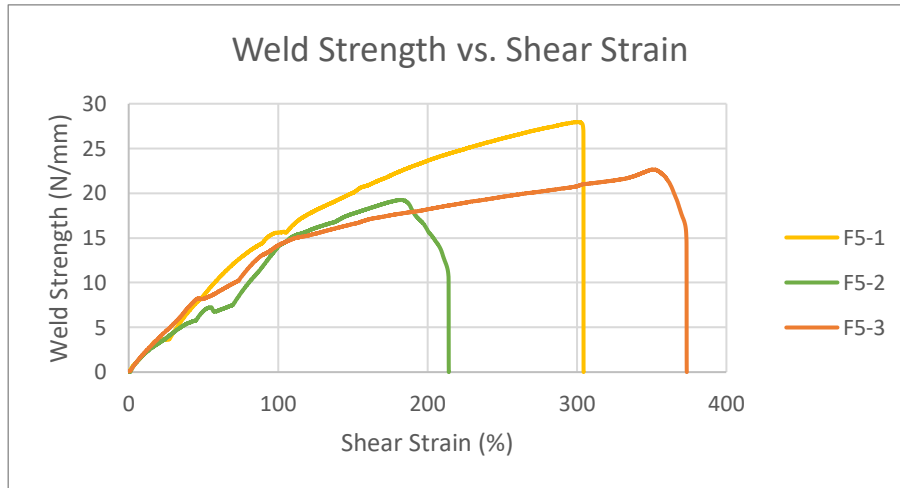
C.5 WELD STRENGTH-STRAIN CURVES (GROUP D)



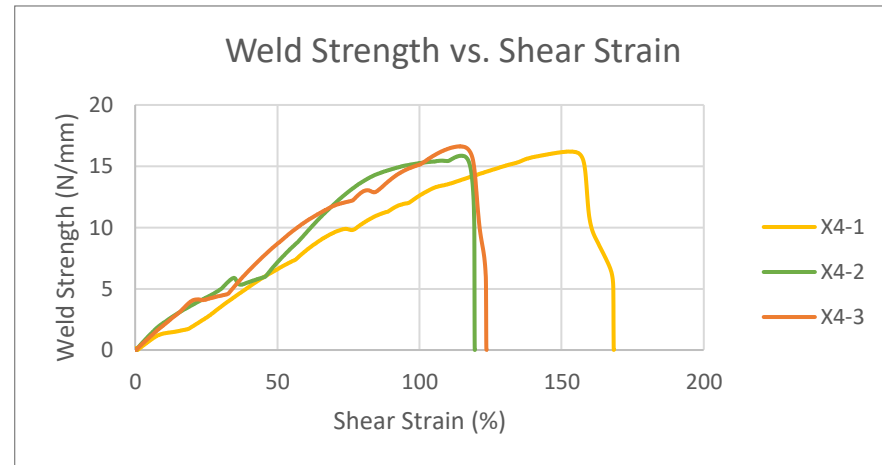
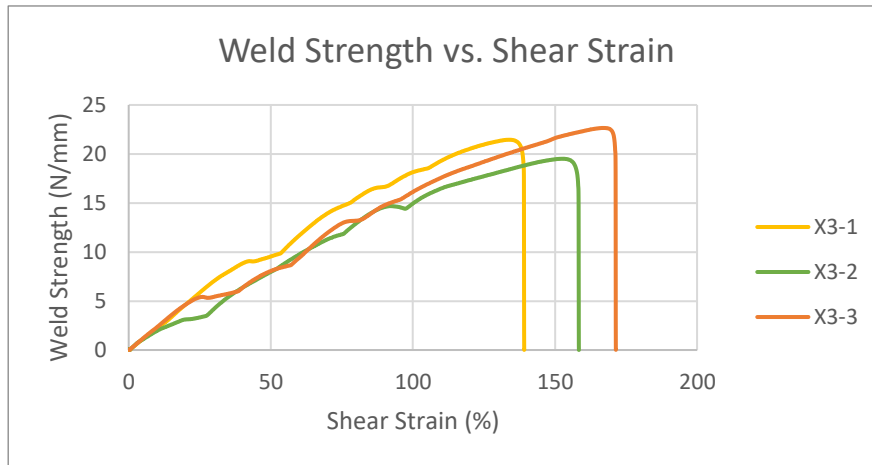
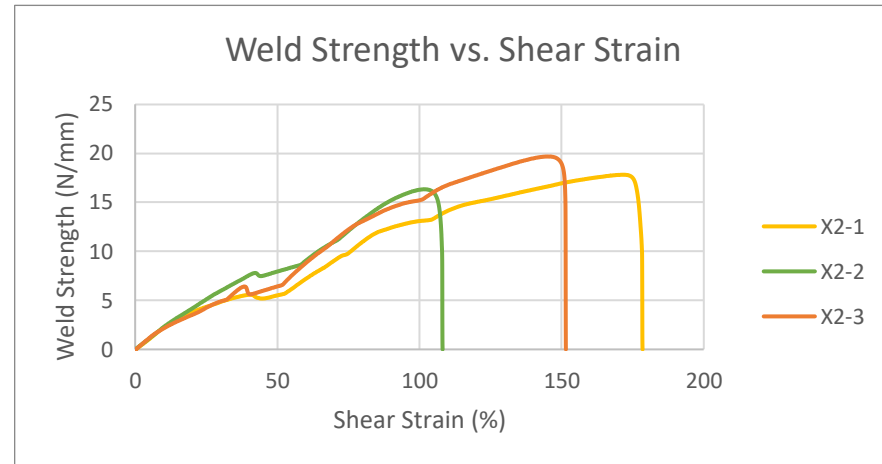
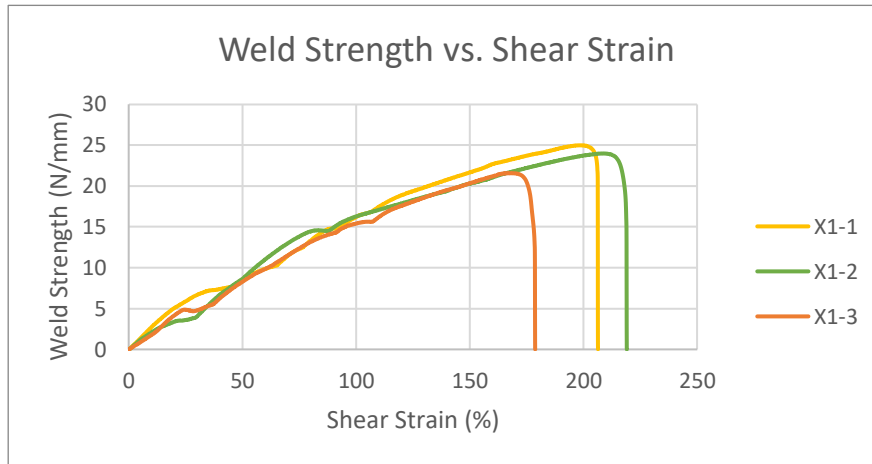


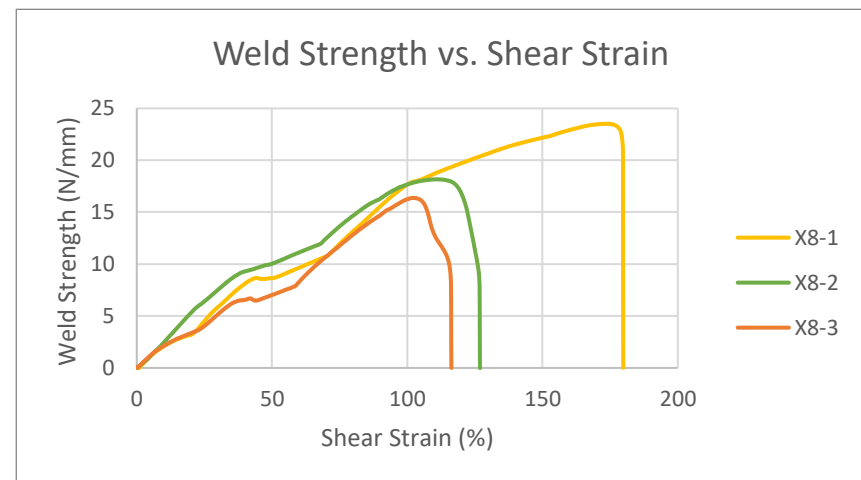
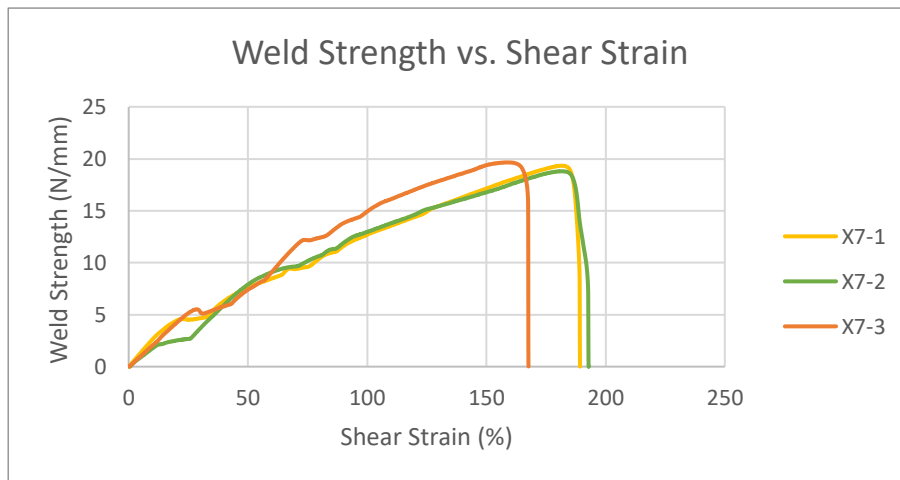
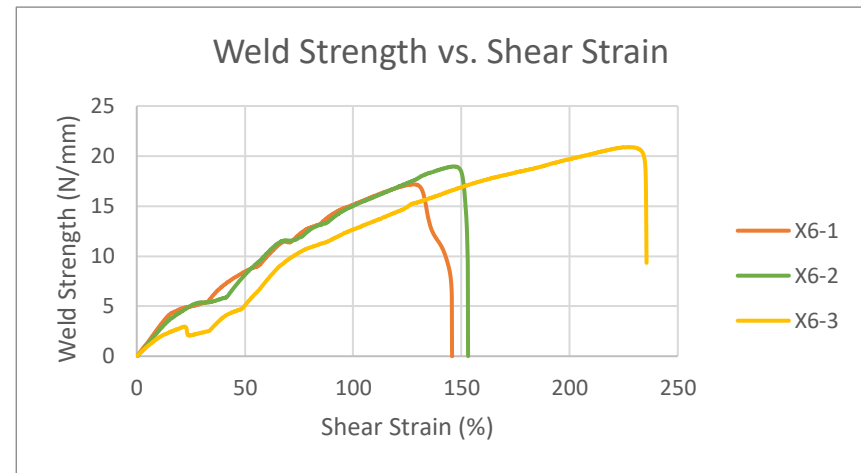
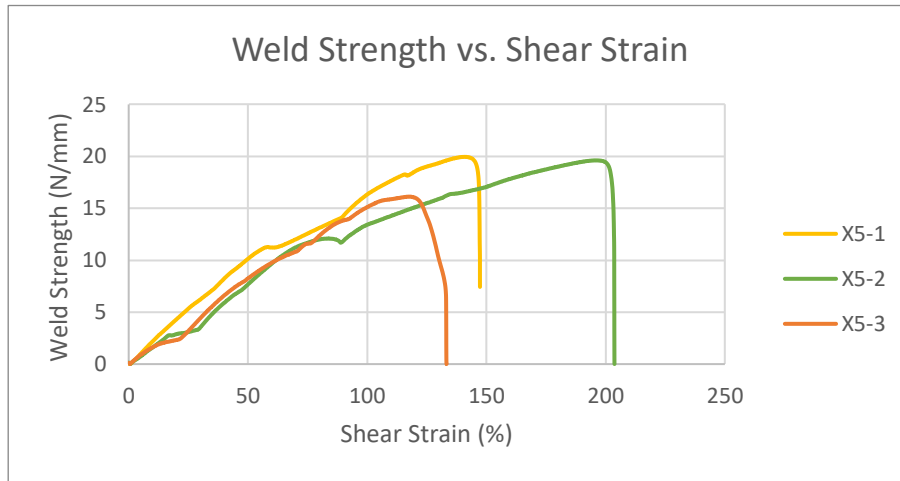
C.6 WELD STRENGTH-STRAIN CURVES (GROUP F)

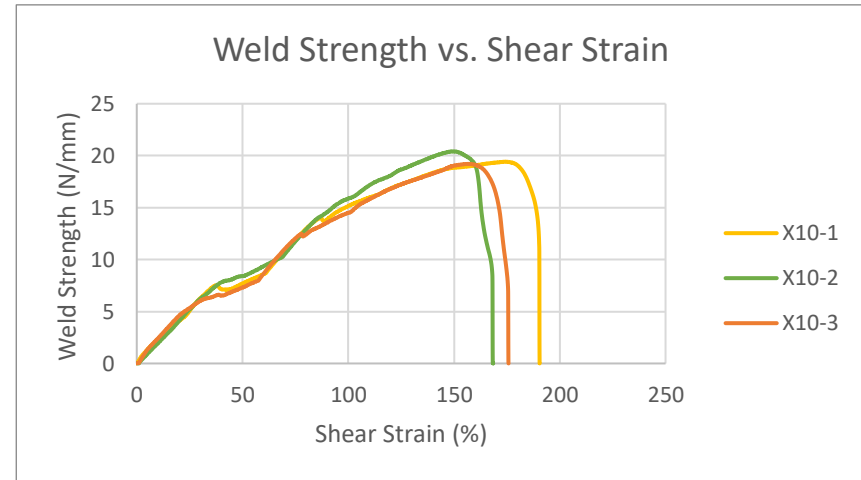
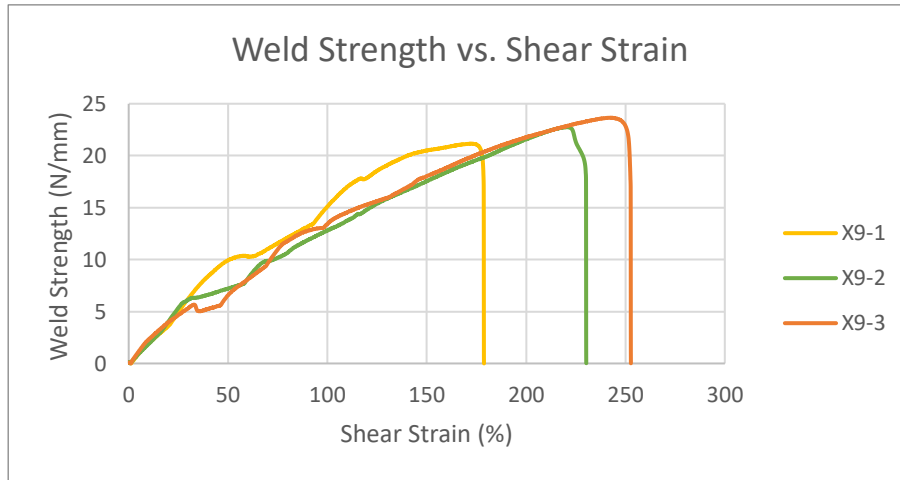




C.7 WELD STRENGTH-STRAIN CURVES (GROUP X)







C.8 STRESS-STRAIN CURVES (BEST SAMPLE)

